EFFECT OF A VARIABLE CONTACT LOAD

ON FRETTING FATIGUE BEHAVIOR

OF Ti-6Al-4V

THESIS

Andrew J. Jutte, 1Lt, USAF

AFIT/GAE/ENY/04-M09

DEPARTMENT OF THE AIR FORCE
AIR UNIVERSITY

AIR FORCE INSTITUTE OF TECHNOLOGY

Wright-Patterson Air Force Base, Ohio

The views expressed in this thesis are those of the author and do not reflect the official policy or position of the United States Air Force, Department of Defense, or the United States Government.

AFIT/GAE/ENY/04-M09

EFFECT OF A VARIABLE CONTACT LOAD

ON FRETTING FATIGUE BEHAVIOR

OF Ti-6Al-4V

THESIS

Presented to the Faculty

Department of Aeronautical and Astronautical Engineering

Graduate School of Engineering and Management

Air Force Institute of Technology

Air University

Air Education and Training Command

in Partial Fulfillment of the Requirements for the

Degree of Master of Science in Aeronautical Engineering

Andrew J. Jutte, B.S.M.E

1st Lieutenant, USAF

March 2004

AFIT/GAE/ENY/04-M09

EFFECT OF A VARIABLE CONTACT LOAD

ON FRETTING FATIGUE BEHAVIOR

OF Ti-6Al-4V

Andrew J. Jutte, B.S.M.E
1Lt, USAF

Approved:

/signed/	
Dr. Shankar Mall (Chairman)	date

/signed/	
Dr. Vinod K. Jain (Member)	date

/signed/	
Dr. Ted Nicholas (Member)	date

AFIT/GAE/ENY/04-M09

Abstract

    Fretting fatigue occurs between components that are in contact and undergo some small amplitude cyclic-type loading which causes a small relative tangential displacement over part of the contacting surface. The occurrence of this phenomenon at the rotor-to-blade interface of turbine engines with dovetail and other similar types of blade-to-disk joints is well documented and a known cause of engine component failures. Nearly all work accomplished to date has examined this problem assuming static contact load conditions even though loading effects in turbine engines are highly dynamic. The primary goal of this study was to investigate the effects of a variable normal contact load on the high cycle fretting fatigue behavior of Ti-6Al-4V. Experimental tests were performed using a new test setup capable of applying a normal contact load varying in amplitude, frequency, and phase as well as measuring shearing force on each side of the test specimen independently. Commercially available finite element code, ABAQUS, was used to perform finite element analysis (FEA) of experimental and idealized loading conditions. Local mechanistic parameters as well as the Modified Shear Stress Range (MSSR) fatigue parameter were evaluated using FEA results. Various correlations between contact width, slip amplitude, fatigue life and a variable contact load for Ti-6Al-4V were established. Furthermore, a variable contact load was determined to have a more damaging effect on fatigue life in comparison to a constant contact load. Predicted values of crack location and orientation using the MSSR parameter were verified experimentally. Two forms of the MSSR parameter were unable to effectively predict fatigue life for variable contact loads. Based on observations of this study a new formulation of the MSSR parameter is proposed which accounts for the effects of a variable contact load as well as constant contact loads.

Acknowledgment

I would like to express my sincere appreciation to my faculty advisor, Dr. Shankar Mall, for his guidance, patience, and support throughout the course of this thesis effort. His insight and experience offered to me was certainly appreciated. I thank the engineering and technical support from the University of Dayton Research Institute during the experimental testing phase of this study. Also, my appreciation goes to fellow AFIT student Major Ki Su Shin of the Republic of Korea Air Force. His guidance and willingness to patiently answer and discuss my many questions was immeasurable helpful during the course of my work.

I also would like to extend appreciation to my parents, family and friends for their support throughout this endeavor. Finally, very special thanks to my girlfriend, a fellow graduate student at the University of Michigan, who always had words of encouragement and motivation to offer.

Andrew J. Jutte

Table of Contents

List of Figures

List of Tables

Nomenclature

a	contact half width
a_{EXP}	experimentally observed contact half width
a_{FEA}	FEA predicted contact half width
a_{max}	maximum contact width experienced during load cycle
a_{min}	minimum contact width experienced during load cycle
A	cross section area
A^*	composite compliance
b	specimen half thickness half
c	stick zone boundary
e	x coordinate of the stick zone
E	elastic modulus
f	coefficient of friction
G	shear modulus
h	depth of penetration
k	influence factor, radius of curvature
N_f	number of cycles to failure; number of fatigue cycles
N_i	number of cycles to crack initiation
P	contact load, applied normal contact load per unit width
P_{max}	maximum contact load applied during load cycle
P_{min}	minimum contact load applied during load cycle
P_o	maximum contact pressure in the contact zone
q	surface shear stress
Q	tangential load, total shear along contact surface
Q_{max}	maximum tangential load
Q_{min}	minimum tangential load
r	fretting pad radius
R	stress ratio
R_1	radius of fretting pad
R_2	radius of fretting specimen
S_{max}	maximum normal stress on the critical plane
S_{min}	minimum normal stress on the critical plane

u	displacement in x-direction
w	specimen width
β	Dunbar's parameter
υ	Poisson's ratio
θ	direction of stress in a material, observed angle of crack orientation
$\Delta\tau$	shear stress range
$\Delta\tau_{crit}$	critical shear stress range
φ_P	phase angle of contact load relative to axial load
σ	axial stress
$\sigma_{1,2}$	principle normal stresses
σ_{axial}	applied axial stress
$\sigma_{axial,\ max}$	maximum applied axial stress
$\sigma_{axial,\ min}$	minimum applied axial stress
σ_N	bulk axial stress
$\sigma_{n,\ max}$	maximum contact stress on critical plane
$\sigma_{setpoint}$	axial load setpoint
σ_T	tangential stress, stress in x-direction in this study
σ_{xx}	contact stress in longitudinal direction (X-axis)
$\sigma_{xx,FEA}$	FEA predicted stress in the X-direction
σ_{yy}	contact stress in the Y-direction
τ	shear stress
τ_a	shear amplitude
τ_{max}	maximum shear stress on critical plane
τ_{max}	minimum shear stress on critical plane
τ_{xy}	shear stress on X-Y plane

EFFECT OF A VARIABLE CONTACT LOAD

ON FRETTING FATIGUE BEHAVIOR

OF Ti-6Al-4V

I. Introduction

1.1. Fretting Fatigue

Fretting occurs between components that are in contact and undergo some small

amplitude cyclic-type loading which causes a small relative tangential displacement over

part of the contacting surfaces. "In situations where the presence of fretting is associated

with a reduction in fatigue life the effect is known as fretting fatigue [33]." It is widely

accepted that fatigue loading combined with an applied clamping or contact load

enforcing surface contact between two bodies undergoing small oscillatory movement

will cause the components to fatigue and fail unexpectedly at stress levels well below

their plain fatigue limit. Yet, there is not an agreement on what is specifically occurring

that causes this phenomenon or what can be done to prevent it.

1.2. Relevance to Air Force

The subject of fretting fatigue is important to the United States Air Force because

fretting fatigue has been attributed to the failure of turbine engines. Specifically, fretting

fatigue has been found to occur in dovetail joints where the turbine blade and turbine

rotor interface as seen in Figure 1.1. The vibration of the turbine engine imposes cyclic

loading on the rotor-to-blade interface joint and induces the conditions for fretting

fatigue. Failure of this joint due to fretting fatigue cannot currently be predicted nor is

there currently an accepted technique to account for fretting in the initial design. Therefore, designers must over-compensate for the potential of fretting by making these dovetail joints more robust than may actually be necessary. Yet, such over-compensation in the design of the joint leads to heavier, less efficient and more costly engines. Moreover, due to the inability to accurately predict failure due to fretting fatigue periodic maintenance inspections, which increase maintenance time and cost, must be performed to ensure cracks do not propagate and lead to catastrophic failure. A better understanding of the failure mechanisms induced by fretting would allow engineers to better design for, prevent, and predict fretting in future engine designs as well as in engines currently in the Air Force's fleet. Better designed engines will also increase engine efficiency, reliability, reduce maintenance time and cost, and improve safety for pilots, crews, and passengers
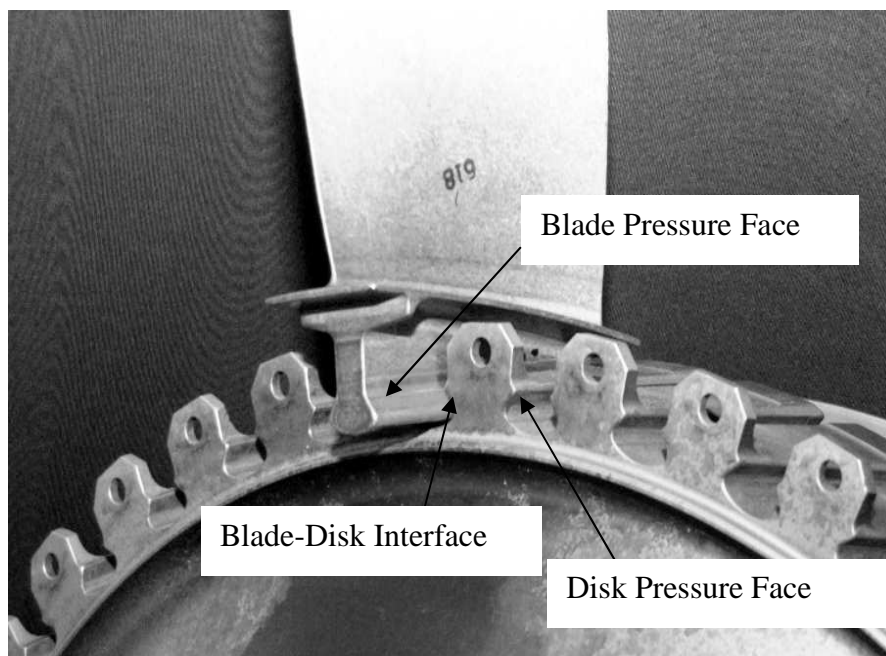
Figure 1.1. Turbine Engine Dovetail Joint

1.3. Simplification of Turbine Engine to an Experimental Setup

The objective of this study was to gain a better understanding of the fretting fatigue behavior of Ti-6Al-4V, a common material used for turbine engine components, so that engineers can better design, maintain, and improve the safety of the Air Force's turbine engine fleet. Therefore, it is necessary to use an experimental setup which simplifies the complex geometry and loading conditions which exist in turbine engines and highlights the fretting fatigue problem as it occurs in turbine engines. Researchers over the years have developed a general test set up with the goal of developing an understanding of fretting fatigue in a way that can be applied in general terms not only to the case of turbine engine components, but to any two components in a configuration prone to fretting fatigue. An experimental simulation of the actual components involved in a fretting fatigue scenario allows for many more tests to be performed at a much lower cost than would be possible using actual components from a turbine engine. Furthermore, an experimental setup allows the desired variables involved in fretting fatigue to be examined in detail systematically.

1.4. Contributing Variables

Several factors are thought to contribute to the overall fretting fatigue phenomena. Researchers are in general agreement that several variables independently or jointly play an integral part in the fretting fatigue process; however, the individual contribution of each factor is not currently fully understood. The major factors thought to influence the fretting fatigue behavior of a material are material properties, environment, applied stresses, displacement between the contacting surfaces and contact pressure between the contact surfaces. These contributing variables directly and indirectly could influence one

another. For example, an increase in the magnitude of the applied contact load increases the area of contact between contacting bodies as well as the local and peak pressure if all other factors are held constant. Therefore, research is continuing in an attempt to isolate and study the effects of the many variables that influence fretting fatigue.

1.5. Purpose of this Study

One variable in the fretting fatigue equation, which has been isolated and studied in the past, is the applied contact load. In this effort several researchers have examined the effect of varying the magnitude of the applied contact load on fretting fatigue. In such studies the contact load is typically held constant for the duration of the experiment. In reality, such a loading case may arise only if the contact load is static and does vary significantly during the lifetime of a joint as in the case of a lap joint. Yet, the contact load experienced by a joint undergoing vibratory loading such as those found in a turbine engine can vary significantly [14]. Therefore, a better understanding of how variations in the applied contact load affects the fretting phenomena is needed so that turbine engine designers and sustainment engineers can better account for its effects. Therefore, the goal of this study is to improve the understanding of how variations in the applied contact load contribute to the fretting fatigue phenomenon. Thus, this study asks the question, what will be the effect of applying a cyclically varying contact load on the fretting fatigue behavior of Ti-6Al-4V?

1.6. Methodology and Objectives

The purpose of this study is to investigate the effects of a variable contact load on the fretting fatigue behavior of Ti-6Al-4V in a systematic way. Therefore, efforts of previous researchers were first examined and studied. Then an experimental test setup

commonly used in the study of fretting fatigue was modified to allow a variable contact load to be applied. The fretting fatigue behavior of Ti-6Al-4V was first established under constant amplitude contact loads using this newly developed experimental configuration. Tests were then conducted with a variable contact load having a sinusoidal waveform. Fretting fatigue specimens were examined to determine the crack location on the contact surface and the size of the contact region. Comparisons were made between the scar patterns of specimens under a constant amplitude contact load and those under a variable amplitude contact load. The stress distribution and regions of stick and slip along the specimen's contact surface were found using finite element analysis (FEA). Crack orientation on the contact surface under a variable contact load was verified using Scanning Electron Microscopy (SEM).

A secondary goal of this study was to examine if an existing fatigue parameter, the Modified Shear Stress Range (MSSR), could accurately predict the number of cycles to failure when the contact load was varied. Using axial, transverse, and shear stresses along the contact surface the MSSR was calculated for each specimen. The MSSR fatigue parameter was evaluated based on its ability to accurately predict crack location, orientation and number of cycles to failure.

Next, research accomplished to date in the areas discussed above and relating to this study above will be summarized in Chapter 2. Chapter 3 will then discuss the experimental setup used in this study. Chapter 4 will then present the finite element model of the experimental setup. Results of experimental and numerical tests will be presented and discussed in Chapter 5. Finally, Chapter 6 will provide conclusions based on the findings of this study as well as recommendations for future work in this area.

II. Background

This chapter will provide a basis for the remainder of this study by presenting basic concepts in the area of fretting fatigue and a review of previous studies, which are relevant to this study. The relation between applied contact load and contact pressure will first be presented and discussed. Second, a common method used to simulate fretting fatigue in an experimental environment will be described. Thirdly, work accomplished to date to better understand the effects of a normal contact load on fretting fatigue and various experiments in this area will be summarized. The concept of predictive fatigue parameters is then presented along with the description of one which has begun to show promise in predicting crack initiation behavior in fatigue situations where fretting is present. Finally, analytical techniques from contact mechanics useful to the study of fretting and which aid in the validation of the Finite Element Model of the fretting fatigue experimental configuration used in this study are presented and discussed

2.1. Relationship Between Applied Contact Load and Contact Pressure

In studying contact load and its effect on the fretting fatigue phenomenon it is important to understand how the applied contact load relates to the stresses in the region of contact. Contact load is often considered a global boundary condition in the fretting fatigue problem. However, the localized confluence of contact load results in a variety of interfacial conditions. Among these interfacial conditions are local contact pressure and peak contact pressure. Therefore, in discussing the effect of contact load it is necessary to relate contact load to local contact pressures, peak contact pressure, and stresses seen at the contacting surface. The relation between these three is largely based on contact geometry. How best to relate these three is yet another source of debate among

researchers and the specifics of the various arguments will not be discussed in depth here.

In early studies contact pressure was related to contact load through the assumed area of contact between two bodies determined analytically. In recent years some researchers have focused on the effect of peak pressure. Yet, still others have focused on the fretting fatigue behavior in terms of the applied contact load. The analytical equations used to relate contact load, local contact pressure, and peak contact pressure will be presented later in this chapter. Therefore, studies on contact pressure effects which are related to the contact load based on an assumed analytically determined contact area will be included in the background to this study contained in the reminder of this chapter. The convention used in this is study will be to relate contact load and pressure in terms of contact load per unit width, i.e. kN/m. To aid in understanding the relationship between the contact load applied and contact pressure as well as to provide a basis for discussion of previous studies, the next section will describe the basic test setup used to study fretting fatigue.

2.2. Typical Fretting Fatigue Experimental Test Setup

In the pursuit to develop a universal understanding of the fretting fatigue phenomenon researchers have developed and adopted a general test setup designed to isolate the problem at hand. Figure 2.1 shows a simplified version of a typical fretting fatigue experimental test setup. Figure 2.1 shows the two bodies of interest; the fatigue specimen and fretting fatigue pad; representative of any two components in contact. Typically a hydraulic test machine is used to grip a fatigue specimen and an axial load, σ_N, is applied to one end while the other end is held fixed. The applied axial load is the fatigue load and typically has a cyclic waveform, i.e. sinusoidal. Simultaneously pads are

pressed against the specimen by a contact load, P, in the direction perpendicular to the direction of the applied axial load. Typically the pads are spherical or cylindrical. These geometries are desirable because the analytical solutions of the stress and displacement distributions have been derived for these cases. The analytical solution for the cylindrical pad case will be discussed later in this chapter. When the axial load is applied to the specimen the specimen expands and contracts based on the elasticity of the material. At the same time the contacting pads remain fixed by a pair of pad holders and in contact with the specimen by the application of a contact load, P. As a result a shear load, Q, develops tangential to the applied axial load as long as the friction between the two bodies is sufficient enough to prevent total slippage, i.e. gross slip. The magnitude of this resulting tangential shear load, Q, which opposes the movement of the pads, is a function of the stiffness of the pad holders. The resulting tangential shear load is typically determined by measuring the difference between the applied axial load and the axial load experienced at the fixed end of the specimen via load cells placed at both ends of the specimen. This difference is equal to sum of the shear loads on each side of the specimen. A moment, M, results from the shear developed between the fretting pad and specimen. The moment is typically applied by a pad holder (not shown). This experimental setup ultimately leads to a crack in the specimen caused by fretting fatigue. In the next section the findings of fretting fatigue research on the effects of contact load using experimental setups similar to the one just discussed will be reviewed.
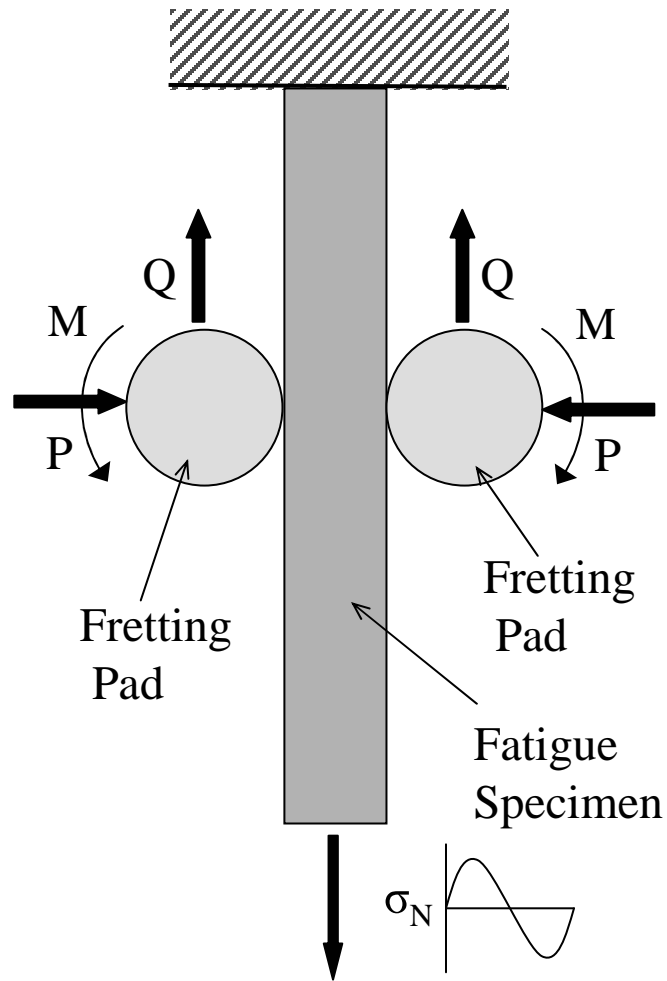
Figure 2.1. Typical Experimental Test Setup

2.3. Summary of Previous Works on Contact Load Effects

Initial work done in the area of fretting fatigue examined the material's response

to various environmental and loading conditions. In recent years studies have continued

in these and other areas in an attempt to better explain the fretting fatigue phenomenon in

general. In particular much research has been done in an attempt to explain the effect of

contact load conditions on the fretting fatigue phenomenon in materials in general and in

some cases Ti-6Al-4V specifically. The next section of this paper will present the major

finding and conclusions of research performed to date in this area with the goal of

providing an outline of what is currently known and unknown about the effects of contact

load on the fretting fatigue behavior of Ti-6Al-4V.

2.3.1. Goss and Hoeppner

In 1973 Goss and Hoeppner conducted a study on the effect of contact pressure on

the fretting fatigue process in titanium. They noted that the major variables affecting

fretting fatigue are material, environment, applied stress, relative displacement between

contacting surfaces, and contact pressure (applied contact load divided by assumed

contact area) between contacting surfaces. Goss and Hoeppner attempted to relate the

macroscopic plane stress fracture toughness to fretting fatigue characteristics of the

material. From their experiments they observed that at lower axial stress levels fretting

fatigue life for titanium shows a stronger dependent on contact pressure than does

aluminum which they also tested. Also, at lower axial stress levels they observed that

when the contact pressure was reduced two things happened in titanium; fretting fatigue

life increased and scatter in the data increased. The increase in fatigue life was said to

indicate that more load reversals were needed to produce a flaw at lower contact loads

that at higher contact loads with the same axial load. This they said indicated that for

titanium contact pressure up to 41.37 MPa is directly related to damage being produced

on the surface during fretting and fatigue life. The increase in scatter in the data they

attributed to variations in the local grain orientation and phase orientation effects in Ti-

6Al-4V. They hypothesized that for fretting damage to lead to a crack the local grain

orientation needs to be such that a crack can propagate from the damage area. From their

observations they concluded that the influence of contact pressure on fretting induced

damage was largely due to variation in microstructure or microscopic toughness and crystallographic effects [9].

2.3.2. Adibnazari and Hoeppner

Adibnazari and Hoeppner continued the work into the effect of contact load conditions and contact pressure. They introduced the concept of a pressure threshold. They stated that there exists a value of contact pressure after which increasing the pressure does not affect the total cycles to failure [

1]. They postulated that above a certain pressure threshold, fretting fatigue failure is only a function of contact and frictional stress, not the increase of these two variables. Using this pressure threshold concept they studied the effect of contact pressure in fretting fatigue on the damage threshold of aluminum and titanium alloys. They concluded that the stress state created by the contact pressure mostly affects crack nucleation and propagation [22].

2.3.3. Nakazawa, Sumita and Maruyama

After Goss and Hoeppner's study a number of other researchers have found that in general fretting fatigue life decreased with an increase in contact pressure; however, other researchers had observed a minimum in fretting fatigue life at a certain contact pressure [27]. The uncertainty of the effect of contact load and in turn contact pressure on fretting fatigue at the time lead Nakazawa et al. to conduct a study in the early 1990's on the subject. They related contact load and contact pressure in terms of stress concentration at the fretting area. Nakazawa et al. define contact pressure as the contact load (normal to the contact surface) applied to the fretting pad divided by the apparent contact area of the fretting pad just as Goss and Hoeppner had done several years earlier. The loading

configuration used by Nakazawa et al. consisted of contact pressures below 160 MPa and an axial fatigue load produced by a sinusoidal wave at a frequency of 20 Hz, under a tension-tension axial load having a stress ratio of 0.1. They concluded that fatigue life showed a dependence on contact pressure in Ti-6Al-4V. For Ti-6Al-4V they found that at higher bulk axial stress amplitude the fretting fatigue life decreased monotonically with increasing contact pressure. Also, at lower bulk stress amplitude Ti-6Al-4V exhibited a minimum at a low contact pressure and decreased again and became constant at high contact pressure. These findings explain why some previous researchers had observed a decrease in fretting fatigue life with an increase in contact pressure while others had observed an increase in fretting fatigue life with a increase in contact pressure [27].

2.3.4. Iyer and Mall

A few years later Iyer and Mall conducted two studies on different aspects of contact load effects. In the first study Iyer and Mall examined the relation between contact pressure and frequency of the bulk axial stress. They reported that contact pressure reduces life at 1 Hz, however, it had no apparent effect on fretting fatigue life at a cyclic bulk stress of 200Hz. They also observed, at a larger contact load (3657 N), a clear dominant stick zone and a narrow slip zone with very little debris. On the other hand, at a lower contact load (1338 N) they observed more severe fretting damage in the form of wear and/or plastic deformation across the entire contact region and the demarcation of the fretting zone being less apparent than at the higher contact load [15].

In another study conducted by Iyer and Mall they conducted an analysis of contact pressure on fretting fatigue life of Ti-6Al-4V. In this study they used experimental results as well as finite element analysis of the stresses along the contact

surface and expanded the work of their previous study adding a contact loading condition of 2230 N to their program of experiments. In this second study Iyer and Mall proposed an explanation for the reduction observed by Hoeppner and Goss [9] and Adibnazari and Hoeppner [

1] in the fretting fatigue life of titanium alloys with increasing contact pressure. Iyer and Mall reported that fretting fatigue loading results in an amplified stress range in the vicinity of contact and could be computed using FEA [17]. They explained that the amplification in the local stress range during fretting fatigue is due to the local build-up of compressive stresses upon unloading. They state that amplification is more severe for smaller cyclic stress amplitudes and thus can be used to explain the more marked reduction in fatigue life due to fretting near the material fatigue strength [17]. This study also shows that the decrease in fretting fatigue life with increasing contact pressure can be related to the increase in the local stress range amplification alone, without any regard to interfacial shear stress or slip amplitude. Furthermore Iyer and Mall evaluated a pair of parameters proposed by Ruiz et al. and widely used in studies previous to theirs. Iyer and Mall reported that the proposed parameters were "unreliable in explaining the effect of contact pressure on fretting fatigue life [17]." Further studies on predictive parameters will be discussed later in this chapter.

2.3.5. Iyer

In further research on fretting fatigue Iyer offered new explanations for the relation between contact load and fretting fatigue life. Up to this point many studies focused on the global boundary conditions such as contact geometry and applied loads. Iyer took a different approach. He stated that it was possible to evaluate the local

mechanistic environment through the use of semi-analytical and numerical methods with the use of finite element analysis (FEA) [16].

2.3.5.1. Local Mechanistic Parameters.

It is Iyer's approach that when considering the classical cylinder-on-flat model of fretting fatigue the important variables in the problem are the "local mechanistic" variables within the contact region and not the global boundary conditions of contact load, pad radius or applied bulk stress [16]. Iyer evaluated local mechanistic parameters including peak contact pressure with the aim of discerning their inter-relationships and individual relevance to fretting fatigue. Iyer identified seven mechanistic parameters as the major contributors to fretting fatigue. The mechanistic parameters identified were: contact pressure, slip amplitude at the interface, the coefficient of friction, the local cyclic tangential shear stress at the interface, the local bulk cyclic stress just beneath the contacting surface and parallel to it, cyclic frequency and the number of fretting cycles. Using FEA he related local conditions to global conditions. Using the relations established from FEA he reported that it is possible to determine what global conditions to apply in an experiment to maintain certain local conditions as constants while varying other local conditions systematically for the purpose of evaluating their effect on fretting fatigue. Iyer found that only peak contact pressure and local maximum bulk stress range were independent variables for determining fretting fatigue life. He also found that all other local mechanistic parameters either did not adversely affect fretting fatigue or were highly dependent on peak contact pressure or the local maximum bulk stress range. Finally he concluded that the peak contact pressure is found to extend fretting fatigue life.

In order for the values of maximum local stress to be evaluated in his study, principal stresses were calculated from finite element output [16].

2.3.5.2. Principal Plane Stresses.

A summary of the principal stresses as explained by Hibbeler [11:208-209] is summarized here. The variation of stresses i.e. σ and τ, with direction, θ, in a material is given as follows.

$$\sigma = \frac{\sigma_{xx} + \sigma_{yy}}{2} + \frac{\sigma_{xx} - \sigma_{yy}}{2} \cos 2\theta + \tau_{xy} \sin 2\theta \tag{1}$$

$$\tau = -\frac{\sigma_{xx} - \sigma_{yy}}{2} \sin 2\theta + \tau_{xy} \cos 2\theta \tag{2}$$

The maximum or minimum in-plane normal stress acting on point is given by the equation

$$\sigma_{1,2} = \left(\frac{(\sigma_{xx} - \sigma_{yy})}{2} \right) \pm \sqrt{\left(\frac{(\sigma_{xx} - \sigma_{yy})}{2} \right)^2 + \tau_{xy}^2} \tag{3}$$

σ_1 and σ_2 are called principle normal stresses and the planes on which they act are called the principal planes. σ_{xx}, σ_{yy}, is and τ_{xy} are the stress components at a particular point in the material. There is no shear acting on the principal planes. The planes for maximum shear stress are 45° from the orientation of the planes for principal normal stress. The equation for the principle shear stress is as follows

$$\tau_{max} = \sqrt{\left(\frac{(\sigma_{xx} - \sigma_{yy})}{2} \right)^2 + \tau_{xy}^2} \tag{4}$$

The use of principal stresses acting on principal planes was further investigated by other researchers and used in the development of predictive parameters which will be discussed further later in this chapter.

2.10

2.3.6. Fernando, Brown, Miller, Cook and Rayaprolu

Nearly all work done to date in the area of contact loading effects on fretting fatigue has been done using constant amplitude contact loads. However, as stated earlier, in many situations where fretting fatigue conditions exist, such as the dovetail joints of turbine engines, contact loads can vary in magnitude and frequency [14]. The lack of experiments into variable amplitude contact loads has been due largely to the lack of testing equipment capable of applying the loading conditions necessary to study such effects. Using fixturing similar to that used by Ruiz [35] it is possible to apply a contact load, which varies in phase with an applied axial load. However, it is not possible to vary the two loads independently. Test configurations have been used in which the contact load varies independently from the axial load. In the early and mid 1990's Fernando et al. [7] developed one of the first testing facilities to study variable contact loads and their affect on fretting fatigue. They were able to control the amplitude, frequency as well as the phasing of applied contact loads on the contact area relative to the phase of the axial load. Using this new testing facility Fernando et al. examined the effects of variable contact load on the fretting fatigue behavior of BS L65 4% copper aluminum alloy. Fernando et al. reported that the fatigue life was noticeably affected by the contact load waveform with variable contact load enhancing the fretting fatigue life at axial loads at or below 125 MPa and contact loads of 1200 N or less. Similar testing of variable contact loads on titanium alloys has not been found in literature.

As seen in many of the studies reviewed, contact load can have a major influence of the fatigue life of specimens when fretting is present. Many researchers have attempted to predict this change in fatigue behavior when fretting is present using fatigue

parameters. The next section will discuss some of the techniques used to develop predictive fatigue parameters as well as details of one parameter that has shown some success in predicting fatigue crack behavior in recent years.

2.4. Predictive Fatigue Parameters

As stated earlier one of the major goals of fretting fatigue research is to provide the engineer or designer with parameters that can be used to accurately predict the fretting fatigue behavior of contacting bodies. Such a parameter would aid the engineer in the design of robust parts reducing engine component weight and cost while increasing engine efficiency and safety. With this goal in mind several studies have been undertaken to develop and evaluate existing predictive parameters for fatigue conditions where fretting exists. To better understand the development of predictive parameters the techniques used in their development will be discussed in the next section.

2.4.1. Predictive Parameter Techniques

In developing predictive parameters the contributing factors to fretting fatigue are evaluated and incorporated into a theory, such as an equation, which attempt to predict the behavior of crack nucleation due to fretting fatigue. The accuracy of the predictive value can then be evaluated based on its ability to predict one or more crack behaviors such as initiation location, orientation, and/or cycles to crack initiation i.e. fatigue life. Additionally parameters can be evaluated on their ability to also predict crack behavior in plain fatigue or fatigue without the fretting effect. Lykins grouped predictive parameters based on the technique used in their development [19]. Lykins defined the groups as those based on empirical techniques, fracture mechanics techniques, fretting fatigue specific techniques, or plain fatigue techniques [19]. Several fretting fatigue researchers

[19,20, 21, 22] have studied predictive parameters based on the aforementioned

techniques on the parameter's ability to accurately predict crack location, orientation,

and/or cycles to crack initiation. In the study conducted by Lykins et al. [20] many of

these initially popular predictive parameters which included the strain-life parameter, the

maximum strain corrected for strain ratio effects, the maximum principal strain corrected

for principal strain ratio effects, the Smith-Watson-Topper (SWT) parameter, the critical

plane SWT parameter, the Fatemi and Socie (F-S) parameter, and fretting fatigue specific

Ruiz parameter on the parameter's ability to predict crack initiation behavior of cycles to

crack initiation and crack initiation location in Ti-6Al-4V undergoing fretting fatigue. In

their study contact load effects are taken into consideration with other applied loads

through the use of FEA. Lykins et al. used FEA to analyze the local stresses and strains

at the point of contact [20]. Local stresses can then be used in the development and

evaluation of predictive parameters. Using FEA stress results and observations from

evaluation of predictive parameters Lykins et al. reported that the maximum strain

amplitude at the contact interface was important in predicting crack initiation [20]. Also

they noted that Ti-6Al-4V responds to fretting fatigue conditions in a manner similar to

plain fatigue conditions when the applied loading was corrected for the effects of contact

and mean stress or strain ratio [14]. Other studies [19, 21, 29] used approaches similar to

that used by Lykins et al. to evaluate the same and other parameters under different

loading conditions. Based on the studies discussed above the predictive parameters based

on plain fatigue techniques have shown promise in being able to accurately predict crack

initiation behavior in situations where fretting is a factor.

2.4.1.1. Plain fatigue techniques.

Plain fatigue techniques are developed based on the stress and/or strain history of the plain fatigue specimen. Plain fatigue predictive parameters can be used to estimate the life of bodies based on the stress or strain history, such as a fretting fatigue specimen. Plain fatigue techniques are applicable to fretting fatigue only if the two are related in terms of stress concentration i.e. stresses occurring at the trailing edge of contact in a fretting configuration can be related stress concentration resulting from a stress riser, such as a notch, in a plain fatigue configuration. As stated by Namjoshi et al. [29] plain fatigue techniques involve correlating the number of cycles to develop a crack of a certain size with the continuum field variables or some parameters developed based on the state of cyclic stress or strain, or any combination of these. In addition, stresses experienced in the region of contact of a body in a fretting fatigue condition are multiaxial in nature. Therefore, if a plain fatigue technique is to be applied to a body undergoing fretting it must incorporate multiaxial states of stress. Numerous multiaxial plane fatigue parameters have been proposed and have been grouped by Namjoshi et al. into two groups; equivalent stress models and critical plane models [29]. Equivalent stress models require the determination of an equivalent cyclic scalar parameter often in terms of the mean stress to be used in conjunction with uniaxial stress versus fatigue life data. However, in a state of multiaxial stress states the definition of a mean stress is difficult. Therefore, using an equivalent stress model is not always possible. On the other hand, several researchers [22,37] have found that critical plane models correlate well with experimental observations. These researchers have observed through experimental tests that fatigue cracks often nucleate on a particular plane. Therefore, in

2.14

recent years predictive parameters have focused on development of parameters based on multiaxial plain fatigue techniques using stresses found on the critical plane.

2.4.1.2. Critical Plane Approach.

Problems are often approached by examining the critical plane when such things as principal axis rotation during cyclic loading are present, cyclic loads occur at more than one frequency, of if there is a difference in phase other than 180° between loads in fatigue. Using a critical plane approach the crack growth is modeled using a combination of normal and shear stress/strains on the critical plane. The normal stress/strains are hypothesized to open cracks reducing the friction between crack surfaces and the shear stress/strain induces dislocation movement along slip lines causing crack nucleation and propagation to occur. Therefore, a technique which involves both plane fatigue techniques for multiaxial states of stress combined with fracture mechanics approach may have the potential to yield a parameter which would be able to predict the cycles to crack initiation, the location and orientation of crack resulting from fretting fatigue. To this end the Modified Shear Stress Range Parameter has been developed and is seen by some as the most likely parameter to effectively predict crack initiation behavior due to fretting fatigue.

2.4.2. Namjoshi, Mall, Jain, Jin (Modified Shear Stress Range Development)

Namjoshi, et al. first proposed the Modified Shear Stress Range Parameter (MSSR) after studying two previous proposed predictive parameters, the Findley Parameter and the Shear Stress Range Parameter [29]. Therefore, to help better understand the theory behind the MSSR parameter the Findley and SSR parameters will first be discussed.

2.15

2.4.2.1. Findley parameter.

The Findley parameter was first proposed by Findley in the sixties and involved the shear stress amplitude, $\tau_a = (\tau_{max} - \tau_{min})/2$ and maximum stress normal to the orientation of maximum shear multiplied by an influence factor, k, and is stated as follows

$$FP = \tau_a + k\sigma_{max} \tag{5}$$

where FP represents the Findley parameter [8]. Using a value of 0.35 for k determined from a previous study [21], Namjoshi et al. found that although the Findley parameter was not able to accurately predict the crack orientation and there was not a good agreement between plain fatigue life data and fretting fatigue life as predicted by the parameter. On the other hand, the Findley parameter did not show a dependence on the pad geometry used. Namjoshi et al. attributed this lack of geometry dependence to the inclusion of normal stress in the calculation of the parameter [29].

2.4.2.2. Shear Stress Range (SSR) Parameter.

Another parameter considered by Namjoshi et al. included the Shear Stress Range Parameter, (SSR), developed by Lykins et al. [21] which is defined as follows

$$\Delta\tau = \tau_{max} - \tau_{min} \tag{6}$$

where $\Delta\tau$ is the shear stress range and τ_{max} and τ_{min} are the shear stress values due to the maximum and minimum globally applied loading respectively. Using a program written by Namjoshi [28], which will be referred to here as the Namjoshi parameters program, the shear stress range was computed on all planes at all points on the specimen's contact region. The plane where the shear stress range is at a maximum is determined to be the critical plane. The Namjoshi parameters program determines the maximum shear stress

range on all planes ranging from $-90^o \le \theta \le 90^o$ in 0.1^o increments at a point using stresses and strains determined by from FEA. The shear stress range parameter was slightly modified to account for the effects of mean axial/shear stress since it has been shown that the mean stress also affects fatigue behavior. Using a technique proposed by Walker [38] to account for mean shear stress ratio effect on the critical plane the shear stress range parameter was then rewritten as

$$(SSR = \Delta\tau_{crit}) = \tau_{max}(1 - R_\tau)^m \tag{7}$$

where τ_{max} is the maximum shear stress on the critical plane, R_τ is the shear stress ratio on the critical plane defined as τ_{min}/τ_{max}, and m is fitting parameter determined to be 0.45 from plane fatigue data [21]. In their study Namjoshi et al. observed that the SSR parameter successfully predicts the location and orientation of crack initiation, however, not for all pad geometries used in their study. Therefore, Najmoshi et al. proposed a new parameter called the Modified Shear Stress Range critical plane parameter (MSSR) with the goal of combining the positive qualities of the Findley and SSR parameters.

2.4.2.3. Modified Shear Stress Range (MSSR) Parameter.

The MSSR parameter proposed by Namjoshi et al. is based the SSR parameter but modified to include effects of normal stress similar in a way similar to the Findley parameter. This parameter eliminates the effects of pad geometry by including both normal and shear stresses, similar to the Findley parameter. Also, contained in the MSSR parameter are aspects of the shear stress range parameter, which was the only parameter Namjohsi et al. found satisfactory in determining both crack location and orientation [29]. The MSSR parameter is stated as

$$MSSR = A\Delta\tau_{crit}^{B} + C\sigma_{max}^{D} \tag{8}$$

where A, B, C and D are constants obtained experimentally and were found by Namjoshi et al. to be 0.75, 0.5, 0.75, and 0.5 respectively. Using this approach the critical plane is determined by the maximum value of the shear stress range, $\Delta\tau$, and not by the maximum value of the MSSR parameter. Using this parameter Namjoshi et al. stated that predicted values of crack orientation and location were in agreement with experimentally observed crack orientations and locations. Also, they reported that the MSSR parameter could be used to estimate fatigue life data for plain as well as fretting fatigue in conjunction with an analysis. However, from their study it was uncertain what the exact impact of normal stress on the critical plane was upon fretting fatigue crack initiation behavior. They concluded that that more tests "involving various pad geometries and loading conditions are needed to evaluate the effect of normal stress on the critical plane [29]." Therefore, a secondary goal of this study is to see if the MSSR parameter can predict the crack behavior as it occurs in a fretting fatigue specimen of Ti-6Al-4V under variable contact load conditions.

From the discussion of predictive parameters it is apparent that understanding the stresses within the region of contact is vitally important. Therefore, the next section will examine analytical methods to determine these stresses. These same analytical methods will then be used to validate the finite element model of the experimental setup used in this study.

2.5. Analytical Model

This study utilizes a fretting fatigue configuration of a cylindrical body (fretting pad) in contact with a flat body (fatigue specimen). In order to understand the effect of normal loading on the fretting fatigue problem it is helpful to examine the surface stresses

at the point of contact. Therefore, it is necessary to discuss the contact mechanics of a cylindrical body and a flat body in contact. The analytical solution for this problem as it applies to fretting fatigue has been discussed in detail by Hills and Nowell [33] and a summary of pertinent information from their discussion follows.

The analytical solution for two bodies in contact is obtained by solving a set of equations based on the displacement relationship for the two bodies, which are assumed to have infinite boundaries. Figure 2.2 shows a diagram of a cylindrical and a flat body in contact.
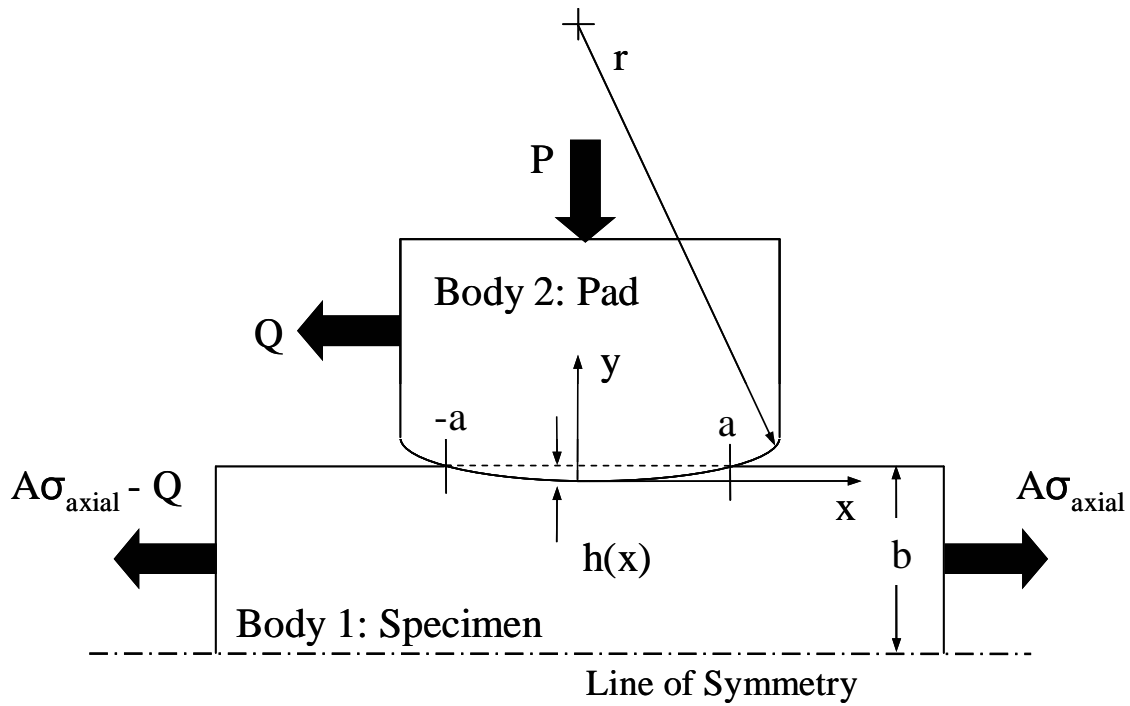
Figure 2.2. Free Body Diagram of Two Bodies Under Fretting Fatigue Loads

In Figure 2.2 σ_{axial} represents the applied cyclic axial stress, P is the applied normal load, Q is the reacted tangential load, a is the contact half length, b is the specimen half thickness, A is the cross sectional area of the half specimen, and h(x) is the

2.19

amount of overlap which would occur if the contacting bodies could freely penetrate each other. The fretting pad has a constant radius, r, and the fretting specimen has an infinite radius along the cross section plane.

Assuming that two corresponding points along each of the contacting surfaces are given a relative displacement in the y-direction given by $v_1(x) - v_2(x)$, then by using the displacement relationship expressed by Hills and Nowell [33] the relationship in the contact region is as follows:

$$\frac{1}{A^*}\frac{\partial h}{\partial x} = \frac{1}{\pi}\int\frac{p(\xi)d\xi}{x-\xi} - \beta q(x) \tag{9}$$

where $h(x) = v_1(x) - v_2(x)$, p is the pressure in the contact zone, and q is the surface shear stress, A^* is the composite compliance defined as

$$A^* = 2\left\{\frac{1-v_1^2}{E_1} + \frac{1-v_2^2}{E_2}\right\} \tag{10}$$

and β is Dundar's parameter defined as

$$\beta = \frac{1}{2A^*}\left\{\frac{(1-2v_1)}{E_1} - \frac{(1-2v_1)}{E_2}\right\} \tag{11}$$

where E is the elastic modulus and υ is Poisson's ratio for the respective bodies. Assuming tangential displacement as $g(x) = u_1(x) - u_2(x)$ a similar equation is obtained as follows

$$\frac{1}{A^*}\frac{\partial g}{\partial x} = \frac{1}{\pi}\int\frac{q(\xi)d\xi}{x-\xi} + \beta p(x) \tag{12}$$

Equation (9) and (12) can be simplified when the two bodies are of the same material as is the case in this study, therefore, $\beta = 0$.

2.20

When two elastically similar bodies are brought into normal contact the resulting displacement of adjoining points on the two bodies are the same when a normal load, P, is applied. The solution to the ensuing pressure distribution, p(x,y), is called the Hertz solution. The Hertz solution states that there will be a peak stress at the middle of the contact surface. For the case of a fretting pad in contact with the fretting fatigue specimen it is possible to solve for the pressure distribution when the assumptions of the Hertz solution are met. The primary assumptions are that the radii of both bodies are large relative to the contact dimensions and that the contacting bodies have infinite boundaries. The assumption that the bodies have infinite boundaries is commonly referred to as the Half Space assumption. The Half Space assumption is considered to be met and the boundaries can be considered infinite if one half of the fretting specimen thickness, b, is equal to or greater than ten times the contact half width, a, or in other words b/a > 10. Fellows et al. [6] found that a finite dimension resulting in b/a = 3 resulted in stress in the x-direction increasing by as much as 20% at the trailing edge of contact due to the applied normal and tangential load. Therefore, violation of the infinite boundary assumption can cause significant deviation from the analytical solution.

In addition to the infinite boundary assumption, it is also assumed that the profile of contact can be idealized by a parabola resulting in a weight function

$$w(x) = \sqrt{(a^2 - x^2)} \tag{13}$$

where, a, is the contact length. Solving equation (12) and then inserting equation (13) the pressure profile yields

$$p(x) = -\frac{\sqrt{a^2 - x^2}}{A * \pi} \int_{-a}^{a} \frac{k\xi d\xi}{\sqrt{a^2 - \xi^2}\,(\xi - x)} \tag{14}$$

2.21

which when the integral is evaluated we find

$$p(x) = -\frac{k}{a}\sqrt{a^2 - x^2} \tag{15}$$

where k is the radius of curvature and is defined as

$$k = \frac{1}{R_1} + \frac{1}{R_2} \tag{16}$$

and R_1 is the radius of the fretting pad, and R_2 is the radius of the fretting specimen. Yet, at this point the contact half width, a, is still unknown. Hills and Nowell state that by employing equilibrium between the contact pressure and applied load per unit width, P, in the contact region it can be found that

$$P = -\int_{-a}^{a} p(\xi)d\xi = \frac{(\pi k a^2)}{2A*} \tag{17}$$

Therefore it can be found that,

$$p(x) = -p_o\sqrt{\left[1 - \left(\frac{x}{a}\right)^2\right]} \tag{18}$$

and the maximum pressure or Hertzian Peak Pressure, p_o, is given by

$$p_o = \frac{2P}{\pi a} \tag{19}$$

The contact half length, a, can now be found as follows

$$a = \sqrt{\frac{2PA*}{\pi k}} \tag{20}$$

For this study the fretting pad radius is R_1=50.8 mm and the fretting specimen having a flat surface has a radius of $R_2 = \infty$. Applying these value to equation (16) and solving equation (20) the contact half-length can be written as

2.22

$$a = \sqrt{\left(\frac{8PR_1}{\pi}\right)\left(\frac{1-v^2}{E}\right)} \qquad (21)$$

The stress in the x-direction along the contact surface resulting from the applied normal

load or equation (18) can be expressed in Cartesian coordinates as

$$(\sigma_{xx})_{normal} = -p_o \frac{\sqrt{a^2 + x^2}}{a} \qquad (22)$$

Building on the equations developed for an applied normal load we now develop the

analytic solution for two cylindrical bodies in contact where both normal load and

tangential load are applied. After applying a normal load per unit width, P, and a

tangential load, Q, there will be regions of stick and slip within the contact region as

shown in Figure 2.3.
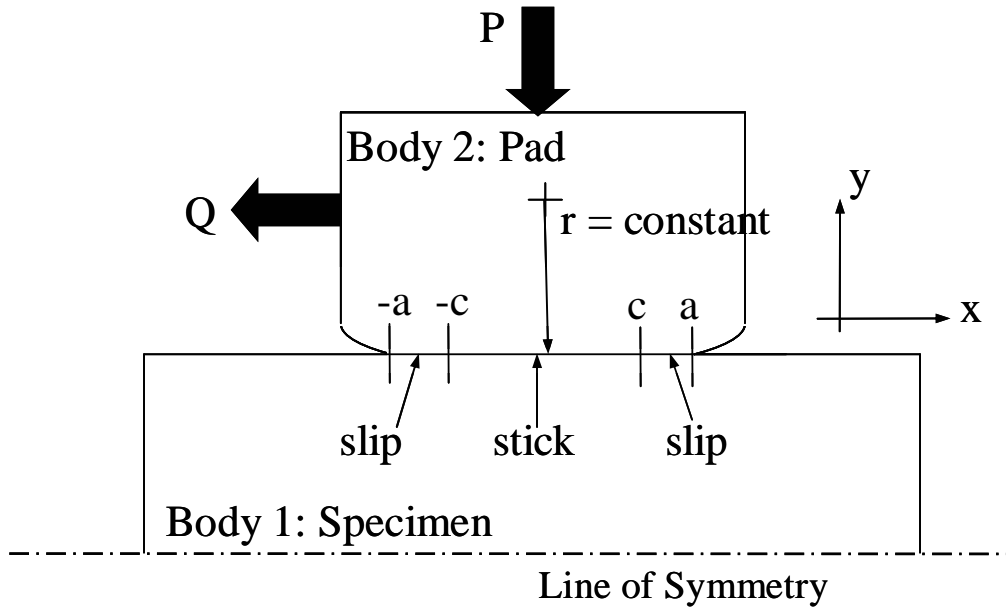
Figure2.3. Partial Slip Condition For Deformed Bodies

2.23

As shown in 2.3 the distance between -c and c defines the stick region and the distance between -a and -c and c and a defines the two slip regions. In the stick region contacting points of the two bodies move together, however, in the slip region contacting points move independently.

The slip region is a result of the interaction between applied loads and frictional forces. For slip (a≥|x|≥c) contacting points are related to the frictional law such that

$$|q(x)| = -fp(x) \tag{23}$$

where f is the coefficient of friction. Here the minus sign indicates compressive surface stress. Moreover, the shear stress opposes relative motion of the surfaces, which gives

$$\text{sgn}(q(x)) = -\text{sgn}\left(\frac{\partial g}{\partial t}\right) \tag{24}$$

where $g = u_1(x) - u_2(x)$ is the relative displacement of the contacting surfaces and t is time. Without the introduction of the time derivative the problem would be purely static and no displacement could occur.

For a point in the region of stick the shear tractions at the point are less than the limiting frictional value (|x|< c) meaning

$$|q(x)| \leq -fp(x) \tag{25}$$

Equations (23) through (25) are based on the Coulomb friction law. Yet, in this situation it is applied at each point under consideration in the contact zone. The area where equation (23) and (25) apply are zones of stick. In this region particles are rigidly adhered to each other and the following relationship applies.

$$u_1(x) - u_2(x) = g(x) = g_o(x) \tag{26}$$

2.24

where $g_o(x)$ is the value of $g(x)$ when the particles enter the stick zone. In the differential form this equation can be written as

$$\frac{\partial u_1(x)}{dx} - \frac{\partial u_2(x)}{dx} = \frac{\partial g(x)}{dx} = g'_o(x) \tag{27}$$

Regions where equations (25) apply are considered under partial slip. The following equation needs to be solved in order to solve for the displacements.

$$\frac{1}{A}\frac{\partial g}{\partial x} = \frac{1}{\pi}\int \frac{q(\xi)}{x-\xi}d\xi \tag{28}$$

Equation (28) can be solved by guessing the extent of the slip regime since the location of the stick or slip region is not known prior to testing. After solving equation (28) by assuming a value of the slip regime one can then verifying if equations (23), (25) and (27) are satisfied. Starting with the assumption of no slip, equation (28) becomes

$$\frac{1}{\pi}\int_{-a}^{a}\frac{q(\xi)}{x-\xi}d\xi = 0 \qquad |x| \le a \tag{29}$$

Similar to equation (12), the form of the shear stress distribution is assumed to be

$$q(x) = \frac{C}{\sqrt{a^2 + x^2}}$$

(30)

where C can be found be considering overall tangential equilibrium

$$\int_{-a}^{a} q(x)dx = Q \tag{31}$$

which gives

$$C = \frac{Q}{\pi} \tag{32}$$

2.25

where Q is the total shear stress along the contact length obtained by integrating the shear

stress distribution. Equation (30) shows that at x=±a the shear stress is infinite.

Therefore, some slip will occur at the edge of contact. It is assumed that some slip will

occur in the region a>|x|≥c, which encloses the central stick zone |x|<c as seen in Figure

2.3 The shear tractions are modeled as a perturbation on the fully-sliding solution so that

$$q(x) = f \cdot p_o \sqrt{1 - \left(\frac{x}{a}\right)^2} + q'(x) \tag{33}$$

where q'(x)=0 is satisfied in the slip zones. Since there is no slip in the stick zones

$g_o(x)=0$ and therefore

$$\frac{1}{\pi} \int_{-a}^{a} \frac{q(\xi)}{x - \xi} d\xi = 0 \qquad |x| \leq c \tag{34}$$

substitution of equation (33) into equation (34) yields

$$\frac{1}{\pi} \int_{-1}^{1} \frac{q'(v)}{v - t} dv = f p_o \left(\frac{c}{a}\right) t \qquad -1 < t < 1 \tag{35}$$

where v=ξ/c and t=x/c. After inverting equation (35), q'(t) takes on the form

$$q'(t) = -f \cdot p_o \frac{c}{a} \sqrt{1 - t^2} \qquad |t| < 1 \tag{36}$$

and by enforcing tangential equilibrium, the stick zone size, c, can be determined

$$Q = \int_{-a}^{a} q(\xi) d\xi = f p_o \left(\frac{c}{a}\right) \int_{-1}^{1} \sqrt{1 - s^2} \, ds - f p_0 \frac{c^2}{a} \int_{-1}^{1} \sqrt{1 - s} \, ds \tag{37}$$

which yields

$$Q = \frac{f \cdot p_o \pi}{2a} \left(a^2 - c^2\right) \tag{38}$$

and using equation (17) the stick zone is found as follows

$$\frac{c}{a} = \sqrt{1 - \left|\frac{Q}{fP}\right|}$$

(39)

Finally the analytical solution, which accounts for the stress in the x-direction, σ_{xx}, along the surface is developed. Nowell and Hills [33] recognized the application of an axial stress causes a shift in the stick zone and in turn a change in the distribution of the shear stress in the contact zone and modifies the solutions by Cattaneo [3] and Mindlin [24]. They beginning with a plane strain assumption and the corresponding strain induced by the axial tensile stress is give by

$$\varepsilon_{xx} = \frac{\sigma(1 - \upsilon^2)}{E}$$

(40)

They continue by assuming that the axial stress applied to body 2 results in displacement gradients that are equal to $-\varepsilon_{xx}$ stated as

$$\frac{-\sigma}{4} = \frac{1}{\pi} \int \frac{q(\xi)}{(x - \xi)} d\xi$$

(41)

The applied axial stress produces a shift in the stick zone, e. This means that the center of contact can lie anywhere from x=e-c to x=e+c. Again, the solution can be assumed to be a perturbation of the full sliding condition, so that

$$q'(x) = f \cdot p_o \sqrt{1 - (x/a)^2} + q'(x)$$

(42)

where q'(x)=0 is satisfied in the slip zones. By substitution into equation (41) and normalizing yields

$$\int_{-1}^{1} \frac{q'(t)}{s - t} dt = \frac{fp_o \pi c}{a} \left[s + \frac{e}{c} - \frac{b}{c} \right]$$

(43)

where s=(x-e)/c, t=(ξ-e)/c and b=σa/(4fp$_o$). Solving equation (43) for e using the following additional consistency equation

2.27

$$\int_{-1}^{1} \frac{\xi + (e/c) - (b/c)}{\sqrt{1-\xi^2}} d\xi = 0 \qquad (44)$$

yields

$$e = b = \frac{\sigma \cdot a}{4f \cdot p_o} \qquad (45)$$

and the solution to q'(x) can be written as

$$q'(x) = -f \cdot p_o \frac{c}{a} \sqrt{1 - \left(\frac{x-e}{c}\right)^2} \qquad (46)$$

and finally the stress distribution in the x-direction as a result of the tangential load is expressed by

$$\left(\sigma_{xx}\right)_{\tan gential} = 2f \cdot p_o - \frac{2}{\pi} \int_{-a}^{a} \frac{q'(x)}{x+a} dx \qquad (47)$$

Therefore, the total stress along the contact surface in the x-direction of the fretting fatigue pad and fretting fatigue specimen can be expressed as the sum of the normal load equation (22), the tangential load equation (47), and the applied axial load and is written as follows

$$\sigma_{xx} = \left(\sigma_{xx}\right)_{normal} + \left(\sigma_{xx}\right)_{\tan gential} + \left(\sigma_{xx}\right)_{axial} \qquad (48)$$

A FORTRAN program has been written by Chan and Lee [4] called "Ruiz" which carries out the numerical analysis for the solution of equation (48). In this study the results of their analysis "Ruiz" program will be compared to the results of the finite element analysis (FEA). Comparison between the analytical solution and the FEA results will be the basis for validation of the finite element model in Chapter IV. In addition to the half space assumption discussed in development of the analytical solution, two other assumptions are worth discussing.

2.6. Fretting Fatigue Analysis Assumptions

This study makes two major assumptions. First, that a steady state condition is quickly achieved and second, that any variation of friction during testing or between tests has a minimal effect on the fretting phenomenon in comparison to the globally applied loads. These assumptions are often used, however, they are discussed here because they are the most significant assumptions made in this study and if they are later found not to be true this work will need to be closely re examined. .

2.6.1. Steady State Assumption

It is typically assumed that a stead-state condition is quickly met in fretting fatigue testing. The assumption is that when the loading conditions are applied and after relatively few cycles the variables including friction, contact width, local stresses and others do not change significantly for the duration of the fatigue test which is the majority of the specimen's life. Nowell and Hill [33] and Iyer [16] and other fretting fatigue researchers made this assumption in their studies.   The danger in making such an assumption is that it would be possible to overlook the root cause of the fretting fatigue phenomenon if in fact the cause of fretting fatigue is a result of a variation of one or more of these variables which are assumed to reach a steady state very quickly.

2.6.2. Coefficient of Friction

Hills et al. [13] have theorized that the coefficient of friction may vary in magnitude under stick-slip conditions. Their estimate for the increase in the coefficient of friction is based on the ratio of shear traction to normal load, Q/P. Using the interpretation proposed by Hills el al. [13] would require a different coefficient of friction be used for each test condition in this study. On the other hand, Iyer and Mall [15] have

2.29

measured the coefficient of friction, μ, to be 0.5 for a configuration similar to that used in this study. Moreover, Lykins determined that a "66% increase in the coefficient of friction causes only a 20% increase in strain amplitude [19]." Therefore the coefficient of friction as determined by Iyer and Mall will be used in this study as input for the finite element analysis test.

2.7. Background Summary

As seen in the previous sections much is still unknown about the fretting fatigue phenomenon. Also it is apparent that the synergistic effect of the variables involved makes the study of the fretting fatigue problem a complex one requiring many different studies with each attempting to shed light on one of the many variables involved. In addition much work has been done on the effects of constant contact loading conditions on fretting fatigue life little, however, very little work has been done on understanding how variable contact load influences fretting fatigue. With these points in mind the primary goal of this study was to expand the understanding of how variable contact loads such as those seen in turbine engines would affect fretting fatigue in a material commonly used in turbine engine components. To accomplish this task a new fretting fatigue test had to be designed and developed. Using this new fretting fatigue experimental setup the variables would need to be controlled and modified systematically to allow the effects of variations in the contact load to be highlighted. The next chapter will discuss how the typical fretting fatigue experimental setup was modified and a new experimental setup developed to aid in the study of the effects variable contact loads.

III. Experiments

This Chapter will present the experiments conducted to study the effects of variable contact load on fretting fatigue behavior of Ti-6Al-4V. First, the details of a new fretting fatigue test configuration used in this study are presented. Then details of the experimental test of this study are described.

3.1. Test Configuration

As stated in Chapter 1, fretting fatigue is a very common problem in aircraft turbine engines. Aircraft turbine engines have complex geometry and loading conditions. Replicating these geometries and loading conditions exactly would make the study of the fretting phenomenon occurring in the blade-disk turbine engine interface joint very complex, time consuming, and expensive. Therefore, the complex geometry and loading conditions of the turbine engine were simplified and a variation of common fretting fatigue experimental setup as discussed in Chapter II is used in this study.

3.1.1. New Variable Contact Load Test Development

The basis for the test setup used in this study was initially developed at Air Force's Turbine Engine Fatigue Facility (TEFF) under contract with the University of Dayton Research Institute (UDRI) during an investigation into the feasibility of using a mulit-axis test stand located at the TEFF to study fretting fatigue [34]. There were two main objectives of the test development. Firstly, to determine if it was possible to use a multi-axis test stand to apply a cyclically varying contact load to a fretting fatigue specimen using a setup similar to the basic experimental configuration discussed in Chapter 2 of this study. Secondly, to see if it was possible to directly and accurately measure the resulting shear load, Q, on each side of the fatigue specimen independently

using flexure springs. In the study by UDRI it was demonstrated that using a multi-axis test stand, servo-hydraulic actuators to apply a contact load, and incorporating software to control the actuators it was possible to apply a cyclically varying contact load to a fatigue specimen in a fretting configuration. In addition, it was demonstrated that the shear load could be measured using a set of calibrated flexure springs [34]. Further details of the development of this new variable normal fretting fatigue test as well as modifications incorporated by this author are available in Appendix A of this study. Also, it is important to note that some data generated from this initial developmental study formed the initial basis for this study. Details of the data used from their study will be discussed later. The next section of this chapter will discuss in detail the newly developed variable contact load test setup as used in this study.

3.1.2. Test Configuration Used in this Study

The experimental setup used to generate data for this study utilizes a servo-hydraulic multi-axis test machine at room temperature in a laboratory environment. A photo of the experimental setup can be seen in Figure 3.1 and a schematic of this setup can be seen in Figure 3.2. The test machine consisted of a rigid steel box frame, a 50 kN lower (vertical) servo-hydraulic actuator, and two 5 kN side (horizontally opposed) actuators. All actuators were controlled using Instron 8800 function generator software. This system allows the user to vary the frequency, waveform, and phase of both the axial load and contact load. The tangential load is a function of the axial load and the stiffness of the flexure springs. Load cells were attached in the vertical servohydraulic load train. Load washers are positioned in line with each side actuator.

3.2
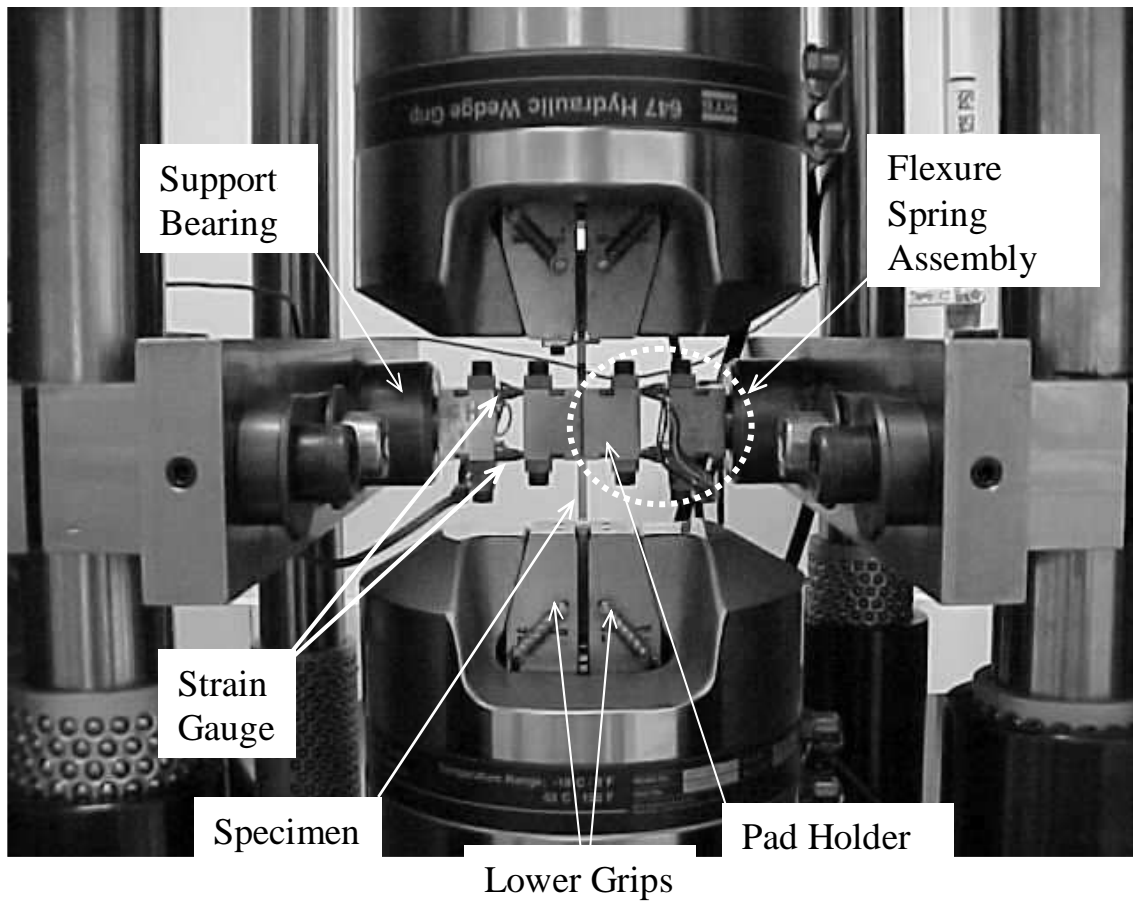
Figure 3.1. Experimental Test Setup

3.3
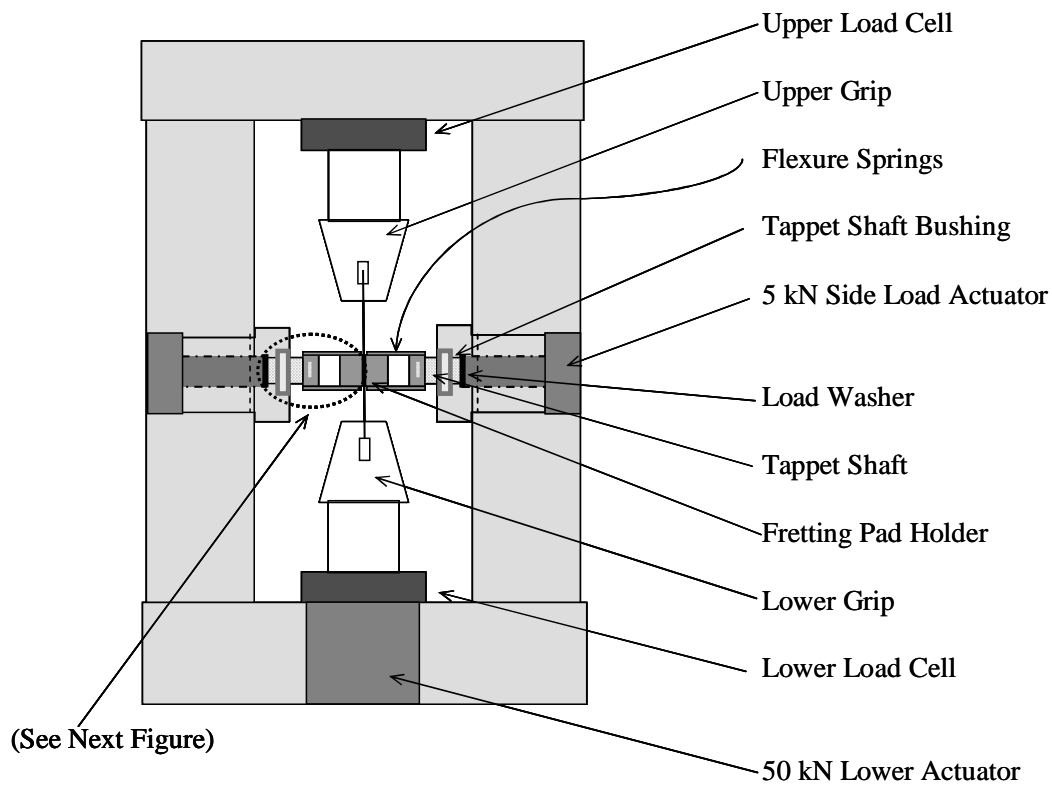
Figure 3.2. Multi-Axis Servohydraulic Test Machine Setup for Variable Contact Loading

Each fretting contact pad is contained within a set of holder blocks. The holder

bocks are suspended from a pair of flexure springs. Figure 3.3 shows a detailed view of

the flexure spring, pad holder, and tappet shaft assembly. The holder blocks are

precision-ground and incorporate design features to ensure the pads are square to one

another and do not have freedom to move within the holder blocks. A block affixed to a

tappet shaft holds each pair of flexure springs. The tappet shaft rides in a self-lubricating

support bearing. The tappet design allows non-critical alignment of the side actuators

within the box frame. In the space between the outboard support bearing and the housing

for each actuator, the actuator shaft pushes on the tappet through a collar that also retains

the load washer in line with the tappet shaft. Finally, a pair of hydraulic wedge grips

holds the test specimen; one is attached to the vertical actuators' carrier plate, and the

other, to the top of the box frame through an extension shaft and load cell.
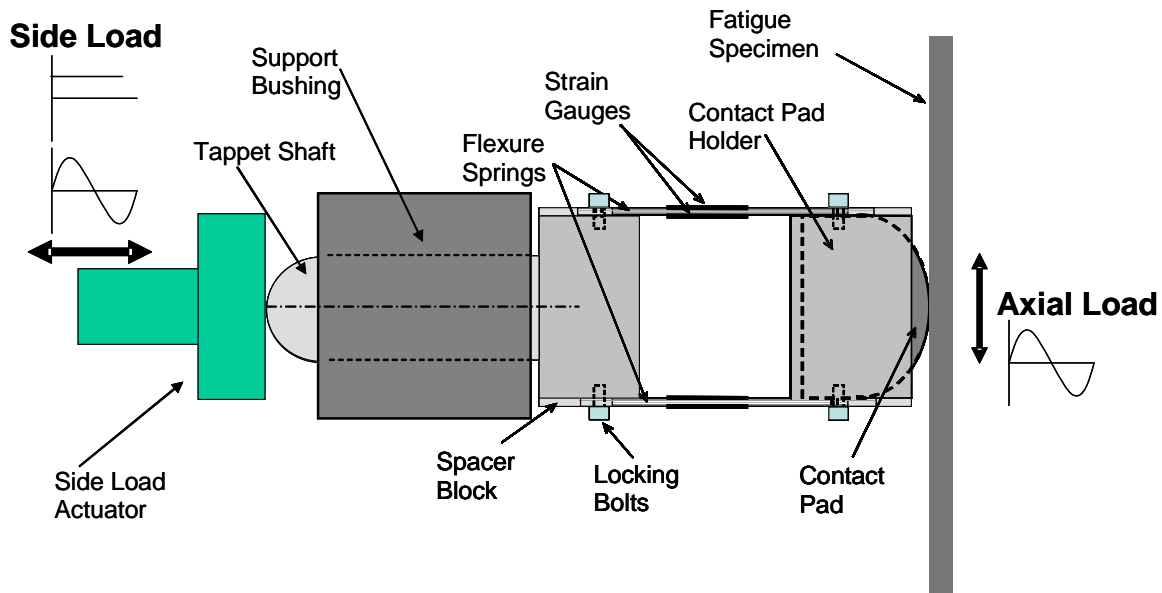
Figure 3.3. Flexure Spring Assembly Detail

3.1.3. Specimen and Pad Geometry

The contacting bodies of each test consisted of a fretting fatigue specimen and

two fretting pads. Dimensions of the gauge section for all dog-boned fatigue specimen

used are as follows: thickness (2b) = 3.81 mm, width (w) = 6.35 mm, cross sectional area

(A) = 24.1935 mm^2. The cylindrical pads used had an end radius of 50.8 mm. The total

overall length of all but one test specimen used was 7 inches with the one other test

specimen having an overall length of 5 inches. Figure 3.4 shows a photo of both the pads

and fatigue specimen labeled with dimensions.
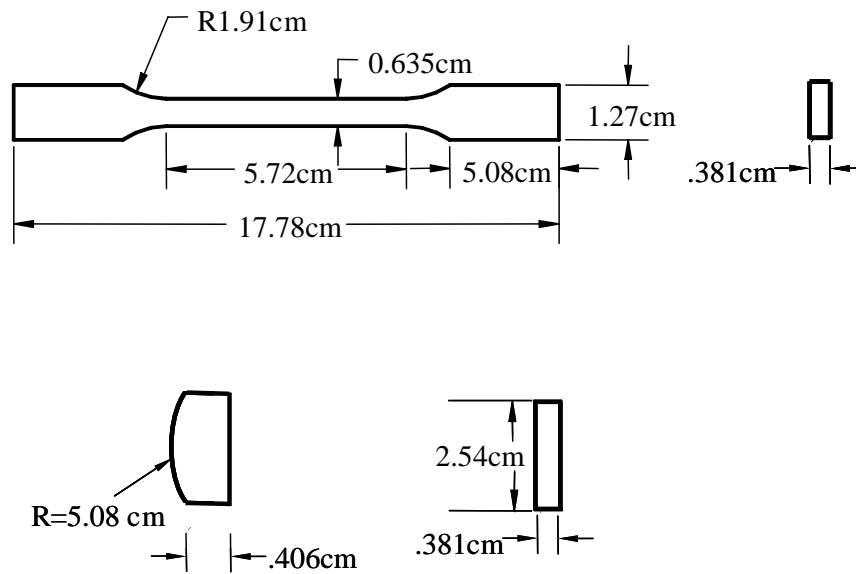
Figure 3.4. Drawing of Specimen and Fretting Pad with Dimensions

3.1.4. Material Property

Both the specimen and the pads used in this study were machined from titanium

alloy, Ti-6Al-4V. Ti-6Al-4V was chosen for this study because of its common use in

turbine engine blades and disks. The modulus of elasticity, E, and Poison's Ratio, υ, of

Ti-6Al-4V used in this and other recent fretting fatigue studies conducted at AFIT were

determined by a contemporary AFIT researcher to be 116 GPa and 0.35 respectfully.

3.1.5. Load Determination and Control

The loading conditions were of greatest importance for this study. This section

will detail how the loads were applied, controlled, and monitored during testing.

3.1.5.1. Axial Load.

The axial load was controlled using feedback from the load cell at the upper end

of the test specimen using Instron 8800 function generator software. The axial load in the

specimen could be measured in one of two ways. One method was to subtract the sum of

the reacted tangential load at the specimen/contact pad interface, $Q_{right}+Q_{left}$, from the

load sensed in the upper load cell and this was equal to the applied axial load, σ_{axial} in the

gauge section of the specimen. This method was used during the test development study

performed by under contract by UDRI [34]. The other method utilized a second load cell

placed at the lower end of the test specimen load train. Using this method the applied

axial load in the specimen gauge section could be determined directly from the lower

load cell. The second method was utilized for data collected in this study.

3.1.5.2. Axial Displacement.

The axial displacement was sensed from a stroke transducer within the vertical

actuator and is conditioned by an Instron 8800 control unit. Axial displacement was

monitored for reference purpose only.

3.1.5.3. Normal Load.

The normal load applied by the contact pads on the specimen was sensed via load

washers positioned in line with each side actuator shaft and which were conditioned by a

charge amplifier. The side load could be controlled by the user via displacement control

of the side load actuators, which was the method used during test development by UDRI

[34], or using feedback control from the side load washers and controlling software,

which was the method used in this study.

3.1.5.4. Shear Load.

The shear load was controlled by the amount of axial deflection or stretching of

the specimen and the stiffness of the flexure springs. Shear load on either side of the

fatigue specimen was sensed by a full-bridge load sensor composed of strain gages

applied to the pad holder flexure springs, and was conditioned using an external bridge

amplifier [34]. The amplifier output could be visually monitored using an oscilloscope. The reacted shear load could also be determined using the load cells at both ends of the specimen load train. The sum of the reacted shear load could be determined by subtracting the load measured by the upper axial load cell from the load measured by the lower axial load cell. The shear load measured by the flexure spring could then be compared to the shear load measured by the load cells in line with the axial load. The difference between the reacted shear load measured by aforementioned methods was attributed to hysteresis in the interface between the tappet shaft of the flexure spring assembly and the bushing, which restricted the tappet shaft's vertical movement (See Appendix A). Variations in the shear load were the main method used to determine crack initiation and propagation. The onset of rapidly varying shear loads was the primary indication of crack initiation and propagation. This variation in shearing loads was visually observed using a two-channel digital oscilloscope. All loading data was monitored and recorded using external data acquisition.

3.2. Experimental Tests

The goal of this study was to determine the effect of variable contact load on fretting fatigue behavior. Therefore, to highlight the effects of contact load it was desirable to keep the axial and shear loads constant between tests while only varying the contact load. The approach taken in this study was to run a test at a constant lower contact load then a test at a higher constant lower contact load and finally a test with a cyclically varying contact load having the same higher (maximum) and lower (minimum) contact loads as the constant contact load cases with all other variables kept the same.

In this study a distinction was made between tests in which the reacted shear load did and did not reverse direction. This study will refer to those test in which shear did not reverse direction during testing as "uni-directional shear tests" or simply "uni-directional" and tests in which the reacted shear load did reverse direction during testing as "bi-directional shear tests" or simply "bi-directional tests". Performing uni-directional and bi-directional shear tests was in part due to the evolution of the capability of the test setup as this study progressed as described in Appendix A. Figures 3.5 and 3.6 display representative load waveforms applied during uni-directional and bi-directional tests respectively. All fretting fatigue tests were conducted under tension-tension axial loading conditions. In order to highlight the effects of contact load, the axial load ratio i.e. ratio of minimum to maximum axial load was controlled as a secondary variable for each test, with a target value of approximately 0.5 for test with uni-directional shear and 0.1 for test with bi-directional shear.
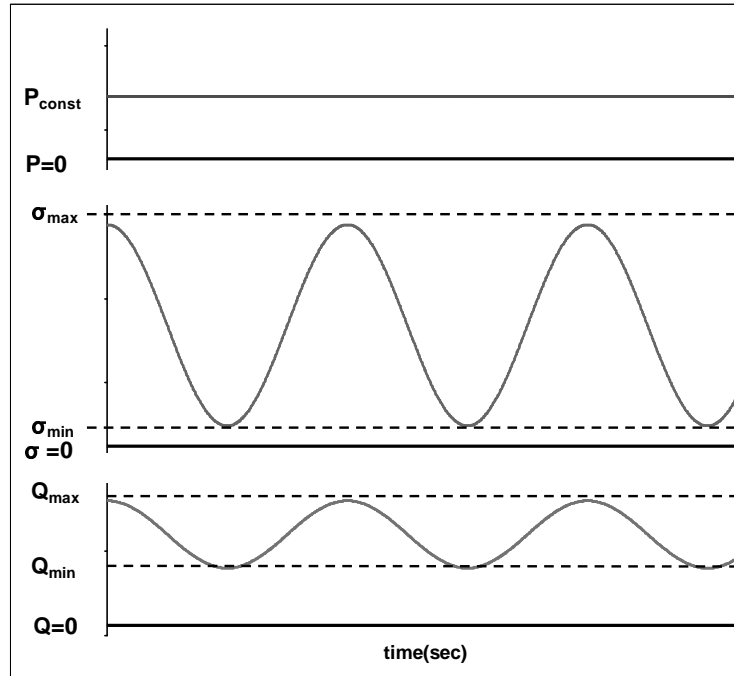
Figure 3.5. Applied Load Relationship for Uni-Directional Tests with Constant Contact Load
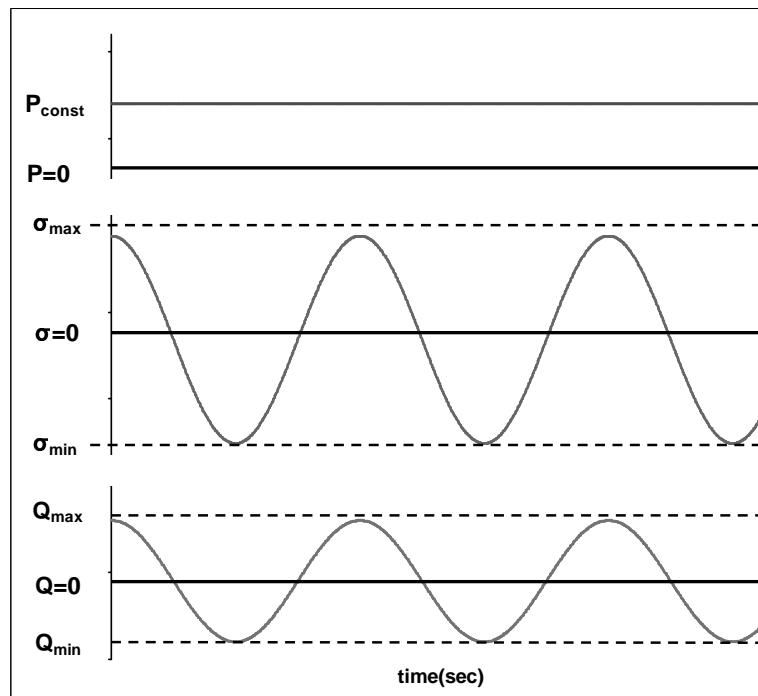
Figure 3.6. Applied Load Relationship for Bi-Directional Tests with Constant Contact Load

3.10

For test with uni-directional shear the amount of axial load applied initially was slightly less than the minimum axial load to be applied during testing. Next, a side load was applied and axial load increased to the desired minimum axial load for testing. Axial load was increased slowly in small increments to ensure shear loads were equal on both sides on contact.

For test with bi-directional shear a predetermined axial load, or axial load setpoint, was first applied to the specimen to give the specimen some initial stretch. The amount of axial load applied initially was typically the same as the mean axial load expected at the point where the reacted tangential load would be near zero. This point was determined by applying a small side load and axial loads in 100 lb load step increments slowly up to the desired maximum axial load and then down to a desired minimum axial load. This technique allowed for an accurate determination of the setpoint. This technique ensured nearly equal amounts of shear would develop on each side of the fatigue specimen during testing. Also, in the case of bi-directional shear test, this technique provided nearly equal positive and negative shear during testing. After the setpoint was determined the contact pads were applied at the desired maximum normal load.

Using the controlling software the axial and constant load waveforms were then applied. Initial amplitude of the axial load was small and the span was increased gradually to prevent gross slip. Reaction shear loads resulted when the applied axial load was increased or decreased and caused the specimen to "stretch" or "contract" relative to the amount it had stretched from axial load point at which the contact load was applied. The magnitude of all contact loads was sufficient to keep the contact pads "stuck" to the

specimen so that the pad and pad holders followed the specimen based on the coefficient of friction for the pad and specimen. During each test the axial load amplitude and setpoint were adjusted to the desired values and in the case of bi-directional shear testing the axial load amplitude and setpoint were adjusted to obtain equal amounts of reacted tangential load in both directions of shear. All loads were adjusted within the first 5000 cycles or less after which they were kept constant.

3.3. Test Details

As mentioned earlier, two basic types of test were performed in this study and for the sake of discussion they have been categorized as uni-directional shear tests and bi-directional shear test. Again, uni-directional shear tests were those tests in which the direction of the reacted shearing load did not change direction whereas in bi-directional shear tests the direction of the shearing load changed direction by 180° during each cycle. For each shearing case constant and variable contact loading tests were performed. The following sub-sections will explain in detail the program of experiments for these two types of tests.

3.3.1. Tests with Uni-Directional Shear

For the uni-directional shear case two peak axial stress conditions, 550 MPa and 600 MPa, were selected with axial load ratios of 0.47 and 0.5 respectively. For the 550 MPa axial stress level constant contact loads of 315 kN/m and 630 kN/m and a variable contact load condition of 315 to 630 kN/m were chosen. Figure 3.7 displays the uni-directional shear test waveform for a variable contact load. Since higher axial stress equates to greater specimen stretch and higher reaction shear load, the side load was increased in proportion to provide sufficient contact friction to transmit the shear load.

Therefore, for the 600 MPa axial stress level constant contact load conditions of 350, 525 and 700 kN/m and variable contact loads of 700 to 350 kN/m and 700 to 525 kN/m were chosen. It was determined for this experimental setup a ratio of shear load to side load of just less than 1/3 as the maximum value for transmitting shear load without contact slippage [34]. The frequency of both the axial load and the contact load was 20 Hz for the uni-directional cases with variable contact load. The waveforms of the axial load and contact load were also kept in phase with respect to each other. This resulted in the maximum contact load being applied at the same time as the maximum axial load with the maximum shear load occurring at this point as well. Two desired peak shear load conditions for the uni-directional were 578 N for the 550 MPa maximum axial stress cases and 667 N for the 600 MPa maximum axial stress level cases.
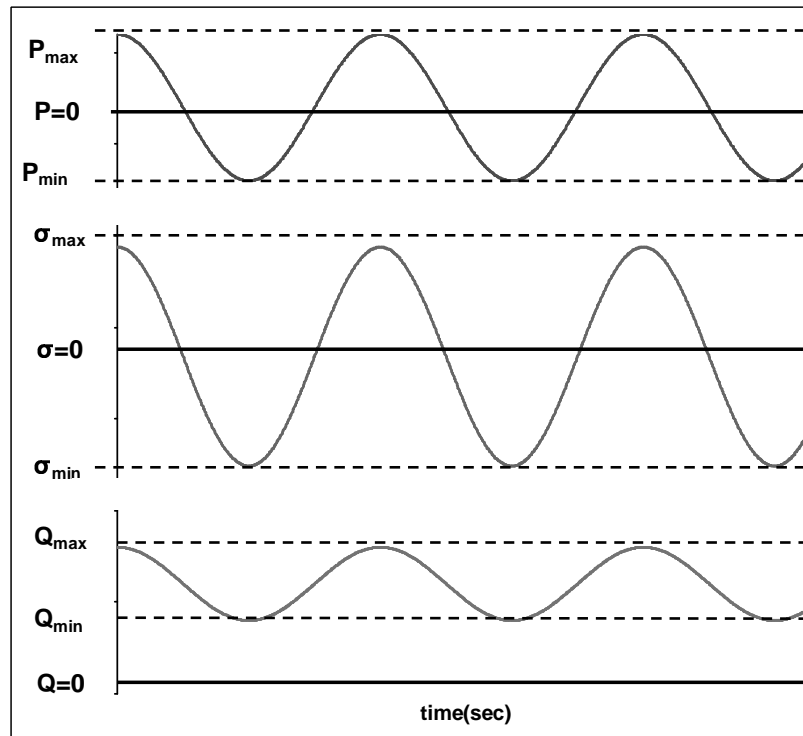
Figure 3.7. Applied Load Relationship for Uni-Directional Shear Test with Variable Contact Load

3.13

3.3.2. Tests with Bi-Directional Shear

For bi-directional shear test only a peak axial load of 600 MPa and an axial load ratio of 0.1 was used along with constant contact load of 350, 525 and 700 kN/m and variable contact loads of 700 to 350 kN/m and 700 to 525 kN/m. The target maximum magnitude of shear loading condition for the bi-directional tests was 333 N in both directions. For the bi-directional cases with variable contact load the frequency of the contact load was twice the frequency of the axial load i.e. 40 Hz. Two different contact load phases were used, $+90^o$ and -90° relative to the axial load. For the -90° phase case the maximum contact load was applied when the maximum axial load was applied as seen in Figures 3.8 and 3.9. For the -90° phase case the minimum contact load was applied when the maximum axial load was applied as seen in Figure 3.9. The phase of the contact waveform was adjusted immediate after each test was started to ensure the maximum contact load was applied at the same times the minimum and maximum axial loads were applied.
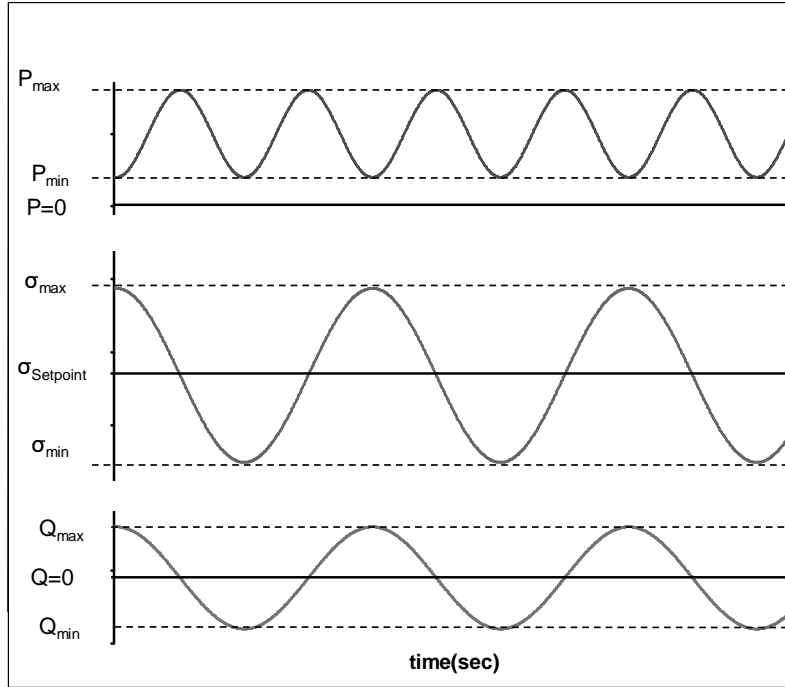
Figure 3.8.   Applied Load Relationship for Bi-Directional Shear Test: 40 Hz Variable Contact Load at 90° phase relative to σ_{axial}
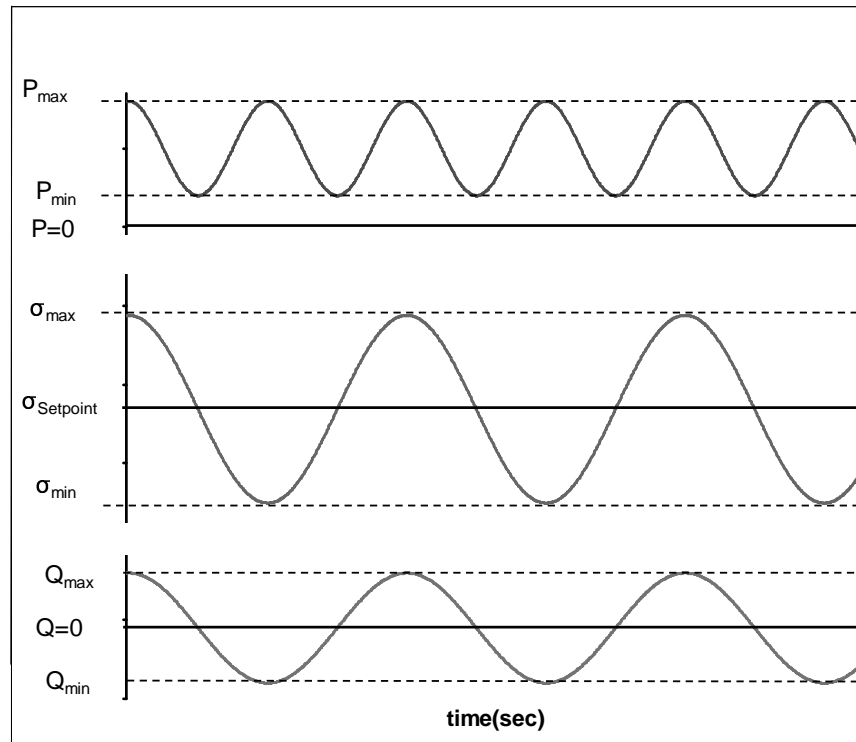
Figure 3.9. Applied Load Relationship Bi-Directional Shear Test with 40 Hz Variable Contact Load at -90° phase relative to σ_{axial}

3.15

The aforementioned loading conditions for both the uni-directional and bi-directional tests were targets and the actual applied loading conditions varied slightly from these desired target loads shown in Table 3.1. In addition to experimental tests, numerical analysis was performed using Finite Element Analysis. The next chapter will discuss why finite element analysis was performed as well as describe the finite element model used in this study.

Table 3.1. Program of Experimental Tests

P_{Max} (kN/m)	P_{Min} (kN/m)	P_{Freq} (Hz)	$\sigma_{N,max}$ (MPa)	R_σ	Q_{max} (N)	R_Q	φ_P (deg)
315	-	20	550	0.47	578	0.08	0
350	-	20	600	0.50	667	0.10	0
525	-	20	550	0.47	578	0.08	0
630	-	20	600	0.50	667	0.10	0
700	-	20	600	0.50	667	0.10	0

P=Variable; Uni-Directional Shear

P_{Max} (kN/m)	P_{Min} (kN/m)	P_{Freq} (Hz)	$\sigma_{N,max}$ (MPa)	R_σ	Q_{max} (N)	R_Q	φ_P (deg)
630	315	20	550	0.47	578	0.08	0
700	350	20	600	0.50	667	0.10	0
700	525	20	600	0.50	667	0.10	0

P=Constant; Bi-Directional Shear

P_{Max} (kN/m)	P_{Min} (kN/m)	P_{Freq} (Hz)	$\sigma_{N,max}$ (MPa)	R_σ	Q_{max} (N)	R_Q	φ_P (deg)
350	-	20	600	0.10	333	-1.00	0
525	-	20	600	0.10	333	-1.00	0
700	-	20	600	0.10	333	-1.00	0

P=Variable; Bi-Directional Shear

P_{Max} (kN/m)	P_{Min} (kN/m)	P_{Freq} (Hz)	$\sigma_{N,max}$ (MPa)	R_σ	Q_{max} (N)	R_Q	φ_P (deg)
700	350	40	600	0.10	333	-1.00	-90
700	350	40	600	0.10	333	-1.00	90
700	350	40	600	0.10	333	-1.00	90

IV. Finite Element Analysis

As stated in Chapter 2, analytical equations and programs such as "Ruiz", which solve the analytical equations, are useful in determining contact width and stresses in the region of contact for the condition of fretting fatigue. Moreover, these analytical techniques require that a half space assumption, i.e. $b/a > 10$, be meet. Yet, the dimensions and applied loads used in this study violate the half space assumption. For instance, the half thickness of the fatigue specimen used in the study is 1.905 mm, i.e. $b=1.905$ mm. For the maximum contact loading condition the contact load is 700.5 kN/m and the resulting contact half width, a, calculated from equation (21) of Chapter 2 is 0.8272 mm. The b/a ratio is found to be 2.3, which violates the half space assumption. Therefore, the analytical solution for the maximum applied contact load will have an error associated with it. Moreover, for the minimum applied contact loads used in this study, i.e. $P=315$ kN/m, the contact half width determined from the analytical equations is 0.5548 mm. The b/a ratio for this case is 3.4, which is again smaller than 10 and in violation of the half space assumption. Therefore, the half space assumption is violated for both the maximum and minimum contact load conditions of this study. Moreover, all other contact loads used in this study fall between these two extremes, therefore, all loading conditions in this study violate the half space assumption requirement that b/a >10. Consequently, another technique is needed to analyze the contact width of and stresses within the contact region that does not rely on the half space assumption being met.

Fortunately, numerical techniques have been developed which do not require the half space assumption to be met. Numerical techniques such as Finite Element Analysis

(FEA) have been shown to be capable of modeling and applicable to the study of the fretting fatigue phenomena. The reminder of this chapter will discuss in detail some of the advantages to using FEA for studying fretting fatigue, the finite element model used in this study, validation of the FEM used in this study, and finally explain how experimental test were numerically modeled.

4.1. Advantages of FEA

In addition to the need for finite element analysis due to half space assumption violations, the use of a finite element model provides several advantages over experimental and analytical techniques. One advantages of Finite Element Analysis is that it provides information otherwise not obtainable through experimental testing or analytical modeling. FEA offers the ability to determine local parameters, p_o, a, δ_{max}, $\tau_{L,max}$, $\Delta\tau_{L,max}$, $\sigma_{L,max}$, $\Delta\sigma_{L,max}$ in the contact region from the applied global boundary conditions, R, P_{max}, P_{min}, Q, $\sigma_{N,max}$ and $\sigma_{N,min}$. Moreover, determination of these local parameters allows for predictive parameters to be developed based on local rather than applied global stresses. Also, use of a finite element model reveals information about the experimental setup, which would otherwise be left unknown. For example, Iyer [16] has noted that a tensile stress concentration arises in the fatigue specimen due purely to the application of the contact load. Also, Magaziner [23] points out that FEA reveals that the contact semi-width is not symmetric about the center of contact. Such advantages make the use of FEA very desirable to the study of the fretting fatigue phenomenon. The following section will describe the finite element model used in this study.

4.2. Finite Element Model Description

The finite element model used in this study is similar to that used by numerous fretting fatigue researchers [19, 28, 29]. The bodies that combine to form the finite element model of the experimental setup will first be described. Then the details of the mesh of the finite element model will be presented.

4.2.1. Finite Element Model Bodies

The three bodies in this model as seen in Figures 4.1 and 4.2 are the fretting pad, the fatigue specimen and fretting pad holder. The coordinate axis is such that the surface of the fatigue specimen lies along the x-axis, and the fretting pad is initially centered vertically on the y-axis.
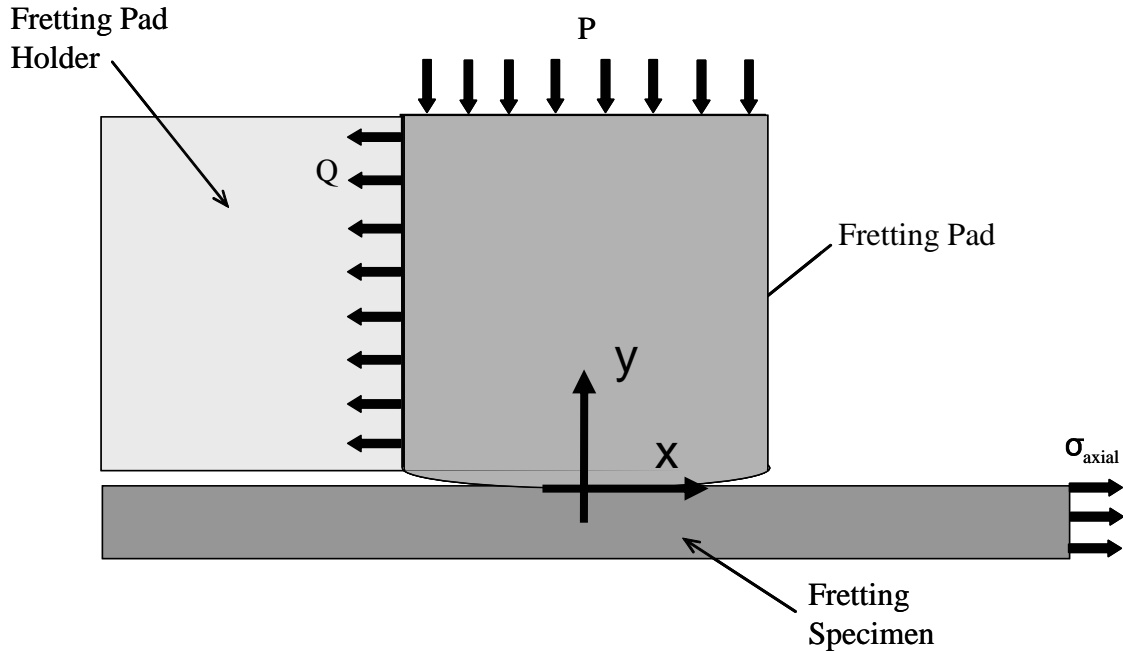
Figure 4.1 . Finite Element Model with Loading and Boundary Conditions
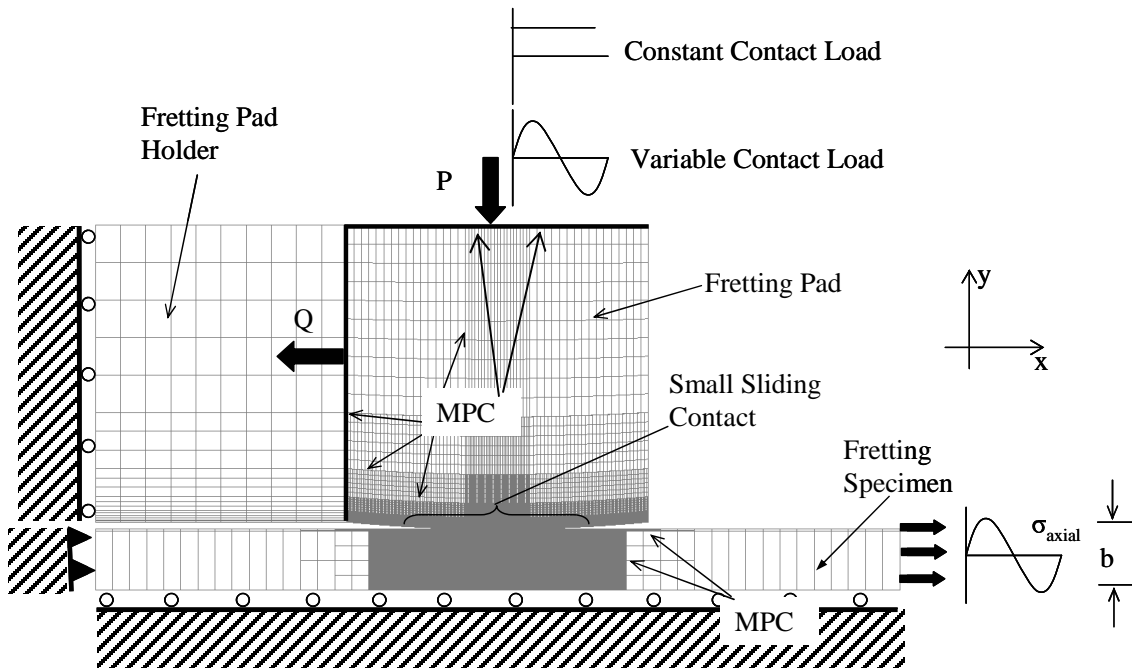
Figure 4.2. Finite Element Model with Loading and Boundary Conditions

As seen in Figure 4.2 the specimen is fixed at its far end in the negative x-direction, restricted from vertical movement along its bottom surface and free to roll in the x-direction and along its bottom edge. Only half the experimental setup needs to be modeled using finite elements because ideally the experimental setup is symmetric along the axial centerline of the specimen. Therefore, the finite element model of the specimen had a thickness b=1.905 mm the same as with the half thickness of experimental test specimen. The range of the specimen is 12.7 mm in both the positive and negative x-direction from the center of contact. The cylindrical pad is rigidly fixed to the pad holder with the pad holder being free to roll in the y-direction along the side opposite to the fretting pad. The cylindrical end radius of the pad is 50.8 mm. Both the fretting pad, fatigue specimen and pad holder have a depth of 6.35 mm. Also, the fretting pad and fatigue specimen have the same material properties as each other as well as the same

4.4

material properties of their experimental counterpart, i.e. an Elastic Modulus of 1.16 MPa and a Poisson's ratio of 0.35. The material properties of the pad holder differ from the other two bodies. The primary purpose of the pad holder in the finite element model is to restrain the pad in the x and y-direction prior to the application of load. Therefore, the material properties of the lateral spring are purposely low so that the pad holder has a minimal effect on the interaction between the pad and specimen. The pad holder has an Elastic Modulus and a Poison's Ratio of 5.0 and 0.3 respectively. The coefficient of friction, μ, was chosen to be 0.5 in all cases. The coefficient of friction needed to be greater than the ratio of Q/P to ensure the numerical solution converged. Next, the mesh of these bodies will be described.

4.2.2. Finite Element Model Mesh

4-node, plane strain elements make up all three bodies of the Finite Element Model. 4-noded elements (bilinear) were chosen instead of 8-noded elements (serendipity), because the mid side node in the 8-noded element introduces an oscillation in the stress state along the contact surfaces as mentioned by Lykins [19]. Contemporary AFIT researcher Major Ki Su Shin has refined a mesh for the study of plasticity and the fretting fatigue phenomenon. His mesh has been refined for the purpose of analyzing local stresses and strains along and near the surface of the fretting fatigue specimen. Therefore, his mesh was adopted for use in this study. As seen in Figure 4.2 the darker regions of the mesh, such as the area near the point of contact, indicate where the mesh is more refined to aid in determining stresses within the contact region. The mesh was less refined in the regions where the values of stresses were not of interest in this study. This decreased the time required to analyze the model. The range of the area of the most

4.5

refined mesh in the specimen is 4.064 mm on either side of the center of contact. On the

contact surface of the specimen, the length and height of the contacting elements is

6.35µm. The contact between the pad and the specimen was defined using the master-

slave algorithm in ABAQUS for contact between two surfaces. Here the master surface

is the fretting pad and the slave surface is the fretting fatigue specimen. The ABAQUS

master-slave algorithm determines which segments on the master surface and which

nodes on the slave surface interact. These master segment/slave node relationships are

then used to establish the contact algorithm for how loads are transferred between the two

contacting surfaces. A multi-point constraint (MPC) was applied at the top of the pad to

prevent it from rotating due to the application of loads. The top nodes of the pad were

forced to move in unison in the y-direction. Also, a multi-point constraint (MPC) was

applied to the boundary between regions where the mesh size of the elements differed.

This prevented the free nodes from penetrating the larger adjoining elements. The next

section will explain the validation of the finite element model described above.

4.3. Finite Element Model Validation

In order to validate the finite element model the results from the finite element

model were compared with analytical results as calculated using the FORTRAN program

"Ruiz". Numerous researchers have used the "Ruiz" program for comparison with their

finite element results [15, 19, 20, 23]. The "Ruiz" program as written by Chan and Lee

solves the analytical equations presented in Chapter 2. The "Ruiz" program, which

solves the analytical solutions, requires the half space assumption be met as discussed in

Chapter 2. Therefore, any experimental test which has resulting contact width, which

violates the half space assumption the analytical solution as calculated by the Ruiz

program will have error. Not unlike the Ruiz program, the finite element method makes use of a basic, yet different, assumption. Stress values determined by the finite element method are calculated using shape functions. Therefore exact values are only determined at specific points or nodes and stress values between these points must be interpolated which, introduces a certain amount of error. Ensuring the size of the mesh used is refined sufficiently in the areas where stress values are of interest can minimize the error induced by this assumption.

4.3.1. Comparison with Ruiz Program

It is most logical to use the loading condition from the study which provides the largest ratio of b/a possible so that error induced by the failure to meet the half space assumption will be as small as possible considering all experimental test cases violate the half space assumption requirements. This loading condition is the case of the minimum applied contact load i.e. P=315.2 kN/m which has a b/a ratio of 3.4 as described at the beginning of this chapter. A shear load of 578.27 N and an axial load of 600.0 MPa were the other loads chosen for the validation study because they are typical of the magnitude of applied loads which accompanied the aforementioned contact load in the uni-directional experimental configuration.

4.3.1.1. Contact width.

The contact width was determined analytically and numerically to be 0.5549 mm. The contact width as determined using the analytical equations independent of the FORTRAN program Ruiz was calculated to be 0.5549 mm as well, matching the numerically and analytically determined values.

4.3.1.2. Stress Curves.

From Figure 4.3, 4.4, and 4.5 it can be seen that the stress curves for the normal stress in the x and y-directions as well as the shear stresses are similar for both the analytical and numerical solutions. As noted by Iyer and Mall [17] because of the geometric constraints the two solutions will never be identical, however, they do come close enough to endorse the finite element model. In this case the maximum value of stress in the x-direction along the specimen contact surface, S_{xx}, was determined numerically to be located at $x = 0.5271$ mm and have a magnitude of 889.35 MPa. Using the Ruiz program the maximum value of S_{xx} was determined to be at $x = 0.5327$ mm with a magnitude of 831.91 MPa resulting in a relative difference from the numerical solution of 6.45%.
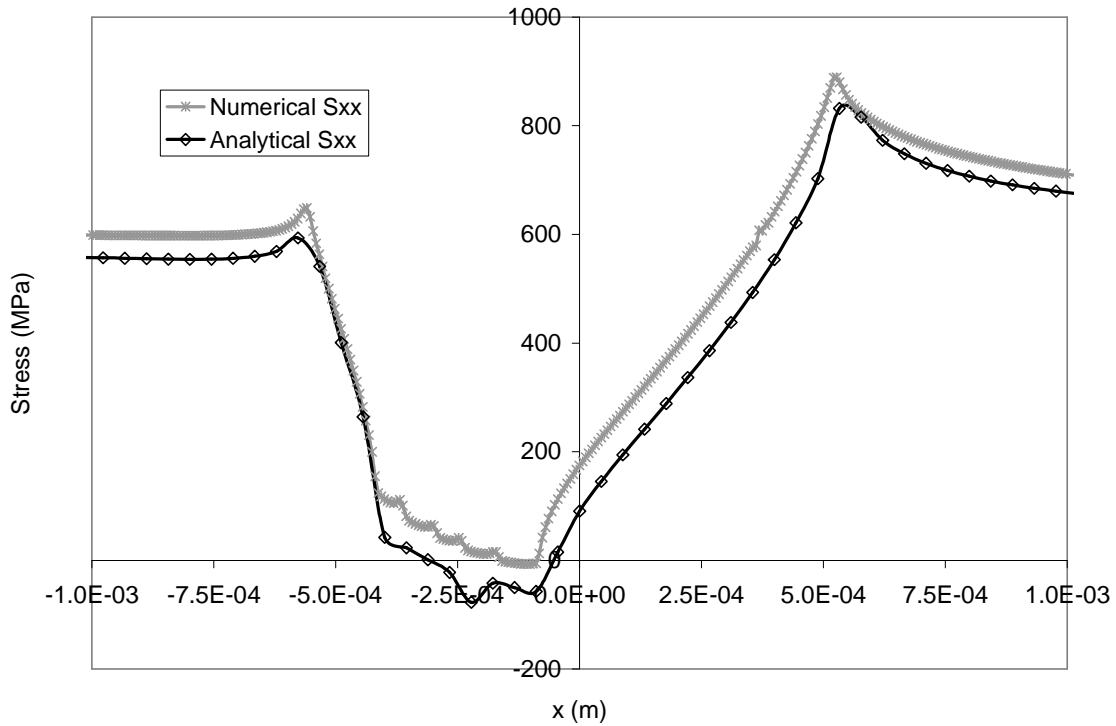
Figure 4.3. Analytical and Numerically Calculated S_{xx} Stress Distribution Curves Along Specimen Surface within Contact Region for FEA Validation

4.8
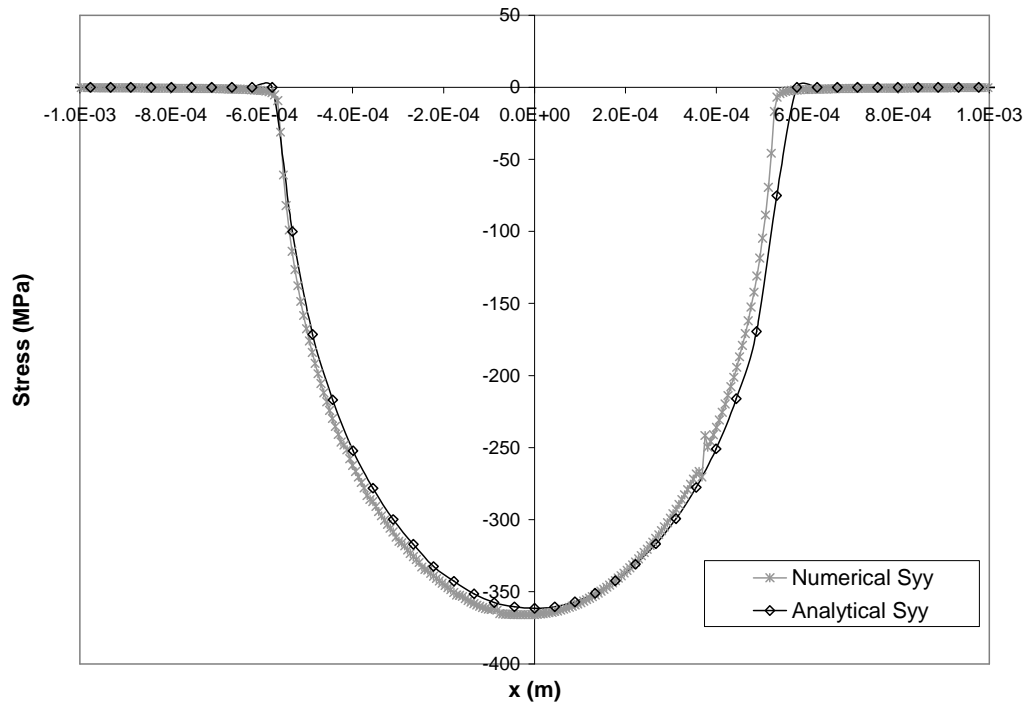
Figure 4.4. Analytical and Numerically Calculated Syy Stress Distribution Curves Along Specimen Surface within Contact Region for FEA Validation
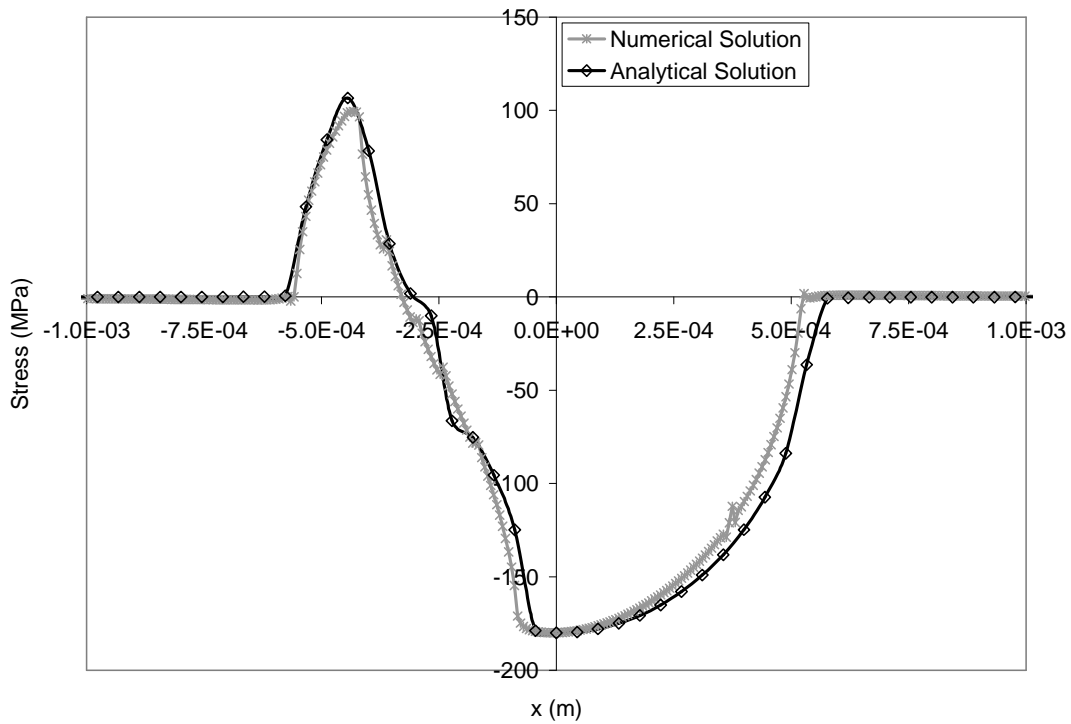
Figure 4.5. Analytical and Numerically Calculated Sxy Stress Distribution Curves Along Specimen Surface within Contact Region for FEA Validation

4.9

4.3.1.3. Peak Contact Pressure.

The magnitude of the peak contact pressure as determined analytically and numerically was 361.7 MPa and 365.93 MPa respectively yielding a relative difference of 1.15% with respect to the numerical solution. The peak pressure as determined by the analytical solution from equation (19) was 361.67 MPa and is in close agreement with the values determined using the FORTRAN program and FEA. The location of the peak contact pressure as determined analytically was at $x = 0.0$ mm. On the other hand, numerically the location of the peak contact pressure is found to be at $x = -0.01905$ mm. This difference in location of the maximum peak pressure is expected since in the case of the numerical solution the location of the peak pressure is shifted due to the application of the applied bulk tension as noted by Iyer [16].

4.3.1.4. Applied Nominal Stresses.

A final condition, which can be used to aid in validating the finite element model, is to examine the magnitude of σ_{xx} at increasing distances from the contact region. The magnitude of σ_{xx} should begin to approach the magnitude of the stress applied to the finite element model as the distance from the contact zone increases. As seen in Figure 4.3 the magnitude of σ_{xx} begins to decrease outside of the contact region and begins leveling off and reaches a value of 600 MPa which is the magnitude of σ_N applied to the finite element model; again confirming the validity of the finite element model. This in addition to the aforementioned comparisons of the finite element analysis results with those of the Ruiz program validates the finite element model for this study. The next section will discuss how the experimental tests were numerically modeled using this finite element model.

4.4. Numerical Test of Experimentally Applied Loads

The finite element model with the boundary conditions, dimensions, and mesh described above was analyzed using the commercially available finite element program ABAQUS on a Unix computer. Loading condition were input as step loads and applied to the finite element model. Finite element analysis would evaluate the stress, strain, and displacement of each node from its original position after each loading step. Each change in load conditions required a new load step to be input and the finite element analysis to be performed again taking the new applied loads into consideration while retaining the results from all previous loading steps. Loading conditions were numerically tested for both the uni-directional and bi-directional shearing scenarios. For both shearing cases constant and variable contact load conditions were applied numerically. The next section will describe how the three globally applied loads, P, Q, and σ_{axial} , were considered as loading steps and how the different experimental loading cases were numerically tested.

4.4.1. Constant Contact Load Test with Uni and Bi-Directional Shear

Loads were applied via three steps for both the uni-directional and bi-directional shear tests in which the contact load was constant. Figures 4.6 and 4.7 are representative of FEA loading steps for uni-directional and bi-directional tests with constant contact load respectively. For constant contact load tests Step 1 applied only the contact load, P_{const}, to the top of the pad as a distributed load. Next, Step 2 applied the maximum bulk axial stress, $\sigma_{axial,\,max}$, as well as the maximum reacted shearing force, $Q_{max,}$ while the contact load, P_{const}, was maintained from the first step. Finally, Step 3 applied the minimum bulk axial stress, $\sigma_{axial,\,min}$, and the minimum reacted shearing force, Q_{min} while maintaining the contact load applied in Step 1. Repeating Step 2 constituted one

complete loading cycle for this case. This was the method used to model all cases with constant contact load regardless of the direction which shear occurred.
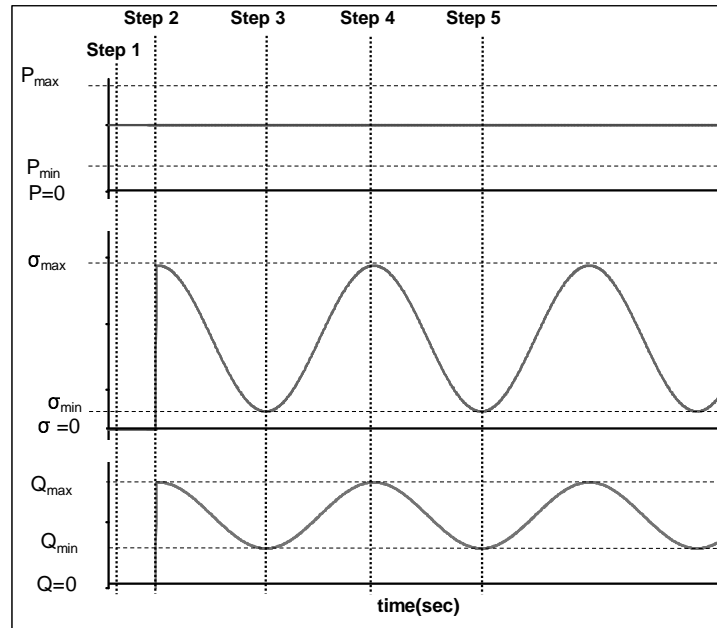
Figure 4.6. FEA Load Steps for Uni-Directional Shear Tests with Constant Contact Load
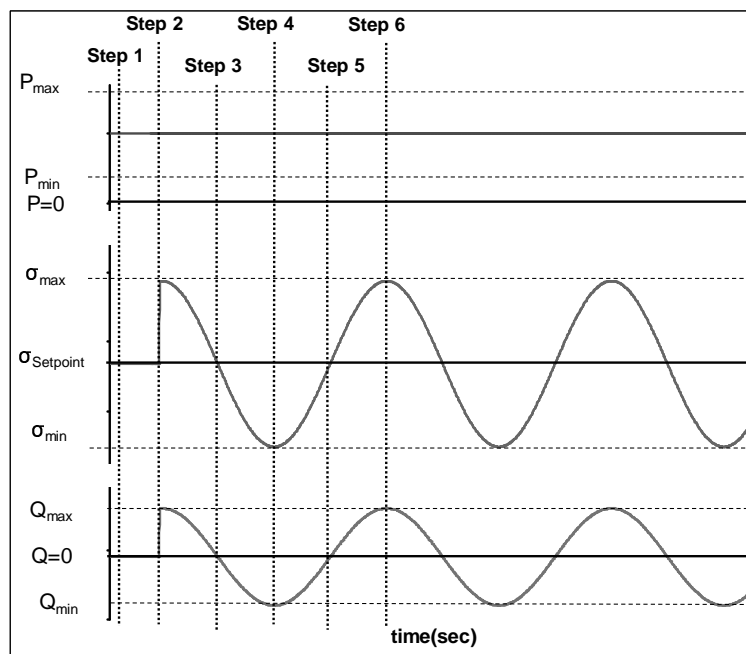
Figure 4.7. FEA Load Steps for Bi-Directional Shear Tests with Constant Contact Load

4.12

4.4.2. Variable Contact Load, Uni-Directional Shear

Figure 4.6 shows the relation of the loading steps for the case of variable contact load with uni-directional shear. Steps 1 and 2 for the analysis of uni-directional shear with a variable contact load were the same as the Steps 1 and 2 for the constant contact load case with the contact load applied during the first two steps being the maximum contact load, P_{max}. Step 3, however, applied a minimum contact load, P_{min}, in addition to the minimum bulk stress, $\sigma_{axial,min}$, and minimum shearing force, Q_{min}. Step 4 and 5 were the same as Steps 2 and 3 respectively.
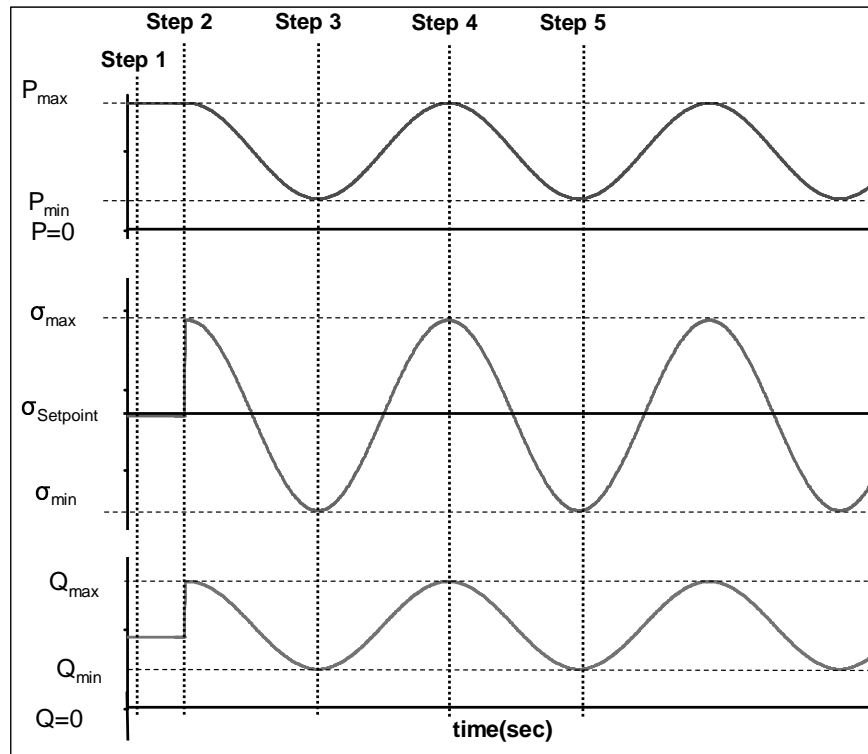
Figure 4.8. FEA Load Steps for Uni-Directional Shear Test with Variable Contact Load

4.4.3. Variable Contact Loading, Bi-Directional Shear

Unlike the previous loading conditions discussed where three load steps were used to apply loads to the finite element model, the case of variable contact load applied with bi-directional shearing required four loading steps as seen in Figures 4.9 and 4.10.
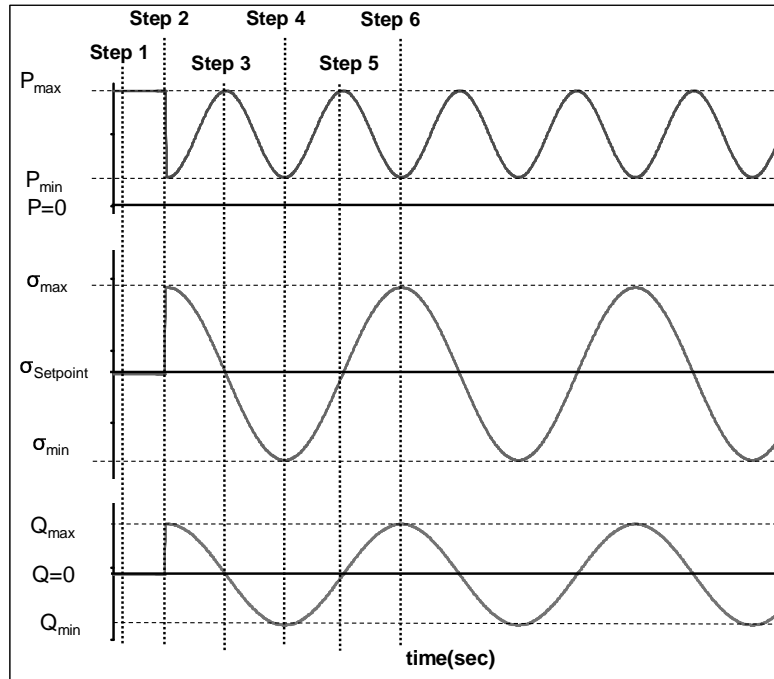
Figure 4.9. FEA Load Steps for Bi-Directional Shear Test: 40 Hz Variable Contact Load at 90° Phase Eelative to σ_{axial}
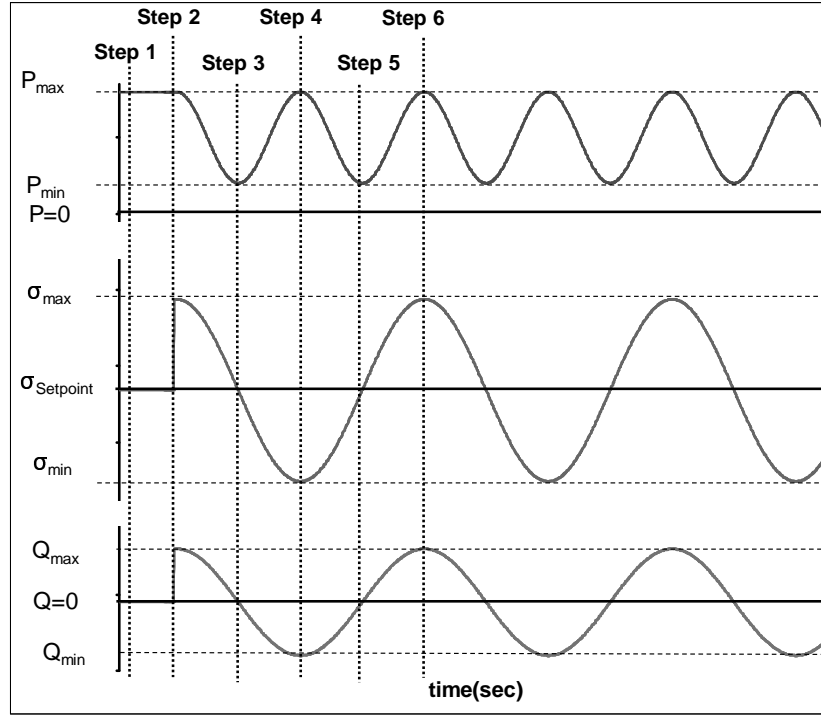
Figure 4.10. FEA Load Steps for Bi-Directional Shear Test with 40 Hz Variable Contact Load at -90$^{\text{o}}$ Phase Relative to σ_{axial}

The need for an additional load step was due to the frequency of the contact load being twice the frequency of the axial load. With the contact load frequency at twice the axial load frequency an additional maximum or minimum contact load is applied between instances of maximum and minimum axial and shear loads. Therefore, in order to include the effects of this additional application of maximum or minimum contact load an additional loading step is added for the cases of bi-directional shear with variable contact load. Nonetheless, as in the two previous cases, Step 1 only applied the maximum contact load, P_{max}. The loads applied during Steps 2, 3, and 4 depended upon the phase of the contact load, $\varphi_{P,}$ relative to the phase of the axial load, i.e. $\varphi_P = +90^{\text{o}}$ versus $\varphi_P = -90^{\text{o}}$

4.15

4.4.3.1. +90° Phase Contact Load Relative to Axial Load.

For the case in which the contact load had a +90° phase relative to the axial load Step 2 consists of a minimum contact load, P_{min}, applied at the same time the maximum axial and shear loads are applied as seen in Figure 4.9. Step 3 applies the maximum contact load, P_{max}, the magnitude of the axial load at the setpoint, $\sigma_{axial,setpoint}$ and a shear value of zero. A shear value of zero is applied in Step 3 because it is assumed to be zero when the axial load is at its setpoint value. Step 4 applies the minimum contact load, P_{min}, minimum bulk stress, $\sigma_{axial,min}$, as well as the minimum shearing force, Q_{min}.

4.4.3.2. -90° Phase Contact Load Relative to Axial Load.

For the other case of bi-directional shear with variable contact loading the contact load is at -90° relative phase to the axial load. For this case Step 2 consists of the application of the maximum contact load, P_{max}, maximum axial load, $\sigma_{axial,max}$, and maximum shear load Q_{max}. Step 3 applies the minimum contact load, P_{min}, the magnitude of the axial load at the setpoint, $\sigma_{axial,setpoint,}$ and a shear value of zero. As in the aforementioned case at the point at which Step 3 occurs the shearing force is assumed to be zero. Step 4 applies the maximum contact load, P_{max}, minimum bulk stress, $\sigma_{axial,min}$, as well as the minimum shearing force, $Q_{min,}$. Reapplying Step 3 and then Step 2 represents one loading cycle for test with bi-directional shear regardless of contact load phase angle.

For each experimental test numerically simulated the appropriate loading conditions based on the experimental test performed in the lab had to be applied to the finite element model. The values of axial load, σ_{axial} and contact load, P, and were taken directly from the loading conditions measured during experimental tests. The values of

4.16

shear load, Q, used for numerical testing were based on the average shear measured on

each side of the specimen by the strain gauges attached to the flexure spring assembly. In

addition to numerical testing using loads taken from the actual experimental tests,

numerical testing was done using idealized load conditions as set forth in the initial

program of experiments and values input into the finite element. Numerical testing using

ideal loading conditions will allow for trends in the predictive parameter to be studies

while the desired variables, i.e. bulk tension and shear, are kept constant. Results from

the FEA will be discussed in the next chapter.

4.4.4. Steady State

Initially loading steps as outlined in the previous sub-section were repeated to

yield at least two complete cycles of loading of each numerical test. Multiple cycles of

loading were used to ensure stresses along the region of contact achieved a steady state

between cycles. To determine if a steady state was reached stresses determined from the

first half-cycle of loading steps, i.e. Steps 2 and 3 for uni-directional shear or Steps 2, 3

and 4 for bi-directional shear, were compared with the stresses resulting from the second

and third application of the same step load following the loading cycle pattern. Figure

4.11 shows a comparison of the output for load Steps 2, 4 and 6 for same loading

conditions used in the FEA validation. It can be seen that the stresses determined from

the finite element model of a uni-directional shear test achieved steady state after Step 4.

For bi-directional test shear values reached a steady state after Step 6. Therefore, stress

values used after these load steps were considered the steady state stress values for each

test.
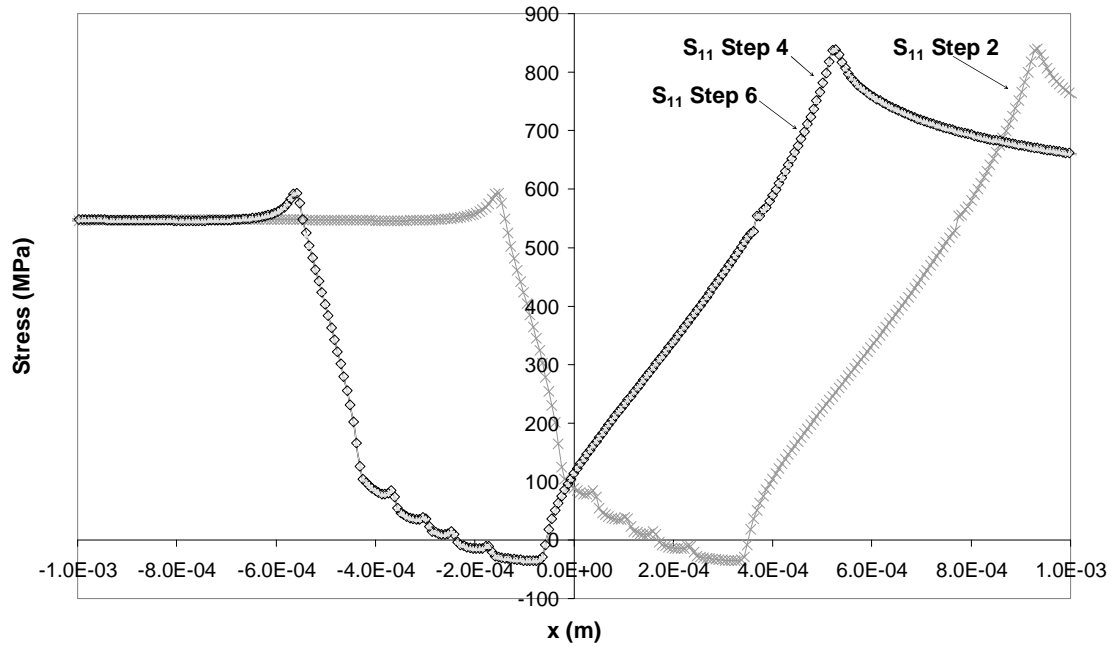
Figure 4.11. Comparison after Steps 2, 4 and 6 of a Uni-Directional Shear Test

In the next chapter, Chapter X, the finite element model discussed previously and the steady state stress values as discussed above will be used to generate stress, strain, and displacement data, which will be used to analyze the fretting phenomenon and to formulate fretting fatigue parameter for fretting fatigue crack initiation. Also, experimental results will be presented and discussed.

X. Results and Discussion

The following chapter will present the results of both experimental test and numerical analysis. Explanations for the effect of variable contact loading on fretting fatigue life will be discussed. The modified shear stress range predictive fatigue parameter will be evaluated based on the output of the finite element analysis. Suggested modifications to the MSSR parameter will also be discussed. Finally new insights and ideas developed through the course of this study will be presented.

5.1. Output of Experimental Tests

The results of twenty-three experimental tests are included in this study. Data for the tests with uni-directional shear was taken from experimental results obtained from the study performed under contract by UDRI [34]. The experimental results are summarized in Table 5.1. A detailed discussion of the experimental results follows.

Table 5.1. Summary of Experimental Results

P=Constant: Uni-Directional Shear

Test #	P_{max} $\frac{kN}{m}$	P_{min} $\frac{kN}{m}$	P_{Freq} Hz	P_φ deg	σ_{max} MPa	R_σ	$Q_{L,max}$ N	$R_{Q,L}$	$Q_{R,max}$ N	$R_{Q,R}$	N cycles	Side of Crack	$2a_{max}$ mm
1	315	-	-	-	556	0.47	569	0.08	560	0.10	1.7E+06	L	1.56
2	350	-	-	-	608	0.51	623	0.13	516	0.07	8.9E+05	L	1.18
3	525	-	-	-	598	0.50	649	0.14	583	0.16	1.2E+06	L	1.61
4	525	-	-	-	603	0.50	636	0.10	592	0.12	6.1E+05	L	1.72
5	630	-	-	-	564	0.47	583	0.08	538	0.03	1.0E+06	L	1.73
6	630	-	-	-	562	0.47	578	0.07	534	0.04	4.8E+05	L	2.01
7	630	-	-	-	555	0.47	574	0.06	565	0.09	8.1E+05	L	1.95
8	700	-	-	-	592	0.49	667	0.17	534	0.08	4.1E+05	L	2.18

P=Variable; Uni-Directional Shear

Test #	P_{max} $\frac{kN}{m}$	P_{min} $\frac{kN}{m}$	P_{Freq} Hz	P_φ deg	σ_{max} MPa	R_σ	$Q_{L,max}$ N	$R_{Q,L}$	$Q_{R,max}$ N	$R_{Q,R}$	N cycles	Side of Crack	$2a_{max}$ mm
9*	630	315	20	0	553	0.46	587	0.09	507	0.04	6.6E+05	R	1.74
10	630	315	20	0	555	0.46	565	0.08	538	0.08	7.1E+05	L	1.59
11	700	350	20	0	600	0.49	654	0.14	534	0.08	2.5E+05	L	2.13
12	700	350	20	0	592	0.46	649	0.11	587	0.10	2.3E+05	L	1.65
13	700	525	20	0	595	0.50	636	0.11	605	0.16	3.5E+05	L	1.83
14	700	525	20	0	595	0.50	641	0.13	587	0.09	2.1E+05	L	2.59

P=Constant; Bi-Directional Shear

Test #	P_{max} $\frac{kN}{m}$	P_{min} $\frac{kN}{m}$	P_{Freq} Hz	P_φ deg	σ_{max} MPa	R_σ	$Q_{L,max}$ N	$R_{Q,L}$	$Q_{R,max}$ N	$R_{Q,R}$	N cycles	Side of Crack	$2a_{max}$ mm
15	350	-	-	-	569	0.10	231	-0.60	255	-0.71	5.9E+04	R	1.21
16	525	-	-	-	588	0.11	222	-0.94	276	-0.81	6.1E+04	R	2.14
17	700	-	-	-	590	0.11	227	-0.78	267	-1.00	5.3E+04	R/L	1.93

P=Variable; Bi-Directional Shear

Test #	P_{max} $\frac{kN}{m}$	P_{min} $\frac{kN}{m}$	P_{Freq} Hz	P_φ deg	σ_{max} MPa	R_σ	$Q_{L,max}$ N	$R_{Q,L}$	$Q_{R,max}$ N	$R_{Q,R}$	N cycles	Side of Crack	$2a_{max}$ mm
18	700	350	36	90	599	0.06	414	-0.16	334	-0.99	6.9E+04	L	2.10
19	700	350	36	90	582	0.02	285	-0.66	387	-0.93	5.0E+04	R/L	1.52
20	700	350	36	90	596	0.05	151	-2.65	329	-1.04	5.1E+04	R/L	2.18
21	700	350	40	-90	591	0.03	196	-1.93	345	1.05	4.6E+04	L	1.66
22	700	350	40	90	592	0.10	222	-0.83	262	-1.02	5.1E+04	R	1.98
23	700	525	40	90	589	0.09	276	-0.79	287	-1.00	5.1E+04	L	1.83

5.1.1. Fatigue Life

Fatigue life was determined for each specimen as discussed in Chapter 3. Stopping tests prior to complete specimen failure allowed for the contact width of the fretting scar to be measured. Tests 15, 16, 18, 20, and 21 could not be stopped prior to specimen failure due to rapid crack propagation at the fretting fatigue loads used in these tests. Fatigue life was found to be less for test with a variable contact load than for test with equivalent higher and lower constant contact loads. Decrease in fatigue life due to

5.2

the application of a variable contact load was most substantial in tests of this study with

uni-directional shear. Fatigue life categorized by contact loading conditions is shown in

Figures 5.1 and 5.2 for uni-directional and bi-directional shear test respectively. Scatter

bars represent the maximum and minimum fatigue life under the same contact loading

condition for cases where multiple specimens were tested under the same axial loads.
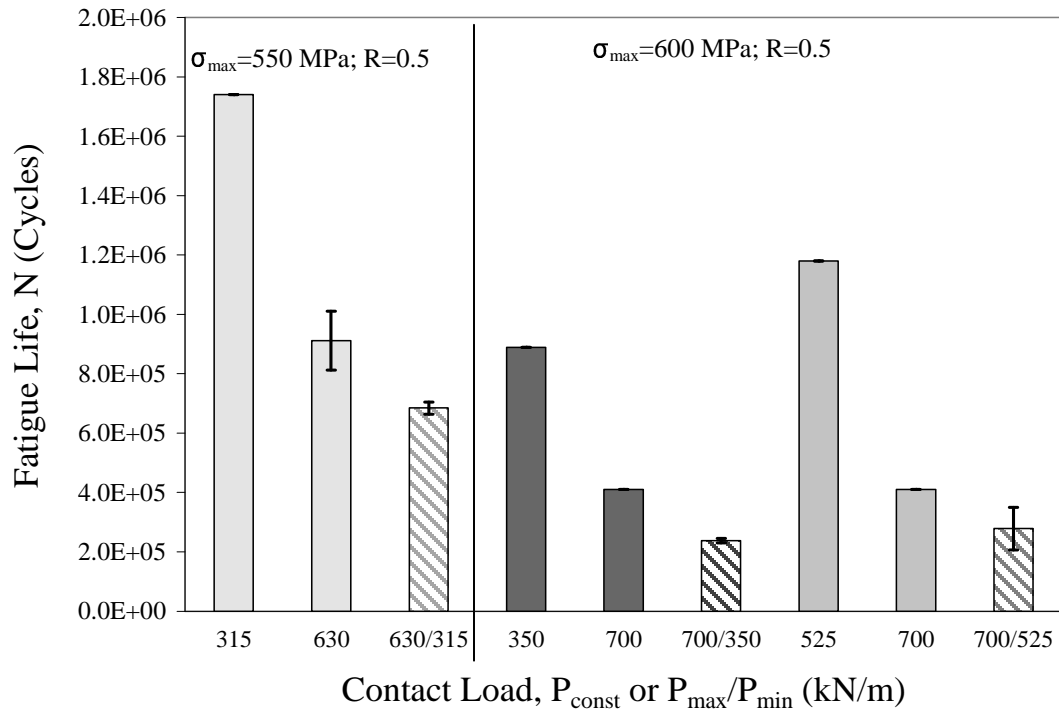
Figure 5.1. Fatigue Life Fatigue Life Comparisons for Various Contact Loading
Conditions with Uni-Directional Shear
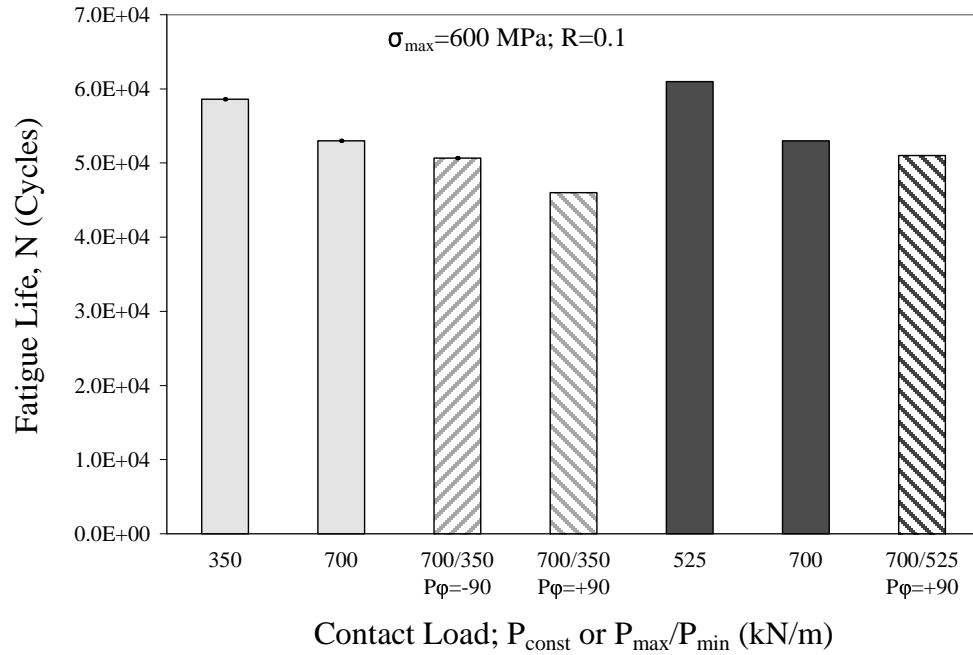
Figure 5.2. Fatigue Life Comparisons for Various Contact Loading Conditions with Bi-Directional Shear

As seen in Figure 5.1, for test with uni-directional shear, fatigue life of specimens with a variable contact load applied was on average 70% less than for an equivalent lower constant contact load case and 33% less then an equivalent higher constant contact load case. As seen in Figure 5.2 the fatigue life for bi-directional shear tests with variable contact loads were on average 17% and 10% less than tests with equivalent higher and lower constant contact loads respectively. These results do not include data for specimens #18, 19 and 20 which had unequal shear spans relative to the left and right hand side of contact. Although test #21 did not have equal shear spans on both sides of contact it is included for the sake of discussion as it was the only bi-directional shear test performed with a phase angle, φ_P, of -90° all other bi-directional shear test had a phase angle of +90°. Next, further details of the experimental results are examined to help yield

5.4

a possible explanation for the trends in fatigue life based on the contact loads as discussed above.

Nakazawa et al. [27] concluded that fatigue life showed a dependence on contact pressure for Ti-6Al-4V, and for higher bulk axial stress amplitude the fretting fatigue life decreased monotonously with increasing contact pressure. This was similar to the trend observed in this study. At higher axial load i.e. 700 kN/m, the fatigue life decreased only slightly relative to lower contact loads i.e. 315 and 350 kN/m, with increase in contact load.

5.1.2. Effective Stress

A simple method for accounting for stress ratio effect on fatigue life is through the use of a simple axial stress parameter, i.e. average axial bulk stress applied to the specimen. Therefore following the method used by Namjoshi et al.[29] the effective stress for each test is plotted versus the number of fatigue cycles as seen in Figure 5.3.
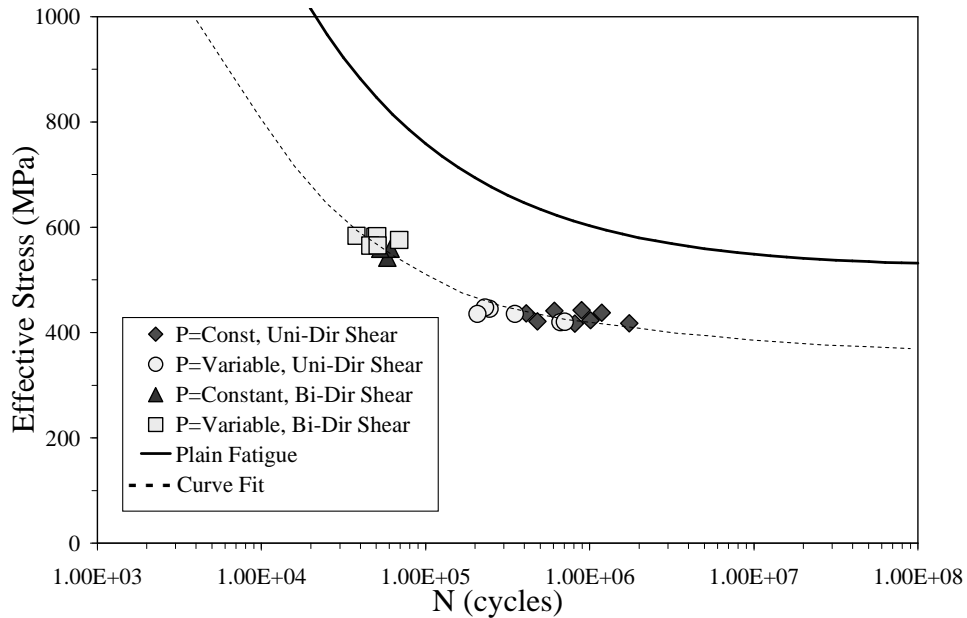
Figure 5.3. Effective Stress versus Fatigue Life Relationship for Uni-Directional and Bi-Directional Shear Test Having Constant and Variable Contact Loads

Effective stress is defined as

$$\sigma_{eff} = \sigma_{max}(1-R)^m \tag{49}$$

where Namjoshi et al determined m=0.45. A curve fit has been drawn for the experimental test data as well as one for plain fatigue data as presented by Namjoshi et al. [29]. As seen in Figure 5.3 tests with uni-directional shear stress had similar effective stresses yet the fatigue life differed. For example, from Figure 5.4 it can be seen that for the constant contact load conditions of 315 and 630 kN/m and the related variable contact load case of P = 315 to 630 kN/m the effective stress was 418, 424 and 420 MPa and the fatigue lives were 1.74E+06, 1.01E+06 and 7.05E+05 cycles respectively.
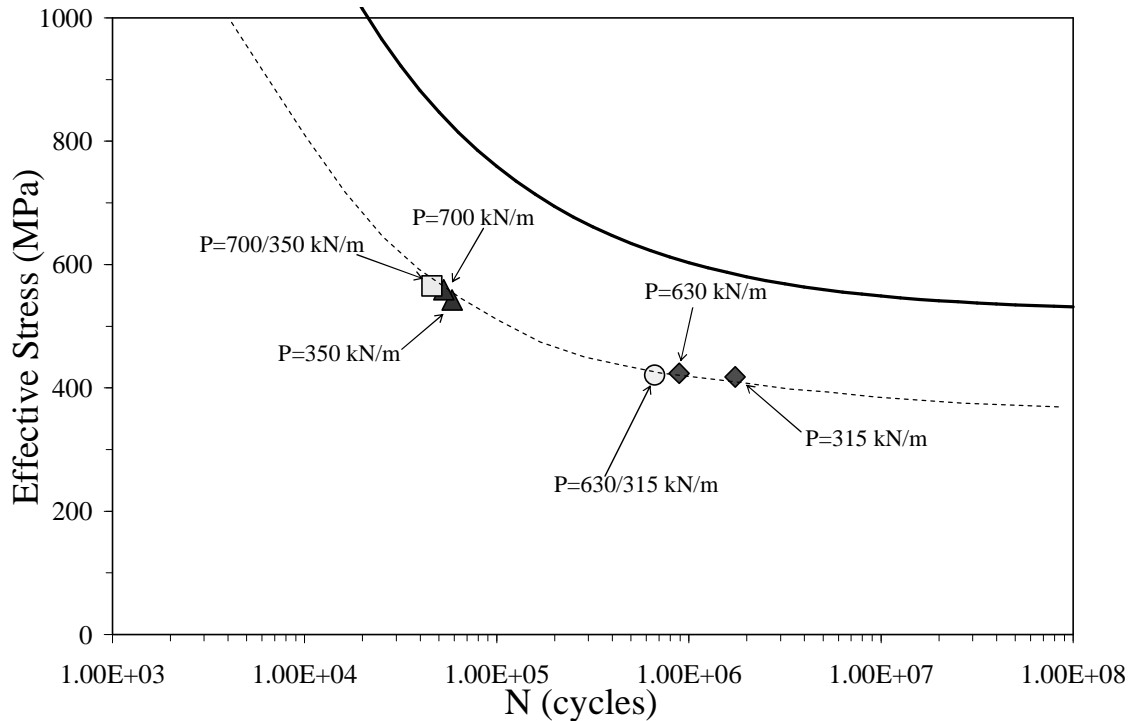
Figure 5.4. Effective Stress versus Number of Fatigue Cycles for Selected Uni-Directional and Bi-Directional Shear Tests.

This trend of decreasing fatigue life with increasing contact load magnitude and a further decrease with variable contact load is not as pronounced for the test with bi-directional shear. As seen in Figure 5.4 the effective stresses of the bi-directional shear test with constant contact loads of 350 and 700 kN/m and variable contact load 350 to 700 kN/m were 542, 559 and 565 MPa respectively and the fatigue lives were 5.86E+04, 5.3E+04 and 5.07E+04 which follows the trend of decreased fatigue life with increased effective stress similar to that for plain fatigue. Therefore, for the test conducted in this study one could say that at the levels of effective stress used for the bi-directional shear test the change in fatigue life may be due at least in part to the differences in effective stresses.

From the effective stress versus fatigue life plots it appears that a parameter other than applied axial stress leads to a decrease in fatigue life for uni-directional test with a variable contact load. The same may be true for the bi-directional shear tests; however, the effects appear to be much less dramatic.

Furthermore, these trends are similar to those observed by Goss and Hoeppner [9]. Goss and Hoeppner noted that titanium showed a strong dependence on normal pressure as compared to aluminum. They concluded that "normal pressure is directly related to the damage produced on the surface during fretting and a fatigue life up to 6000 Psi (41.35 MPa) [9]." They attributed greater fatigue life at lower normal loads to an increase in the number of cycles needed to produce a flaw at at the same axial stresses. This is one possible explanation for differences in fatigue life for different constant contact loads; however, it does not explain the trend observed for variable contact loads.

In trying to shed more light on the factors influencing the decrease in fatigue life

for test under variable contact load the resulting scar pattern and contact width were examined.

5.1.3. Contact Width

The scar pattern for each specimen was examined. Fatigue scars in general had a large "stick zone" in the center area with darker thin lines on the edges demarcating "slip zones" at the leading and trailing edges of the contact area. Uni-directional shear test had noticeably darker lines at the trailing edge of contact which was most likely due to debris accumulation occurring primarily at the trailing edge since the shear traction on the surface was not fully reversing. The width of the resulting scar pattern for each specimen was measured and the results listed in Table 5.1. Figure 5.5 shows the scar patter for Specimen 5. Photos of scar patterns for the remaining specimen can be seen in Appendix B.
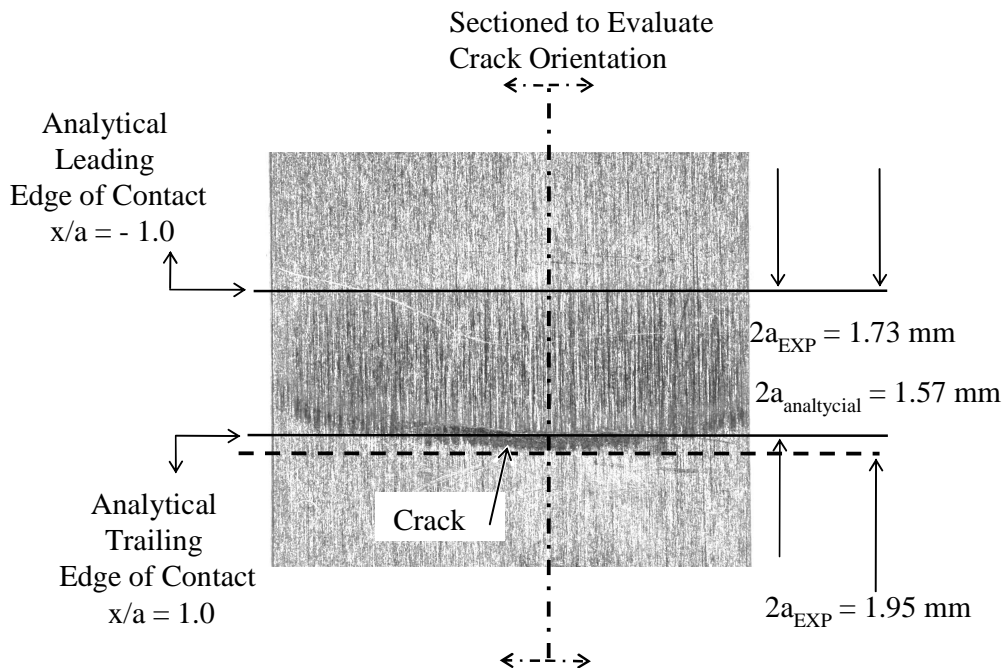
Figure 5.5. Scar Pattern (Test # 5)

5.8

Specimens tested at higher contact loads i.e 700 kN/m, showed a clear, dominant stick zone. The stick zones of specimen tested at lower contact loads were less distinguishable within the region of contact. The contact width was assumed to be equal to the maximum width of the scar pattern for each specimen.

The contact widths, 2a, for specimens 1, 5 and 10 under corresponding contact loads of 315 kN/m constant, 630 kN/m constant and variable 315 to 630 kN/m were determined to be 1.56E-03, 1.735E-04 and 1.59E-03 m respectively. Interestingly, specimen under a variable contact load had contact widths on average between those of specimen tested at the same constant contact loads equal to P_{max} and P_{min} for test with a variable contact load. Figure 5.6 highlights this trend by displaying the contact widths for specimen under the various loading conditions with uni-directional shear categorized by loading condition.
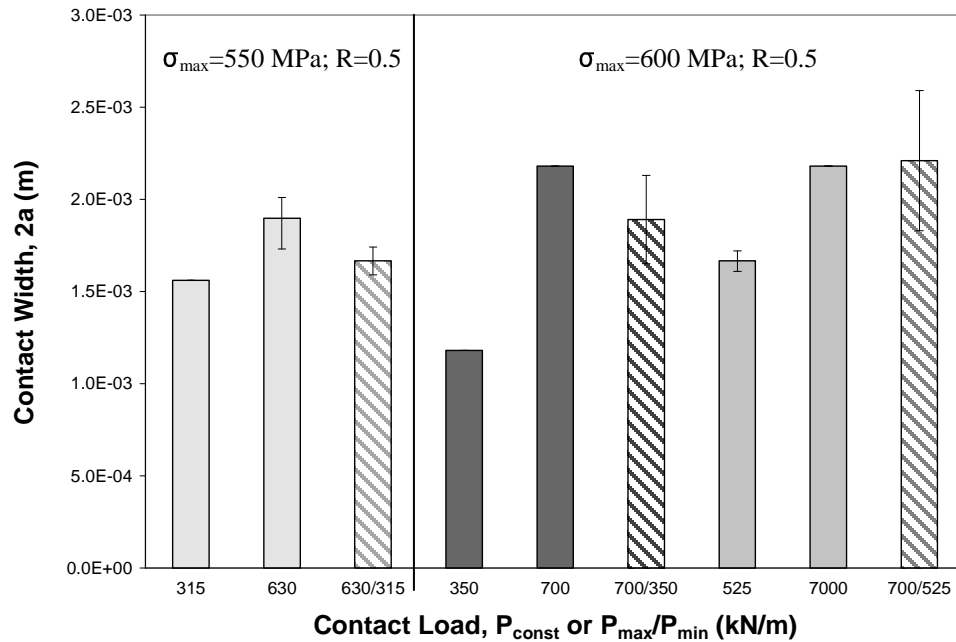
Figure 5.6. Specimen Contact Widths for Constant and Variable Contact Load with Uni-Directional Shear

5.9

The trend seen among the constant contact load tests of 315 and 630 kN/m and test with a variable contact load of 630 to 315 kN/m is repeated among the specimen tested at constant contact loads of 350 and 700 kN/m and a variable contact loads of 700 to 350 kN/m. For the specimen tested at constant contact loads 525 and 700 kN/m and tests at variable loads of 700 to 525 kN/m it is not so clear that this trend is continued, i.e. contact width for a variable load is between that of test with the same higher and lower constant contact loads. Specimens 13 and 14, which had variable contact load 750 to 525 kN/m, had scar patterns which were not uniform i.e. triangular or tapered, i.e. not completely in contact over the entire width of the specimen. When the contact widths for these two specimens are averaged they do fall between the contact width of the specimen under the related constant contact loads of $P = 525$ and $P = 750$ kN/m. However, unlike the specimen of the other variable contact loads of $P = 630$ to 315 kN/m and $P = 700$ to 350 kN/m, taken separately the contact width of the two specimen under the variable loading condition of $P = 700$ to 525 kN/m do not fall between the contact width of the specimen under related constant contact loads. Therefore, it is unclear if the trend of variable contact load test having contact widths between constant contact load of the same higher and lower loads is less distinctive for contact loads of 525 and 750 kN/m as result of higher contact loads or uneven contact.

In the case of bi-directional shear test this trend is not as distinct as in uni-directional shear tests. As seen in Figure 5.7 that for the contact width of specimen under variable contact loading conditions are similar to the contact width of specimen under the same maximum constant contact load. This is in agreement with the trend seen previously where the fatigue life of a specimen under variable contact load, which

although slightly less, was similar to the fatigue life of specimen tested at a constant

contact load equal to P_{max}. Therefore, for the bi-directional shear tests the only trend

observed thus far was a slight decrease in fatigue life under a variable (sinusoidal) contact

load compared to that of specimen with the same higher but, constant contact loads.
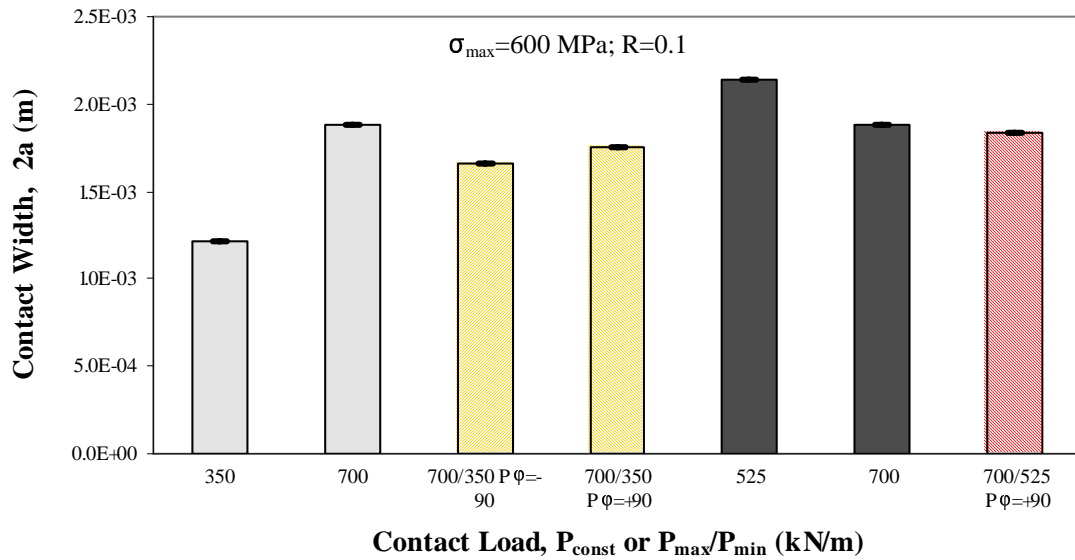
Figure 5.7. Specimen Contact Widths for Constant and Variable Contact Load with Bi-Directional Shear

Furthermore, the relationships between fatigue life and contact width for uni-

directional and bi-directional shear test are shown on the next page in Figures 5.8 and 5.9

respectively. It can be seen that fatigue life is dependent on loading condition and not

contact width, which is a function of contact load, regardless of shear direction. For both

uni-directional and bi-directional shear tests fatigue life is less for test with a variable

contact load than test with higher and lower constant contact loads although the contact

width is between that of test with constant contact loads equal in magnitude to P_{max} and

5.11

P_min of the variable case. Next, crack behavior observations are presented and discussed and will later be used to evaluate the fatigue parameter.
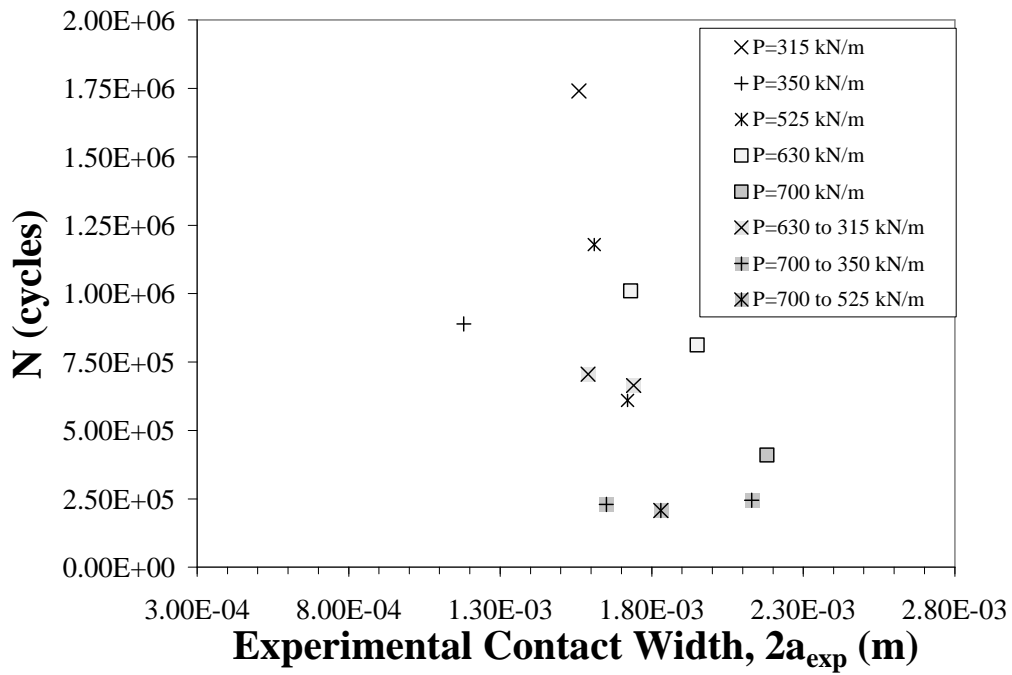
Figure 5.8. Fatigue Cycles versus Contact Width Relationship for Test with Uni-Directional Shear
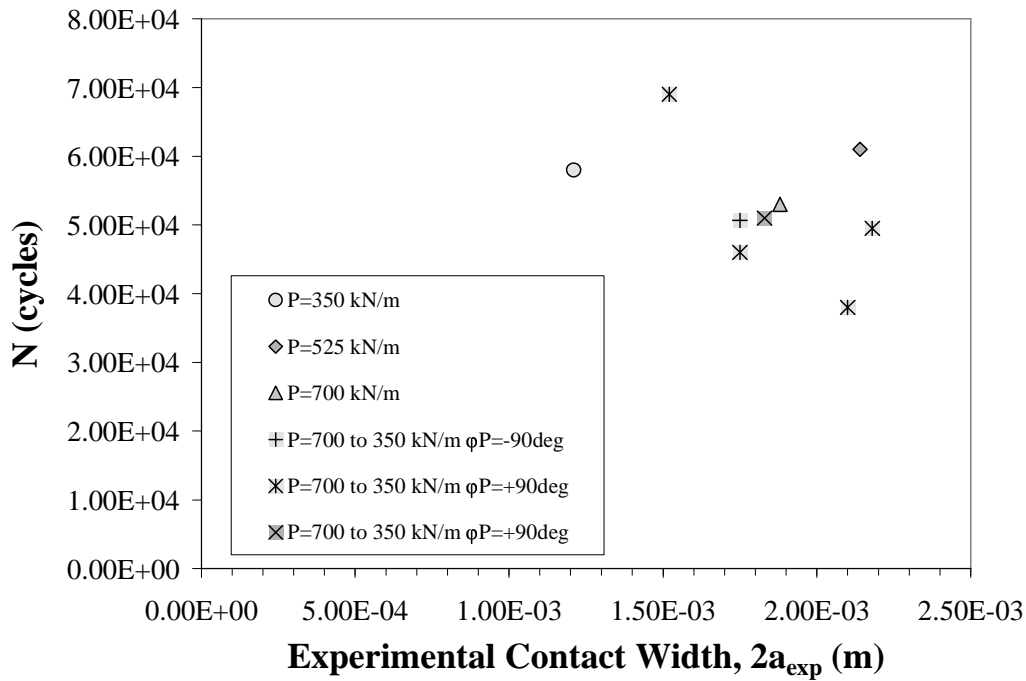
Figure 5.9. Fatigue Cycles versus Contact Width for Bi-Directional Shear

5.1.4. Crack Location

The prediction of crack location is one of the several measures of a predictive

fatigue parameter; therefore, the crack location was determined for the each experimental

test. Figure 5.5 shows the fretting fatigue scar from the 900 kN/m constant contact load

with uni-directional shear. The crack location was found to occur near the trailing edge

of contact or near $x/a = 1.0$. This was typical of all specimens. Therefore, as expected,

cracks initiated along the trailing edge of contact, this is where the highest axial stress

occurs. Another criterion for parameter evaluation is crack orientation.

5.1.5. Crack Orientation

Crack orientation was determined by mounting a sectioned specimen and

systematically grinding and then polishing to ensure the sectioned surface was at the

center of the crack initiation zone. Zones of crack initiation were identified as the region

of discoloration on the failed specimen surface as seen in Figure 5.10. Crack orientation for Specimen #18 is shown in Figures 5.11. Specimen #18 was chosen because the specimen had ruptured; exposing the fracture surface. As seen in Figures 5.11 the crack orientation from the contact surface was found to be -50°. The next section will present and discuss the results of the finite element analysis. For further understanding of the factors influencing the trends in contact load versus fatigue life seen thus far i.e. a variable contact load decreases fatigue life, results were analyzed from FEA.
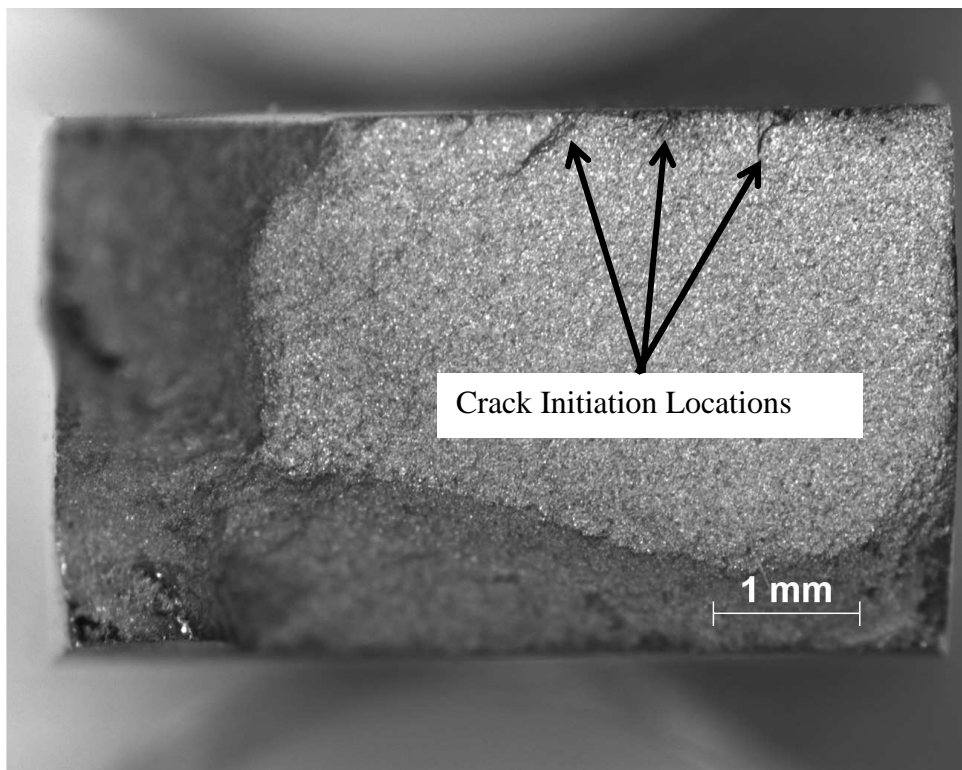
Figure 5.10. Crack Initiation Locations on Fracture Surface for Specimen # 18.

5.14
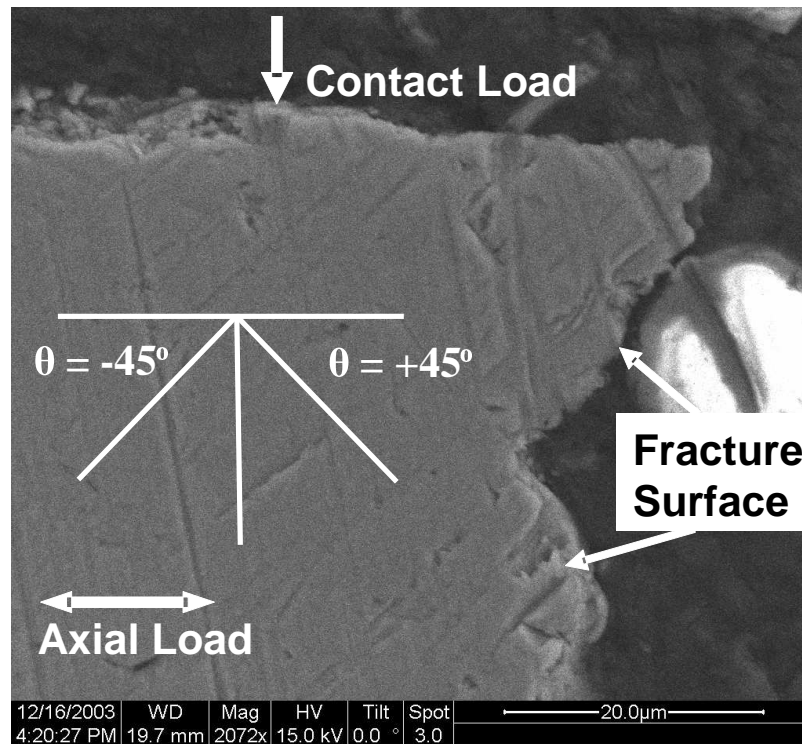
Figure 5.11. Crack Orientation of Specimen #18

5.2. Finite Element Analysis of Experimental Test

As described in the previous chapters, finite element analysis was used to model the experimental test. Table 5.2 lists the input values used to model the experimental tests. The main purpose of obtaining FEA results of experimental test conditions was to allow the MSSR predictive fatigue parameter to be determined so a relationship between the predictive parameter and fatigue life can be established. The results of FEA using experimental test loads are presented in Table 5.2.

Table 5.2. FEA Input Based on Experimental Test Results

Test #	P_{Max} (kN/m)	P_{Min} (N)	P_{Freq} (Hz)	σ_{max} (MPa)	R_σ	$Q_{L,max}$ (N)	$R_{Q,L}$	$Q_{R,max}$ (N)	$R_{Q,R}$	P_φ (deg)
P=Constant: Uni-Directional Shear										
1	315	-	20	556	0.47	569	0.08	560	0.10	-
2	350	-	20	608	0.51	623	0.13	516	0.07	-
3	525	-	20	598	0.50	649	0.14	583	0.16	-
4	525	-	20	603	0.50	636	0.10	592	0.12	-
5	630	-	20	564	0.47	583	0.08	538	0.03	-
6	630	-	20	562	0.47	578	0.07	534	0.04	-
7	630	-	20	555	0.47	574	0.06	565	0.09	-
8	700	-	20	592	0.49	667	0.17	534	0.08	-
P=Variable; Uni-Directional Shear										
9	630	315	20	553	0.46	587	0.09	507	0.04	0
10	630	315	20	555	0.46	565	0.08	538	0.08	0
11	700	350	20	600	0.49	654	0.14	534	0.08	0
12	700	350	20	592	0.46	649	0.11	587	0.10	0
13	700	525	20	595	0.50	636	0.11	605	0.16	0
14	700	525	20	595	0.50	641	0.13	587	0.09	0
P=Constant; Bi-Directional Shear										
15	350	-	20	569	0.10	231	-0.60	255	-0.71	-
16	525	-	20	588	0.11	222	-0.94	276	-0.81	-
17	700	-	20	590	0.11	227	-0.78	267	-1.00	-
P=Variable; Bi-Directional Shear										
18	700	350	36	599	0.06	414	-0.16	334	-0.99	90
19	700	350	36	582	0.02	285	-0.66	387	-0.93	90
20	700	350	36	596	0.05	151	-2.65	329	-1.04	90
21	700	350	40	591	0.03	196	-1.93	345	1.05	-90
22	700	350	40	592	0.10	222	-0.83	262	-1.02	90
23	700	525	40	589	0.09	276	-0.79	287	-1.00	90

5.3. Finite Element Results using Idealized Load Conditions

Because loads other than contact loads varied slightly from one test to another, trends from FEA results using idealized load conditions are more valuable. Therefore, this section will focus on the trends observed from FEA of the systematic variation of contact load while axial stress and shear loads are held constant. Table 5.3 lists input values used in this analysis where $\sigma_{axial,max}$, $\sigma_{axial,min}$, Q_{max}, and Q_{min} are held constant while only contact load magnitude and waveform are varied. Trends in surface stresses

5.16

within the contact region for test with constant and variable load conditions were observed. Summaries of the trends observed from this analysis will be discussed next.

Table 5.3. Summary of FEA Input Based on Idealized Test Loads

Ideal Test #	Pconst (kN/m)		P$_{Freq}$ (Hz)	σ$_{N,max}$ (MPa)	R$_σ$	Q$_{max}$ (N)	R$_Q$	φ$_P$ (deg)
P=Constant: Uni-Directional Shear								
1	315		20	550	0.47	578	0.08	0
2	630		20	550	0.47	578	0.08	0

Ideal Test #	Pmax (kN/m)	Pmin (kN/m)	P$_{Freq}$ (Hz)	σ$_{N,max}$ (MPa)	R$_σ$	Q$_{max}$ (N)	R$_Q$	φ$_P$ (deg)
P=Variable; Uni-Directional Shear								
3	630	315	20	550	0.47	578	0.08	0

Ideal Test #	Pconst (kN/m)		P$_{Freq}$ (Hz)	σ$_{N,max}$ (MPa)	R$_σ$	Q$_{max}$ (N)	R$_Q$	φ$_P$ (deg)
P=Constant; Bi-Directional Shear								
4	350		20	600	0.10	333	-1.00	0
5	700		20	600	0.10	333	-1.00	0

Ideal Test #	Pmax (kN/m)	Pmin (kN/m)	P$_{Freq}$ (Hz)	σ$_{N,max}$ (MPa)	R$_σ$	Q$_{max}$ (N)	R$_Q$	φ$_P$ (deg)
P=Variable; Bi-Directional Shear 7								
6	700	350	40	600	0.10	333	-1.00	-90
7	700	350	40	600	0.10	333	-1.00	90

5.3.1. Local Stresses Along Contact Surface

Using FEA local stresses along the contact surface were determined for both uni-directional and bi-directional shear tests.

5.3.1.1. Uni-Directional Shear Tests:

For test with uni-directional shear with maximum axial, shear and contact load applied it was found that the maximum stress in the x-direction is located near the trailing edge i.e. $x/a = 1$, and is equal for test with a variable (sinusoidal) and higher constant contact loads as seen in Figure 5.12 on pg 5.19 where "a" is the contact width from FEA.

On the other hand, as seen in Figure 5.13 when σ_{axial}, Q, and P are at their minimum values the maximum stress in the x-direction, S_{11}, for a variable (sinusoidal) contact load at the leading edge i.e. x/a = -1, has a magnitude between that of the two constant contact load cases. Shear stresses along the surface also show this trend as seen in Figure 5.14 and 5.15. Stresses in the y-direction, S_{22}, are nearly identical at the trailing edge for the variable and higher constant contact load cases when maximum loads are applied as seen in Figure 5.16. Moreover, S_{22} along the contact surface is nearly identical for the variable and the lower constant contact cases at the minimum loading condition as seen in Figure 5.17. It is expected that S_{22} along the surface would be nearly identical for the lower constant and variable contact load cases at the point where the minimum axial load is applied.   This is because for a variable load (sinusoidal in phase with axial load and at the same frequency) the minimum axial load is applied at the same time the minimum contact load is also applied; which, are the same loads applied in a case with an equivalent lower but constant contact load at the point the minimum axial load is applied. Slightly different trends between stresses along the contact surface at the maximum and minimum loading conditions were seen between the tests of constant and variable contact load for test with bi-directional shear.

5.18

Figure 5.12. Comparison of S_{11} Along Contact Surface for Constant 350 kN/m, Constant 700 kN/m, and Variable 350 to 700 kN/m Contact Loads of Idealized Uni-Directional Shear Tests with $\sigma_{axial,max}$ Applied

Figure 5.13. Comparison of S_{11} Along Contact Surface for Constant 350 kN/m, Constant 700 kN/m, and Variable 350 to 700 kN/m Contact Loads of Idealized Uni-Directional Shear Tests with $\sigma_{axial,min}$ Applied

5.19
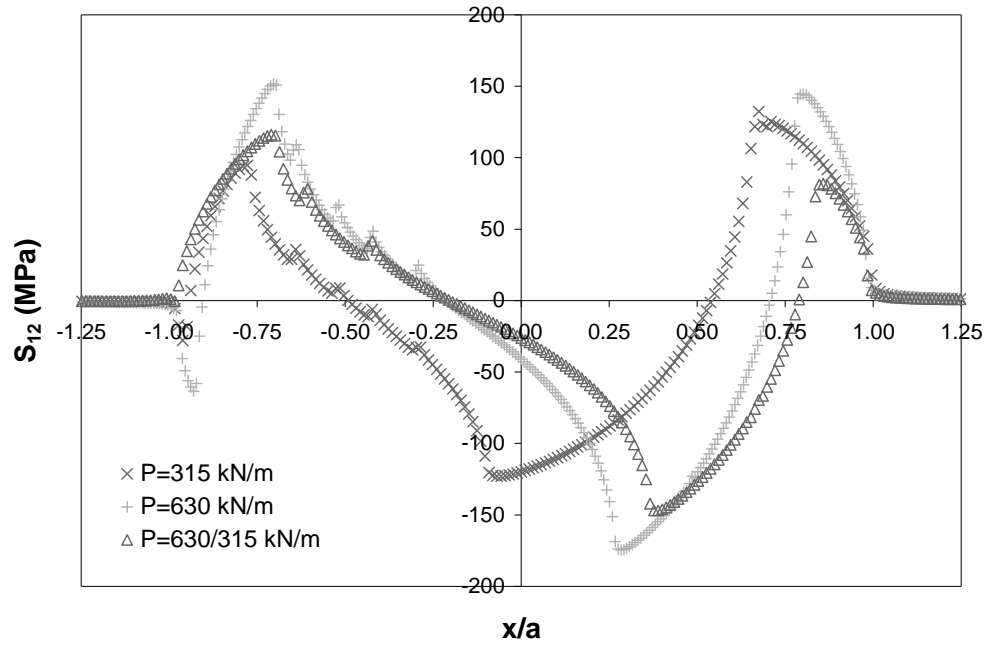
Figure 5.14. Comparison of S_{12} Along Contact Surface for Constant 350 kN/m, Constant 700 kN/m, and Variable 350 to 700 kN/m Contact Loads of Idealized Uni-Directional Shear Tests with $\sigma_{axial,max}$ Applied.
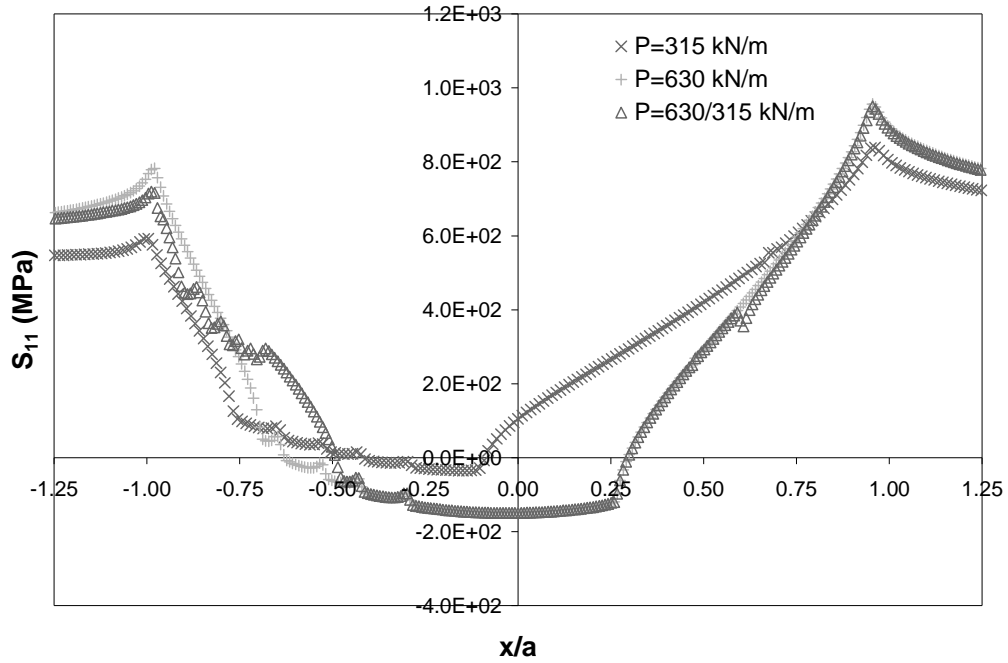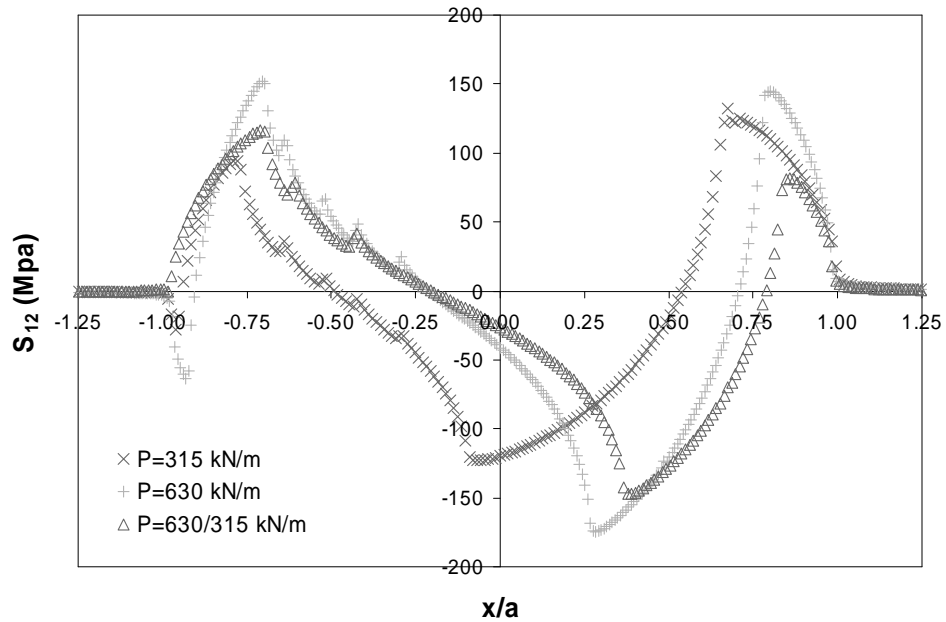

Figure 5.15. Comparison of S_{12} Along Contact Surface for Constant 350 kN/m, Constant 700 kN/m, and Variable 350 to 700 kN/m Contact Loads of Idealized Uni-Directional Shear Tests with $\sigma_{axial,min}$ Applied.

5.20

Figure 5.16. Comparison of S_{22} Along Contact Surface for Constant 350 kN/m, Constant 700 kN/m, and Variable 350 to 700 kN/m Contact Loads of Idealized Uni-Directional Shear Tests with $\sigma_{axial,max}$ Applied..
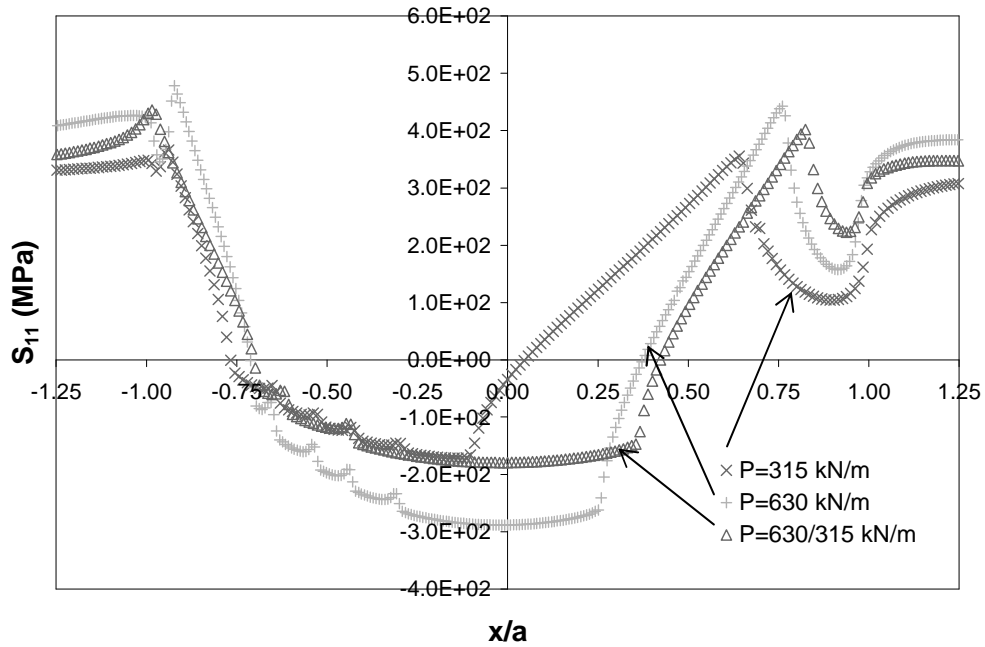

Figure 5.17. Comparison of S_{22} Along Contact Surface for Constant 350 kN/m, Constant 700 kN/m, and Variable 350 to 700 kN/m Contact Loads of Idealized Uni-Directional Shear Tests with $\sigma_{axial,min}$ Applied.
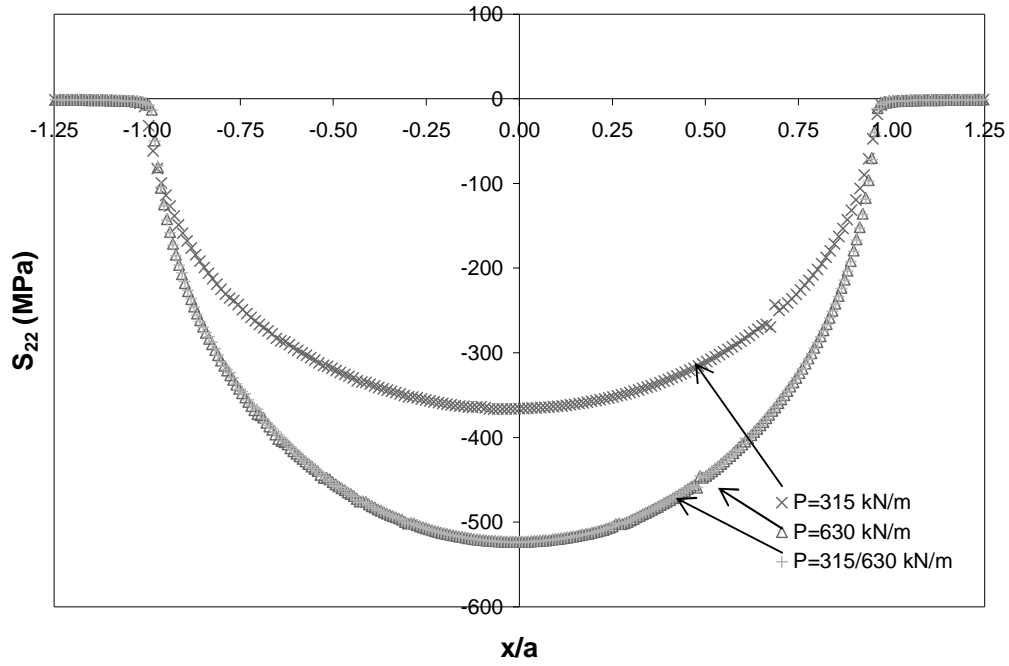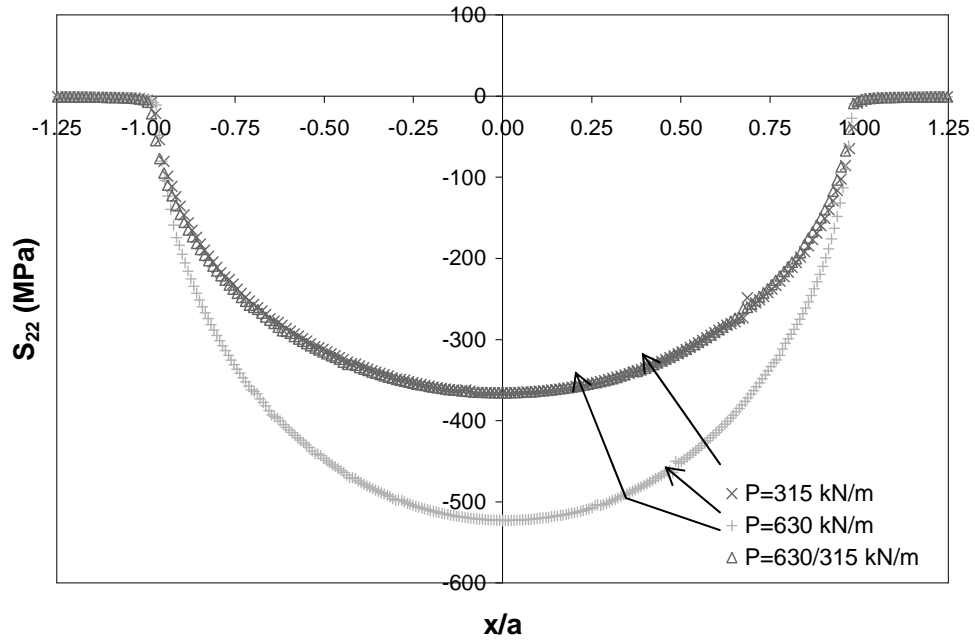
5.21

5.3.2. Bi-Directional Shear Tests

When maximum axial load is applied, the magnitude of the contact load applied for the case of sinusoidal contact load is dependent upon the phase and frequency of the contact load. In the case of the test 6 and 7 of the idealized loading conditions the value of the contact loads for the -90° and $+90^o$ phase variable contact loads correspond to their maximum and minimum values respectively at the point the maximum and minimum axial stress is applied. As a result the maximum stresses S_{11}, S_{12} and S_{22} and contact widths are nearly identical for the variable contact load case with -90° phase and the higher constant contact load with only a slight variance in the shear stress between the center of contact and leading edge with it being greater at the higher constant contact load. All resulting stresses was well as contact widths are nearly identical for the lower constant and $+90^o$ phase variable contact load cases.

Furthermore, for the case of minimum axial loading, a trend similar to that described above is observed. The maximum stresses are nearly identical for the variable contact load case with -90° phase and the higher constant contact load with no variance in shear tractions. When minimum axial loads are applied the resulting principle stresses as well as contact widths are nearly identical for the higher constant and -90° phase variable contact load cases with the maximum value of S_{11} and S_{12} for the -90° phase case being slightly lower then for the higher constant contact load case. These relations can be seen in Figures 5.18 thru 5.23 starting on pg 5.24.

These results are expected because the same loads are being applied to the cases of higher constant contact load and -90° phase variable contact load at the points of maximum and minimum axial loading. Likewise for the lower constant contact load and

$+90^o$ phase variable contact load have the same loading conditions at the instance of maximum and minimum axial loading.

From the above observations based on finite element analysis of the ideal loading conditions it can be said that at no point does the maximum stress for any variable contact load case exceed that of constant contact load cases with the same directions of applied shear. In addition to stresses along the contact surface, relative slip range was determined and compared for the various contact load conditions using FEA results of the tests from the idealized contact load conditions.

Figure 5.18. Comparison of S_{11} Along Contact Surface for Constant 350 kN/m, Constant 700 kN/m, and Variable 350 to 700 kN/m Contact Loads of Idealized Uni-Directional Shear Tests with $\sigma_{axial,max}$ applied.
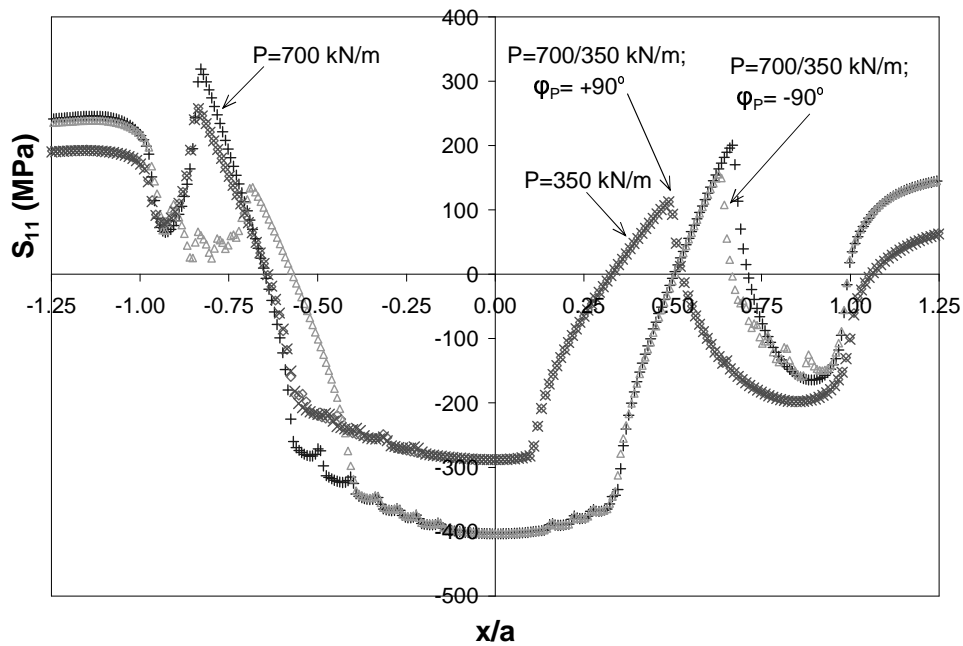
Figure 5.19. Comparison of S_{11} Along Contact Surface for Constant 350 kN/m, Constant 700 kN/m, and Variable 350 to 700 kN/m Contact Loads of Idealized Uni-Directional Shear Tests with $\sigma_{axial,min}$ Applied.
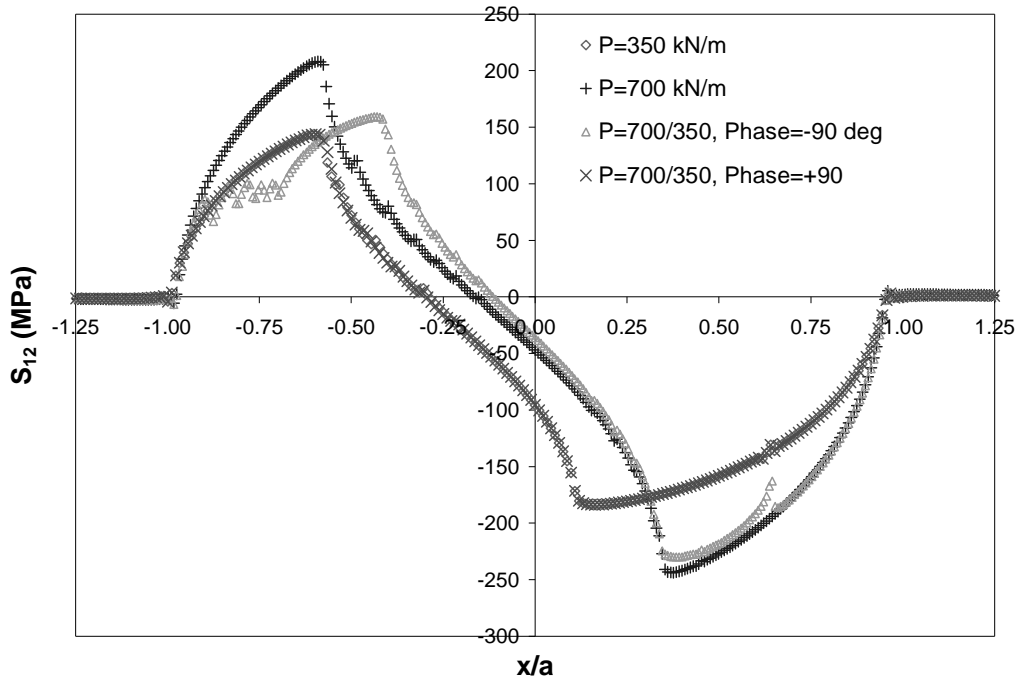
Figure 5.20. Comparison of S_{12} Along Contact Surface for Constant 350 kN/m, Constant 700 kN/m, and Variable 350 to 700 kN/m Contact Loads of Idealized Uni-Directional Shear Tests with $\sigma_{axial,max}$ Applied
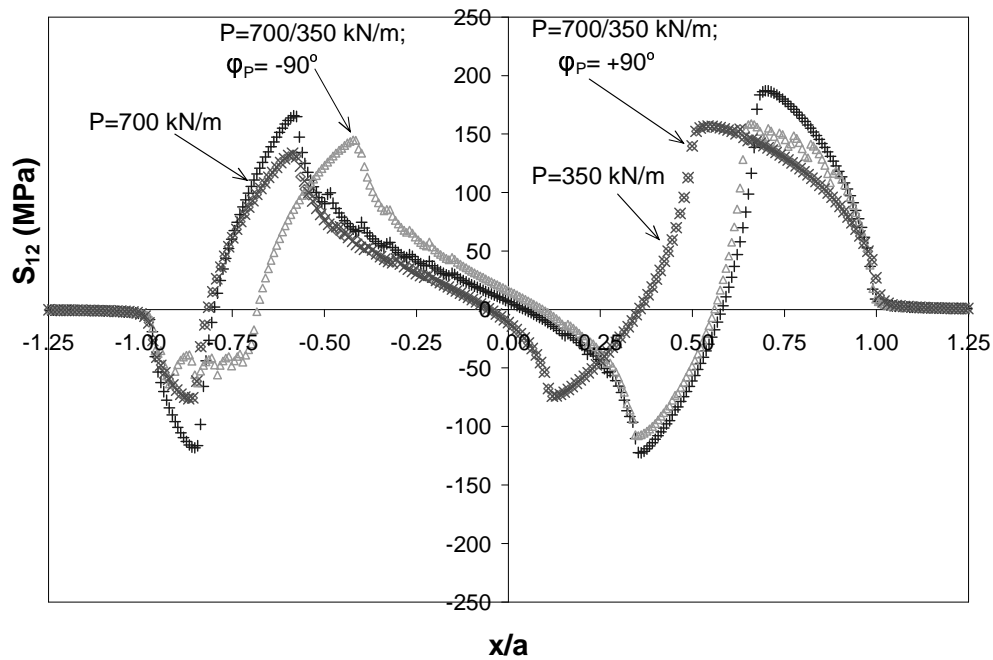
Figure 5.21. Comparison of S_{12} Along Contact Surface for Constant 350 kN/m, Constant 700 kN/m, and Variable 350 to 700 kN/m Contact Loads of Idealized Uni-Directional Shear Tests with $\sigma_{axial,min}$ Applied

Figure 5.22. Comparison of S_{22} Along Contact Surface for Constant 350 kN/m, Constant 700 kN/m, and Variable 350 to 700 kN/m Contact Loads of Idealized Uni-Directional Shear Tests with $\sigma_{axial,max}$ Applied
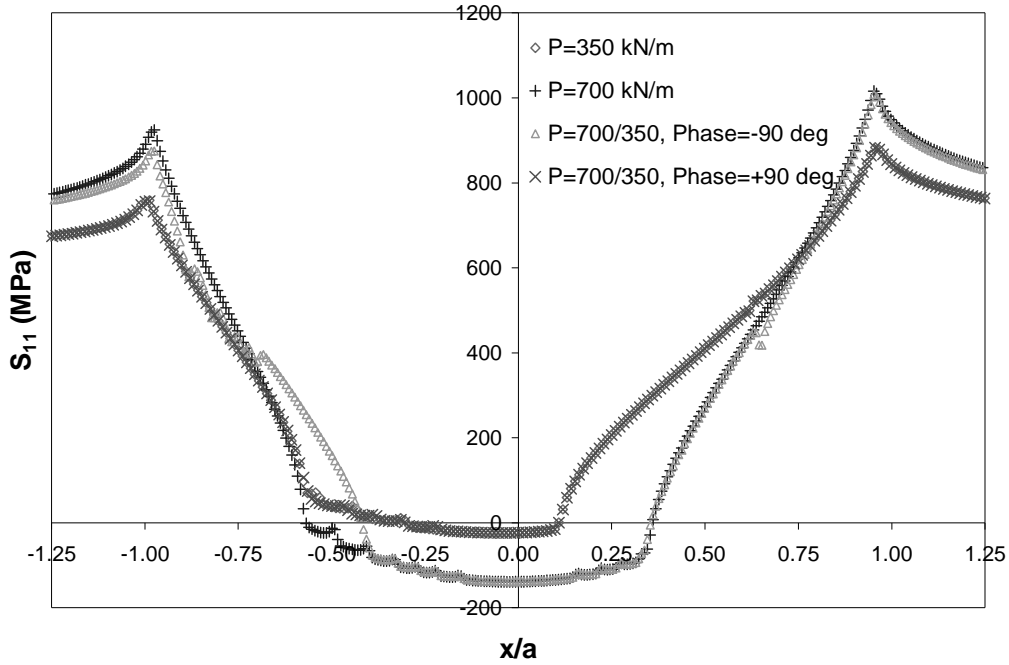

Figure 5.23. Comparison of S_{22} Along Contact Surface for Constant 350 kN/m, Constant 700 kN/m, and Variable 350 to 700 kN/m Contact Loads of Idealized Uni-Directional Shear Tests with $\sigma_{axial,min}$ Applied.

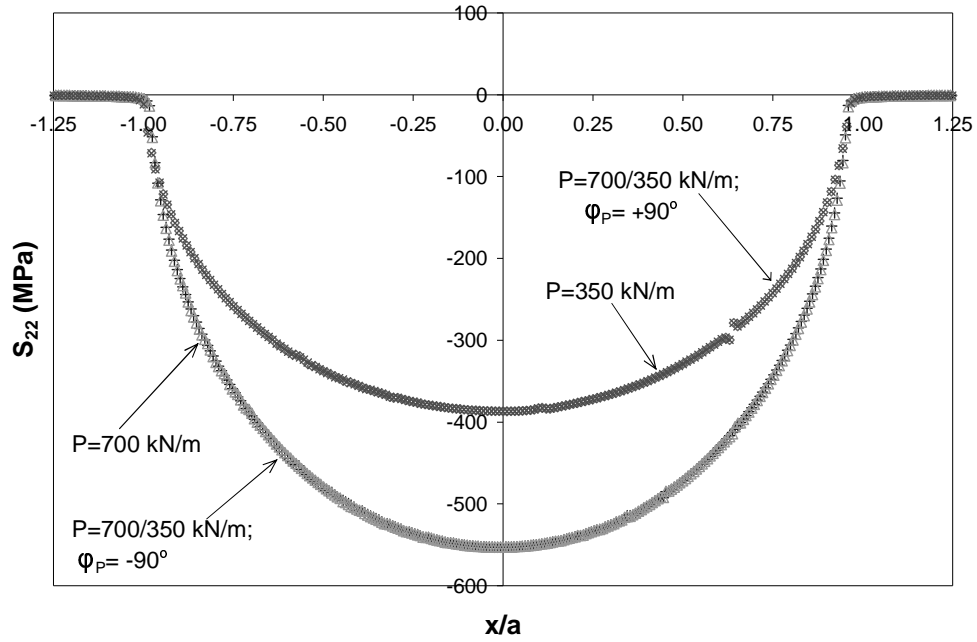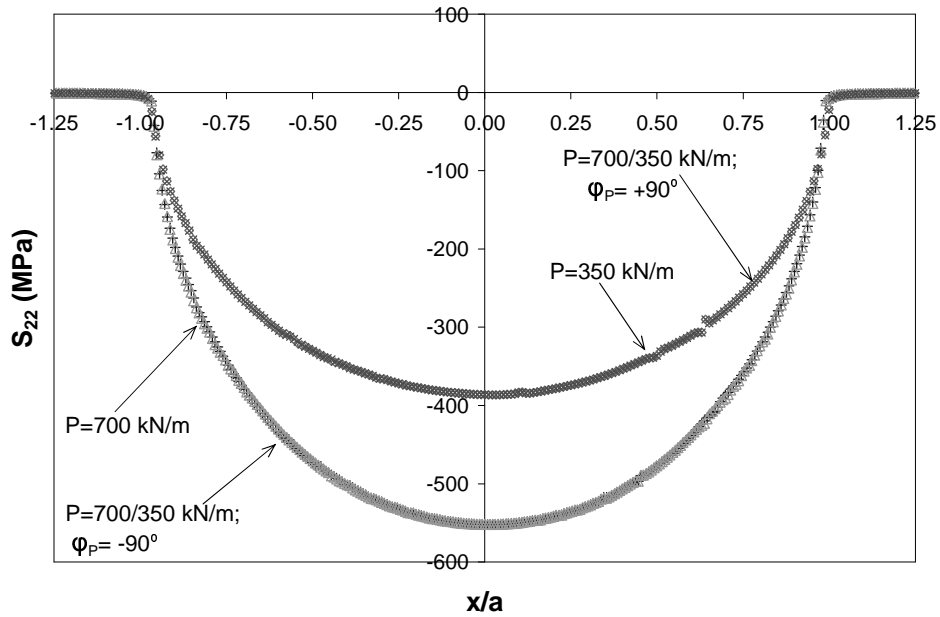### 5.3.3. Relative Slip Range

Relative nodal displacements along the surface of contact can be determined by FEA. After the normal load, P, is applied the fretting pad and fatigue specimen are in contact. After Q and σ_{axial} are applied the fretting pad and fatigue specimen remain in contact, however, regions of stick and slip will develop as discussed in Chapter 2. Regions where nodal points along the surface of the pad and specimen, which were in contact prior to loading, and have no displacement in the x-direction, u_1, relative to each other after axial and shear loading are said to be "stuck". This region where the pad is "stuck" to the specimen is labeled the stick region. The slip region is denoted by the set of points in contact along the surface of the pad and specimen that have a displacement relative to each other after load is applied. This relative displacement is called slip. The magnitude of the relative slip can vary with loading conditions and as a result the location and size of the stick and slip zones can vary during a loading cycle. The difference in relative slip for the same point along the surface of contact at two different points in the loading cycle is known as the relative slip range with slip amplitude being defined as half of the slip range. The relative slip range reveals which region on the contact surface remains in a "stick" condition throughout the loading cycle and which regions change between conditions of stick and slip throughout the loading cycle. Where the slip range is equal to zero indicates the region remains in a stick condition throughout the entire loading cycle. All other regions in contact are in a slip condition at some point in the loading cycle. The slope of the slip range is an indication of the magnitude of the slip range at a give location along the contact surface. The end of the slip region is marked by

the point where the slope of the slip range decreases and becomes constant at increasing distance along the x axis.

5.3.3.1. Uni-Directional Shear.

Using the idealized loads the relative slip range was determined for the constant contact, uni-directional loading cases of P = 315 kN/m, P = 630 kN/m and for a variable contact loading with the same magnitude contact loads. Figures 5.24, 5.25, and 5.26 starting on pg 5.29 show the relative slip at maximum and minimum loading conditions for uni-directional shear tests with lower constant, higher constant and variable contact loads respectively. Regions of slip for each cycle begin where the magnitude of relative slip is non-zero and ends where the slope of the relative slip becomes constant. The comparison of relative slip ranges for the same three uni-directional shear tests from the idealized loads are shown in Figure 5.27. From Figure 5.27 it can be seen that the region of stick is greatest for the higher constant contact load case with the region of stick for the variable contact load case falling between that of the higher and lower constant contact loads.

This may explain why the contact widths for the experimental test with variable contact load were between those the lower and higher constant contact load test. Also, from Figure 5.27 the region of slip is greatest for the variable contact load case.

Figure 5.24. Relative Slip Between Fatigue Specimen and Fretting Pad of Idealized Uni-Directional Shear Tests, P_{const} = 315 kN/m

Figure 5.25. Relative Slip Between Fatigue Specimen and Fretting Pad of Idealized Uni-Directional Shear Tests, P_{const} = 630 kN/m
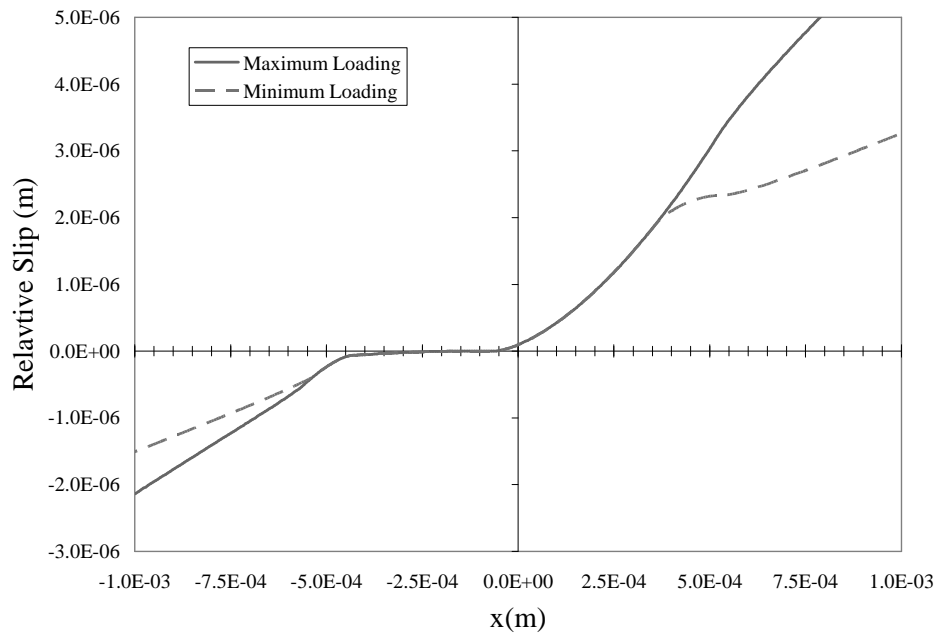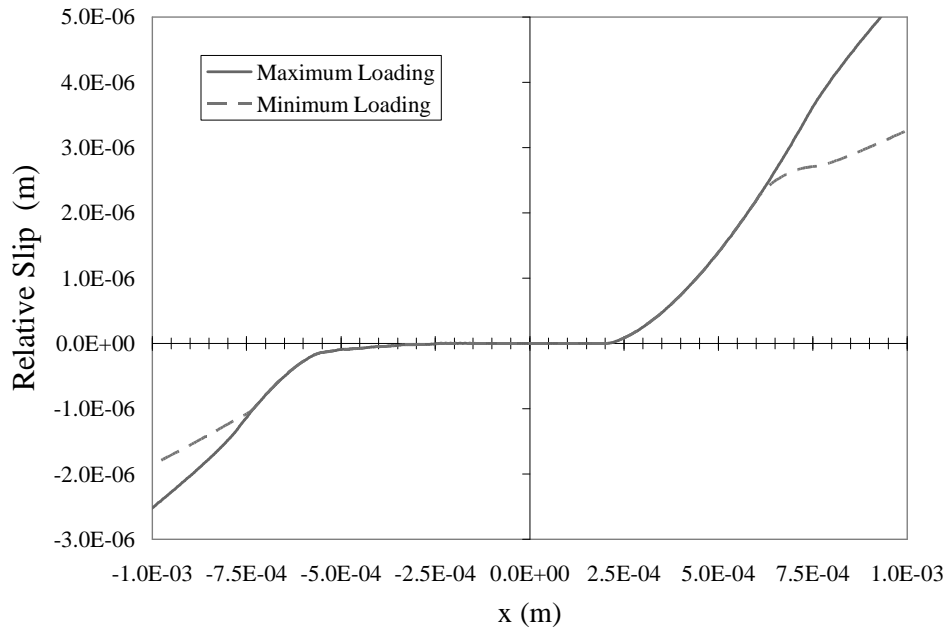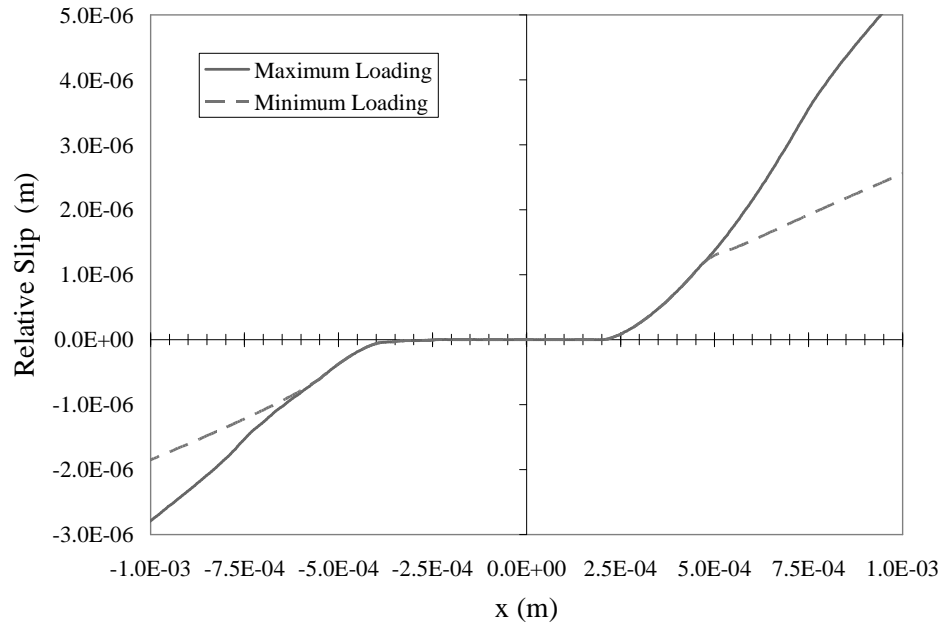
Figure 5.26. Relative Slip Between Fatigue Specimen and Fretting Pad of Idealized Uni-Directional Shear Tests, $P_{max} = 630$ kN/m and $P_{min} = 315$ kN/m
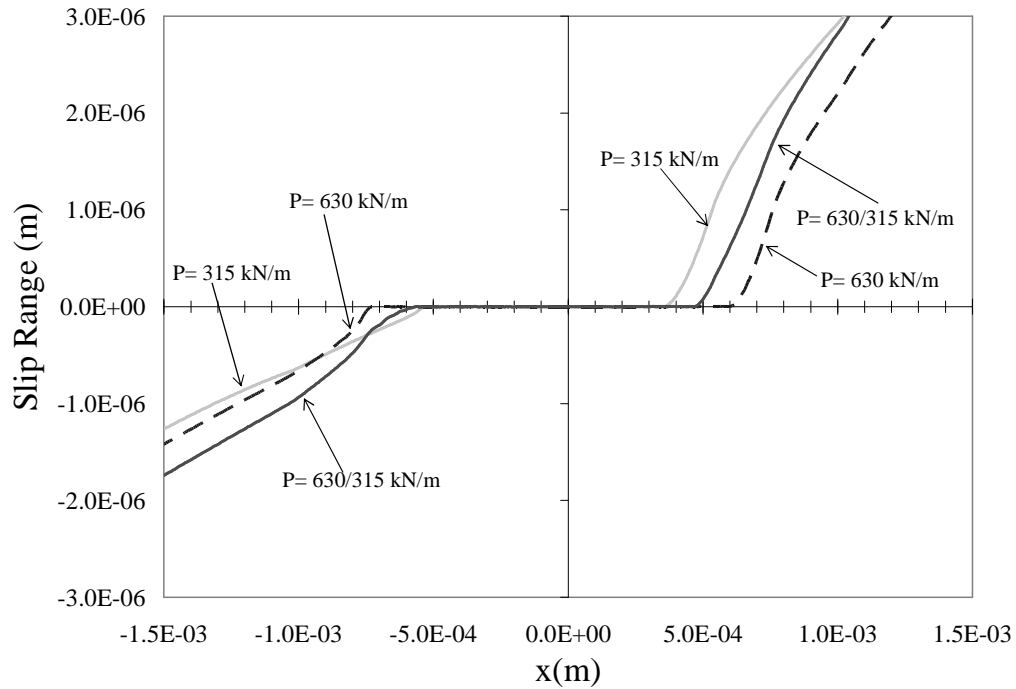
Figure 5.27. Relative Slip Range Comparisons of Idealized Uni-Directional Shear Tests with Constant 350 kN/m, Constant 700 kN/m, and Variable 350 to 700 kN/m Contact Loads.
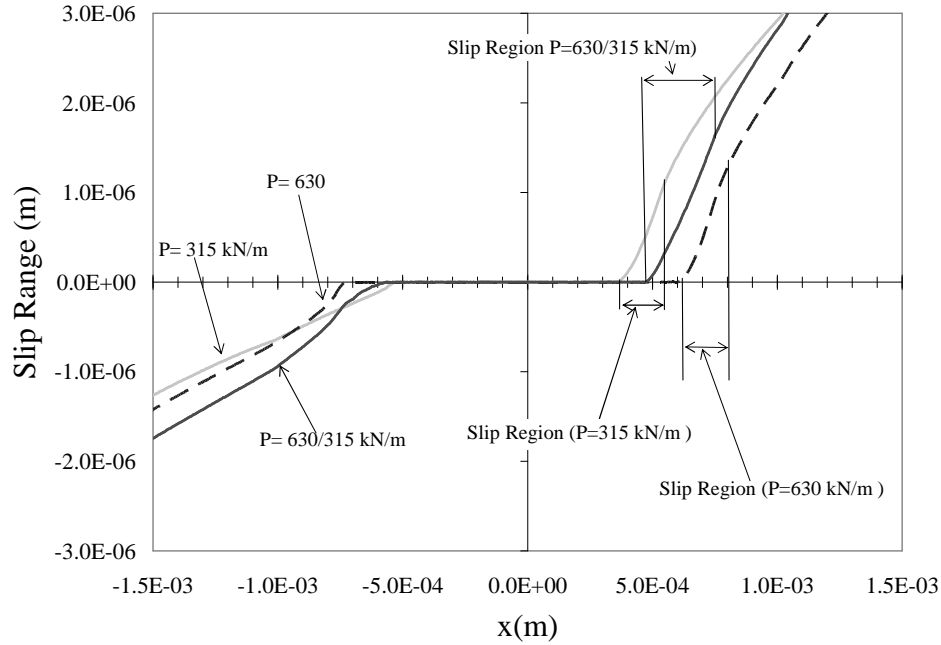
Figure 5.28. Slip Range Comparisons For Idealized Tests 1,2 and 3 with Uni-Directional Shear

5.3.3.2. Bi-Directional Shear.

The bi-directional shear tests have different contact trends than the uni-directional shear test as seen in Figure 5.29. This is most likely due to the difference in frequency and phasing of the contact load relative to the axial load between the uni-directional and bi-directional tests. In the case of the variable contact load case for which $\varphi_p = -90^o$, $P_{max}=700$ kN/m is applied at the same time the maximum axial stress is applied. The slip range for this case and the constant contact load case of $P_{const} = 700$ kN/m are similar. The same is true for the variable contact case with $\varphi_p = +90^o$ and the constant contact load case of $P_{const} = 350$ kN/m. On the other hand, the variable case with $\varphi_p = -90^o$ the stick zone through the loading cycle appears to be slightly less that that for the constant 700 kN/m contact load, however, only at the leading edge.
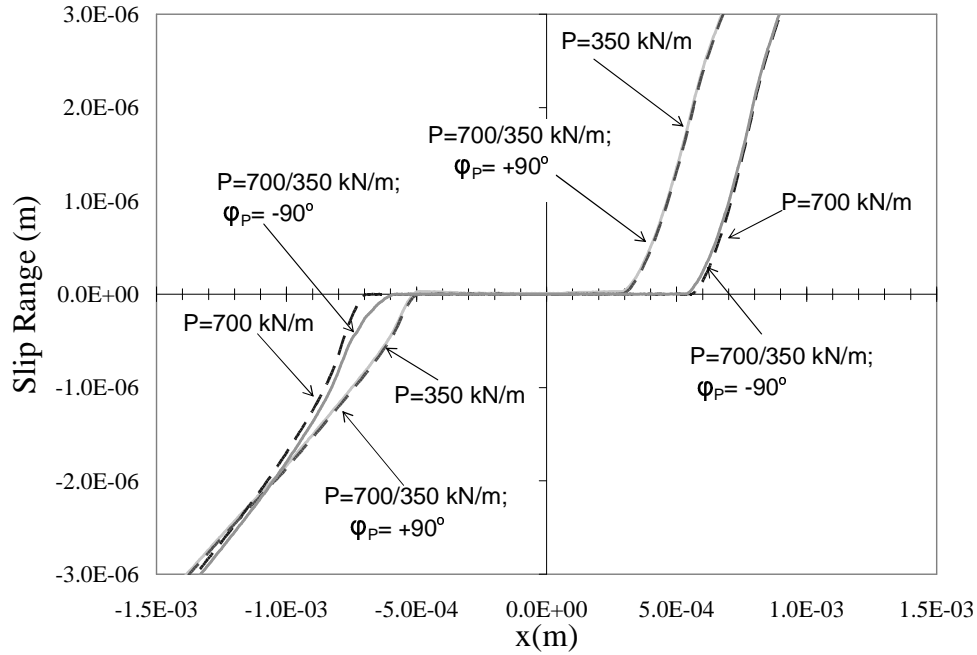
Figure 5.29. Relative Slip Range Comparisons for Idealized Load Test 4,5, 6 and 7 with Bi-Directional Shear.

5.4. Modified Shear Stress Range Parameter

The MSSR parameter, as discussed in Chapter 2, was evaluated for each experimental test as well as for loads used in the idealized loading cases. Predicted values of fatigue life, crack location and crack orientation based on the MSSR parameter are compared to the experimental results previously presented. Additionally, using stress results from the idealized loading conditions trends in the MSSR parameter were studied. Finally, changes to the modified shear stress parameter are proposed to account for the effect of a variable contact load

5.4.1. Namjoshi Parameter Program Output for Experimental Results

The relevant details of the MSSR parameter were discussed in Chapter 2. Using the "parameters program" written by Namjoshi [28], the MSSR parameter, as described in Chapter II, was determined using FEA results at locations along the specimen surface,

5.32

which were in the contact region. Output from the Namjoshi program based on stress

output from FEA are summarized in Table 5.4. The predicted values for crack location,

orientation and fatigue life will next be compared with those from experimental results.

Table 5.4. Summary of Modified Shear Stress Range Fatigue Parameter Terms Determined from FEA Stress Output and Namjoshi Parameter Program for Experimental Tests

P=Constant: Uni-Directional Shear									
Test #	P_{max} (kN/m)	P_{min} (kN/m)	P_{ϕ} (deg)	$\Delta\tau_{max}$ (MPa)	τ_{eff} (MPa)	S_{max} (MPa)	S_{min} (MPa)	θ (deg)	x/a
1	315	-	-	343	392	466	89	38	-0.93
2	350	-	-	350	411	503	125	37	-0.92
3	525	-	-	367	435	281	-113	-54	-0.92
4	525	-	-	371	438	542	144	36	-0.92
5	630	-	-	376	440	542	130	36	-0.93
6	630	-	-	375	439	540	131	36	-0.93
7	630	-	-	373	436	537	129	36	-0.93
8	700	-	-	383	457	578	159	36	-0.93

P=Variable; Uni-Directional Shear									
Test #	P_{max} (kN/m)	P_{min} (kN/m)	P_{ϕ} (deg)	$\Delta\tau_{max}$ (MPa)	τ_{eff} (MPa)	S_{max} (MPa)	S_{min} (MPa)	θ (deg)	x/a$_{max}$	x/a$_{min}$
9	630	315	0	376	436	528	121	36	-0.94	-1.33
10	630	315	0	375	436	285	-123	-53	-0.94	-1.33
11	700	350	0	393	444	221	251	28	-0.91	-1.29
12	700	350	0	380	435	216	234	27	-0.91	-1.29
13	700	525	0	395	461	378	210	32	-0.84	-0.97
14	700	525	0	382	455	575	169	35	-0.93	-0.93

P=Constant; Bi-Directional Shear									
Test #	P_{max} (kN/m)	P_{min} (kN/m)	P_{ϕ} (deg)	$\Delta\tau_{max}$ (MPa)	τ_{eff} (MPa)	S_{max} (MPa)	S_{min} (MPa)	θ (deg)	x/a
15	350	-	-	466	452	430	-68	40	-0.94
16	525	-	-	504	496	488	-62	40	-0.95
17	700	-	-	503	496	489	-60	40	-0.82

P=Variable; Bi-Directional Shear									
Test #	P_{max} (kN/m)	P_{min} (kN/m)	P_{ϕ} (deg)	$\Delta\tau_{max}$ (MPa)	τ_{eff} (MPa)	S_{max} (MPa)	S_{min} (MPa)	θ (deg)	x/a$_{max}$	x/a$_{min}$
18	700	350	90	507	482	320	-226	-50	-0.66	-0.93
19	700	350	90	522	488	458	-117	40	-0.66	-0.93
20	700	350	90	509	478	322	-233	-50	-0.67	-0.94
21	700	350	-90	558	538	518	-100	39	-0.94	-0.94
22	700	350	90	483	466	442	-77	40	-0.67	-0.94
23	700	525	90	457	442	39	398	-65	-0.81	-1.15

5.4.1.1. Crack Location Prediction.

Crack location, x/a, was predicted to be near the trailing edge of contact for all constant contact load tests as seen in Table 5.4. In Table 5.4 two crack locations, x/a_{max} and a/a_{min}, were determined for test with variable contact. a_{max} and a_{min} correspond to the maximum and minimum contact widths occurring during the load cycle. Notice that for variable load test the location of crack initiation most often occurs at the edge of contact corresponding to the point when maximum axial load is applied. For the uni-directional crack initiation is predicted near the trailing edge of a_{max}. For the bi-directional shear test with a phase angle, φ_P, of -90° the crack initiation is predicted near the trailing edge of , a_{max} which occurs when $P=P_{max}$ and $\sigma_{axial}=\sigma_{axial,max}$. For bi-directional shear test with $\varphi_P =$ +90° crack initiation prediction ed at the edge of contact, a_{min} which occurs when $P=P_{min}$. and axial load is maximum. Specimens 13 and 23 show exceptions to this trend. It can be said that the MSSR parameter's prediction of crack location is dependent on the applied axial load. Nonetheless it did predict the general location of crack initiation location i.e. near the trailing edge of contact for all test.

5.4.1.2. Crack Orientation Prediction.

Crack orientation as determined using the MSSR parameter was compared to the experimentally observed crack orientation angle for Test #18 as seen previously in Figure 5.15. The predicted and observed angles were in close agreement with both equaling -50°. The third criterion for evaluation of the MSSR fatigue parameter is its ability to predict fatigue life.

5.4.1.3. Fatigue Life Prediction.

In principle the MSSR parameter as set forth by Namjoshi et al. [29] and discussed in Chapter 2 should increase in value as fatigue life decreases. Therefore, based on experimental results obtained in this study the MSSR parameter should be greater for test with a variable normal load than for those with a constant normal load all else being the same. The MSSR parameter as presented by Namjoshi et al. was determined for the experimental test of this study using FEA and compared to the curve which Namjoshi et al. fit to their results. As seen in Figure 5.30 the MSSR parameter as determined for test of this study does not fall along this curve fit. Also, the parameter fails to increase in value for loading conditions i.e. variable contact load, which has been observed to decrease fatigue life as seen in Figures 5.31and 5.32 with the exception of the bi-directional shear test with $\varphi_P = -90^{\circ}$. Table 5.5 on pg 5.54 list the values of the MSSR parameter for the experimental tests as determined using the formulation described above.
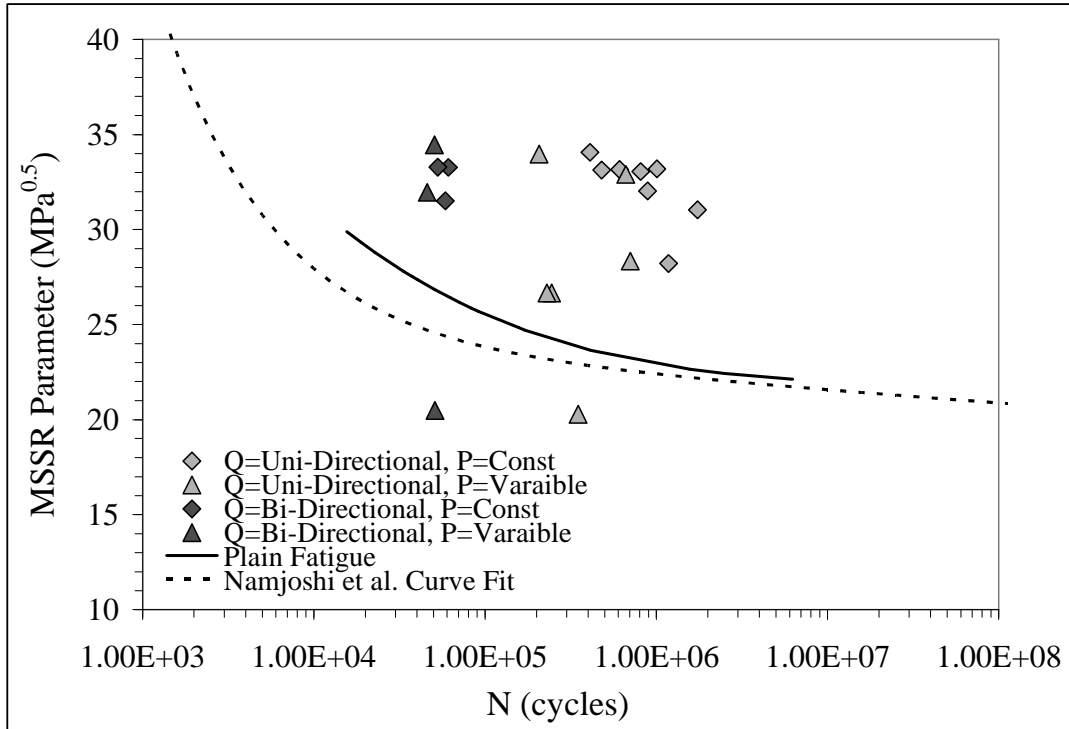
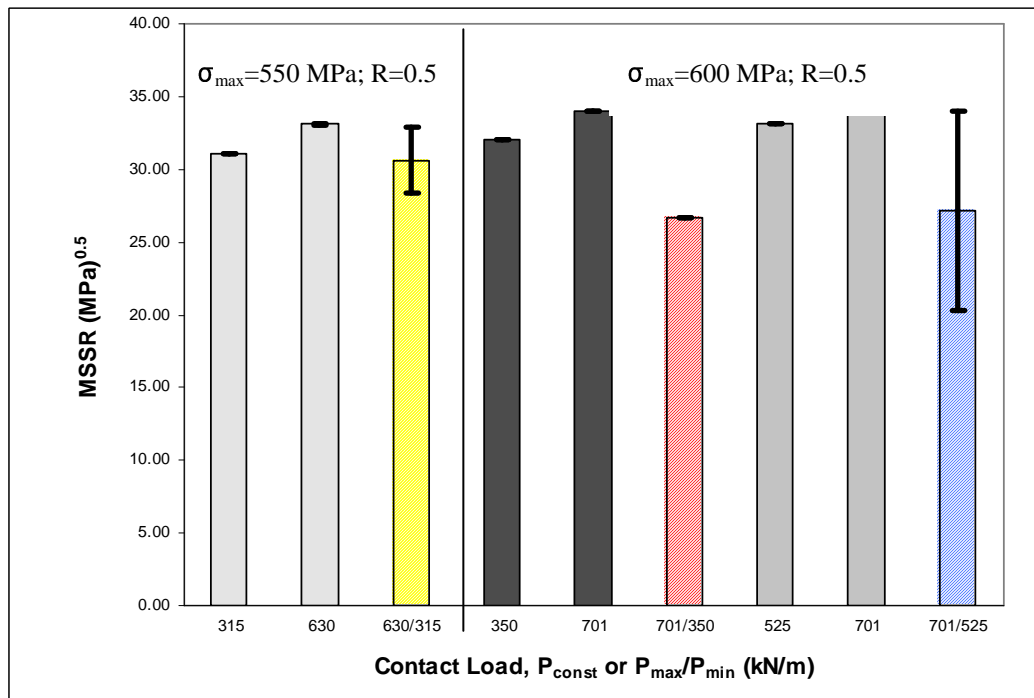Figure 5.30. MSSR for Experimental Test Determined using Namjoshi et al. Method and Stresses from FEA

Figure 5.31. MSSR for Experimental Test determined using Namjoshi et al. Method and Stresses from FEA
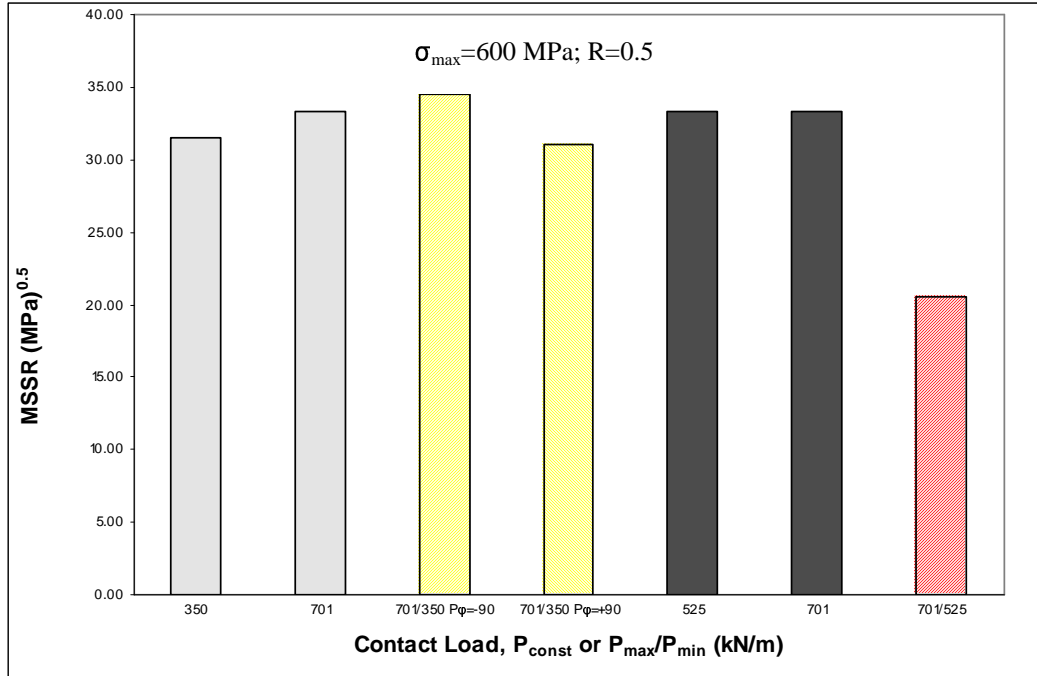
Figure 5.32. MSSR as Defined Namjoshi et al For Experimental Test with Bi-Directional Shear

5.4.1.4. Alternate MSSR Parameter Formulation Fatigue Life Prediction.

Contemporary AFIT researcher Maj Ki Su Shin has suggested a slight variation to the MSSR parameter. He has suggested using the absolute difference between the maximum and minimum values of normal stress on the critical plane i.e. $|S_{max}-S_{min}|$, at the point which shear stress range on the critical plane, $\Delta\tau_{max}$, is maximum, rather than using the maximum value of the normal stress, S_{max}, at the same point. Figure 5.33 shows a plot of the MSSR parameter values for test of this study using the formulation of the MSSR parameter just described. The MSSR parameter values do collapse well for constant contact loads, however, this formulation fails to collapse the data in a desirable range for variable contact load tests. Also, as seen in Figures 5.34 and 5.35, this formulation of the MSSR parameter also fails to increase in value for variable loading

conditions, which have been observed to decrease fatigue life. Again the bi-directional shear test with $\varphi_P = -90^o$ is the only exception. Table 5.5 lists the values of the MSSR parameter for the experimental tests as determined using the formulation described above.
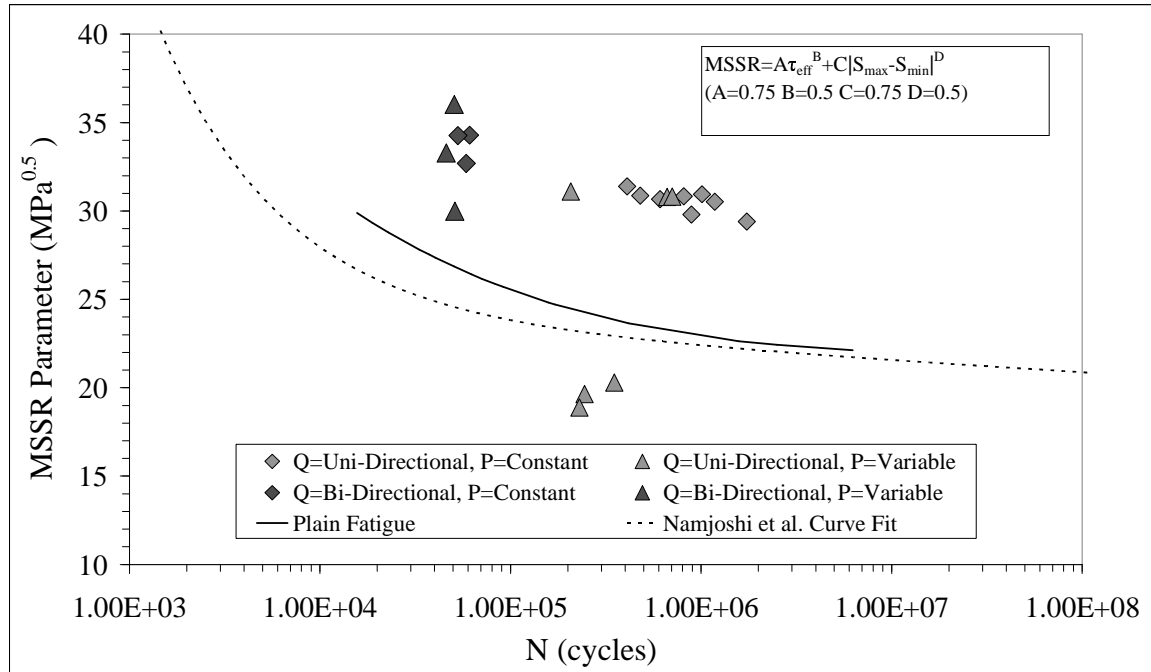

Figure 5.33. MSSR Determined Using Absolute Difference Between S_{max} and S_{min} at Surface Location with Maximum Shear Span Using Stresses from FEA.

Figure 5.34. MSSR Using Absolute Difference Between S_{max} and S_{min} at Surface Location with Maximum Shear Span using Stresses from FEA for Uni-Directional Shear Tests with Various Loading Conditions.

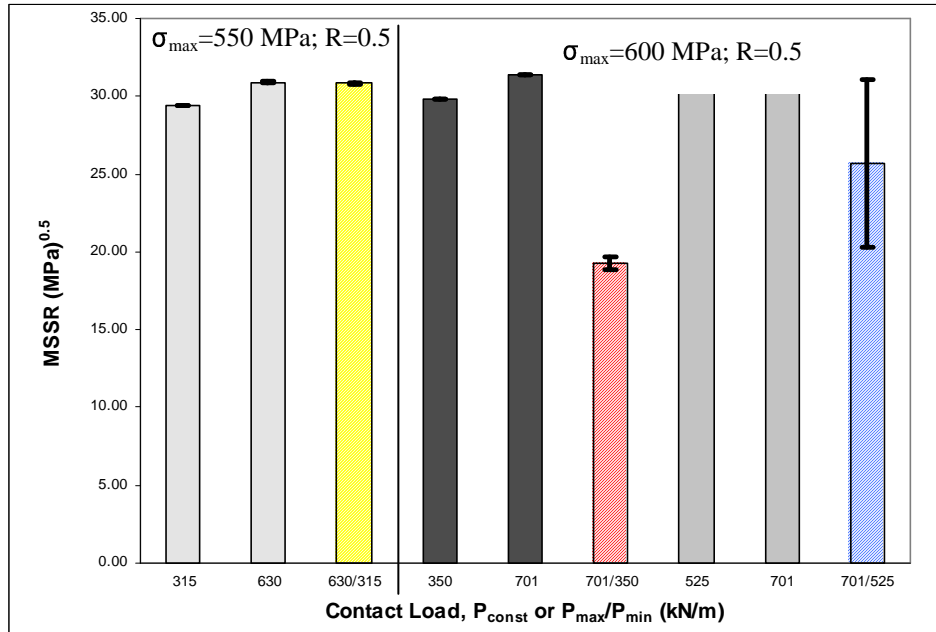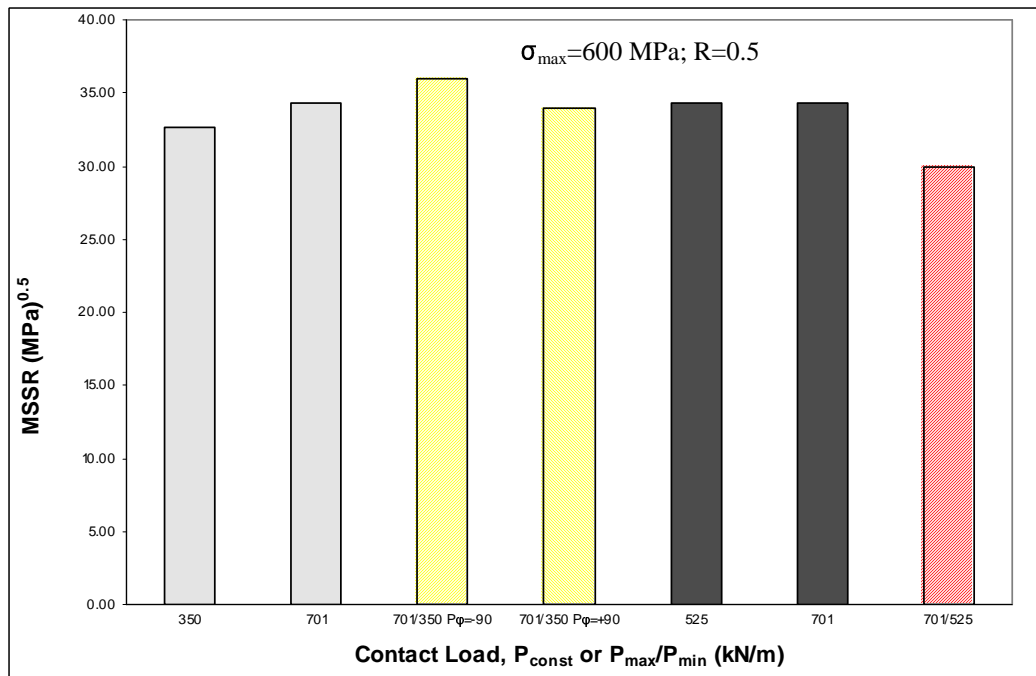Figure 5.35. MSSR Determined Using Absolute Difference Between S_{max} and S_{min} at Surface Location with Maximum Shear Span using Stresses from FEA for Bi-Directional Shear Tests with Various Loading Conditions

5.39

5.4.2. Namjoshi Parameter Program Output for Numerical Tests

As seen thus far the two methods of formulating the MSSR predictive fatigue

parameter failed to predict fatigue life for experimental tests with variable contact load.

In experimental testing axial and shear loads varied somewhat between tests. The results

of both MSSR parameters discussed above include these variations in axial and shear

loads.   On the other hand, in the tests of the idealized cases, which were discussed in a

previous section, axial shear loads were held constant. Therefore, the influence of a

variable contact load and waveform on the MSSR parameter can be studied and the

influence of variations in the shear and axial loads can be eliminated. Also, trends

observed from the MSSR parameter as determined from the results of the idealized load

conditions may reveal a general trend in the MSSR parameter and/or provide insight into

a modification which could be made to the parameter to yield the desired results for all

contact load conditions. Table 5.6 on pg 5.55 lists the value output from the parameters

program as well as the MSSR parameter values as determined for the numerical studies

using the two methods discussed above.

5.4.1.4. Prediction of Fatigue Life Trend.

Results from the idealized loading conditions reveals neither method described

above yields a desirable trend relative the trend in fatigue life with respect to contact load

as observed experimentally for both uni-directional and bi-directional shear tests. The

MSSR value of the uni-directional shear test with variable contact load falls between that

of the higher and lower constant contact load. Also the MSSR values for the bi-

directional shear test with variable contact load and $\varphi_P = -90^o$ and $\varphi_P = +90^o$ are nearly

equal to the MSSR parameter for the higher and lower constant contact loads respectively.

5.4.1.5. MSSR Parameter Details.

Further insight into the MSSR parameter's ability to predict fatigue life can be obtained by examining the trends in the terms, which compose the parameter. Figures 5.36 5.37 and 5.38 starting on pg 5.42 shows $\Delta\tau_{max}$, τ_{eff}, S_{max}, S_{min}, and $|S_{max}-S_{min}|$ values along the contact surface for idealized loading cases 1, 2 and 3 with uni-directional shear. Figures 5.40, 5.41, and 5.43 starting on pg 5.44 show comparisons of $\Delta\tau_{max}$, τ_{eff}, S_{max}, S_{min}, and $|S_{max}-S_{min}|$ for the three idealized uni-directional shear tests. Notice from Figures 5.40, 5.41, and 5.43 that for the variable normal loading case, Case 3, the maximum value of all these terms which make up the MSSR parameters as discussed previously i.e. τ_{eff} and σ_{max} for MSSR defined by Namjoshi et al. [29] and when τ_{eff} and $|S_{max}-S_{min}|$ are used to calculate the MSSR, are all less in value that for the same terms for constant contact load cases 1 and 2 with the same lower and higher contact loads respectively. Also, note from Figure 5.38 that for Case 3 with a variable contact load $\Delta\tau_{max}$ and τ_{eff} reach their maximum values at different locations unlike for constant contact load Cases 1 and 2. Therefore, with the formulation of the MSSR parameter as discussed in the previous sections it is not mathematically possible for the MSSR to be greater for the variable case because the terms τ_{eff}, σ_{max}, and $|S_{max}-S_{min}|$, are all less than those for the higher and lower constant contact loads at the point which the MSSR is calculated, i.e. surface location, x, at which shear stress range, $\Delta\tau(x)$, is at its maximum value, $\Delta\tau_{max}$. For the variable load case $|S_{max}-S_{min}|$ is a near the location of minimum

5.41

value of $\Delta\tau_{max}$ and a maximum at the point where τ_{eff} is a maximum as seen in Figure 5.38. The same is not true for the uni-directional shear test with a constant load.
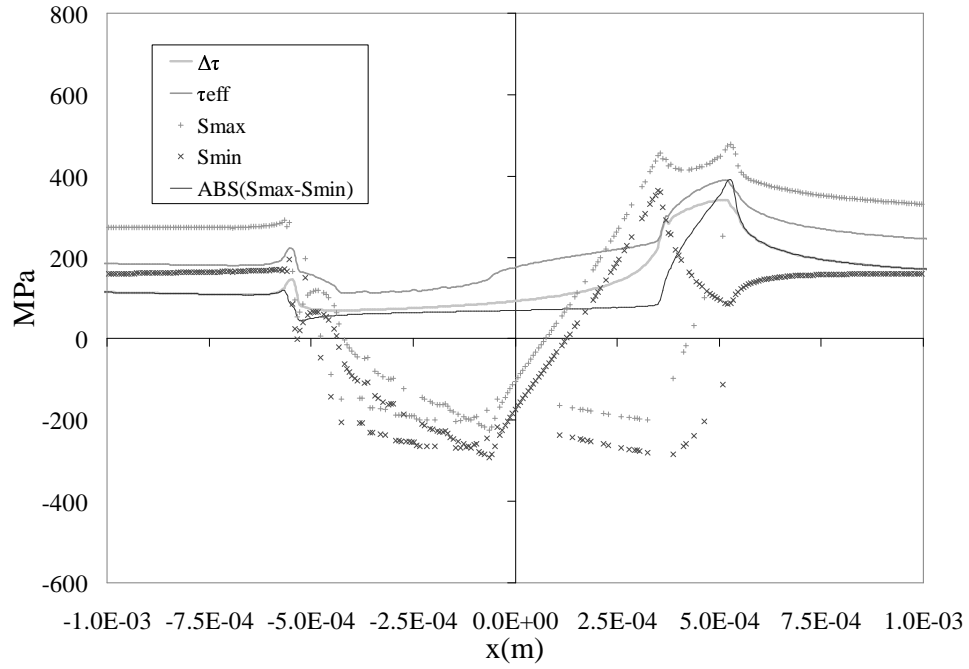

Figure 5.36 . MSSR Terms Along Contact Surface of Idealized Uni-Directional Shear Test, $P_{const} = 315$ kN/m
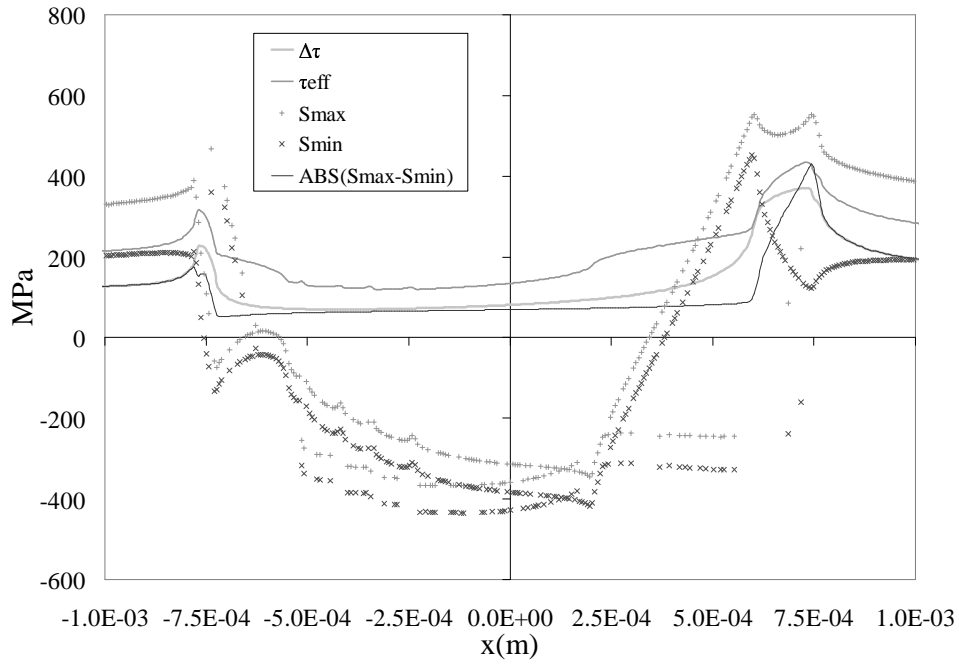
Figure 5.37. MSSR Terms Along Contact Surface of Idealized Uni-Directional Shear
Test, P_{const} = 630 kN/m
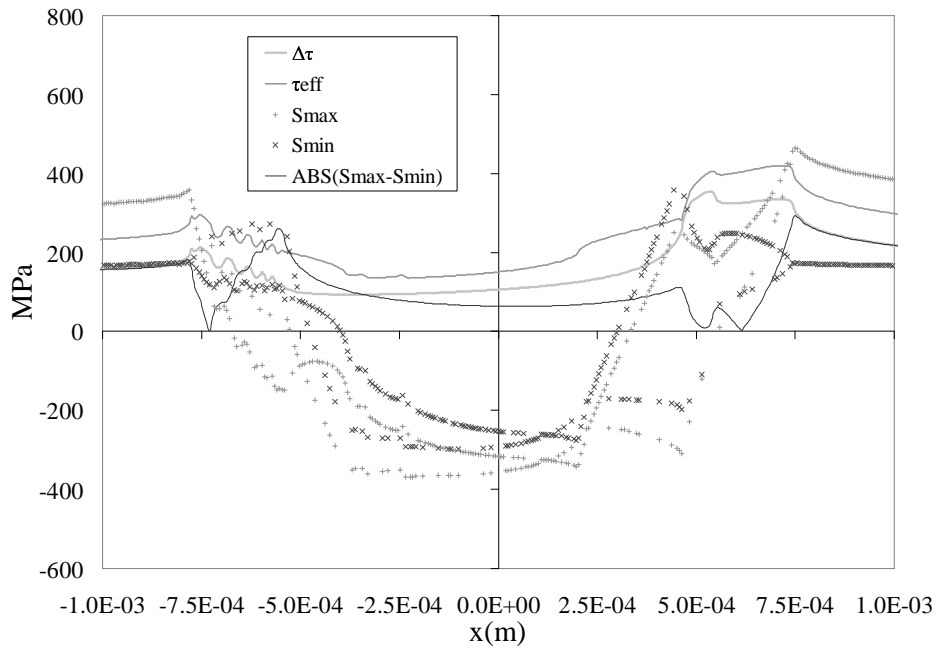
Figure 5.38 MSSR Terms Along Contact Surface of Idealized Uni-Directional Shear
Test; P_{max} = 630 kN/m, P_{min}=315 kN/m

Figure 5.39. Comparison of MSSR Term, $\Delta\tau$, Along Contact Surface for Idealized Uni-Directional Shear Test.

Figure 5.40. Comparison of MSSR Term, τ_{eff}, Along Contact Surface for Idealized Uni-Directional Shear Test

5.44

Figure 5.41. Comparison of MSSR Term, S$_{max}$, Along Contact Surface for Idealized Uni-Directional Shear Test
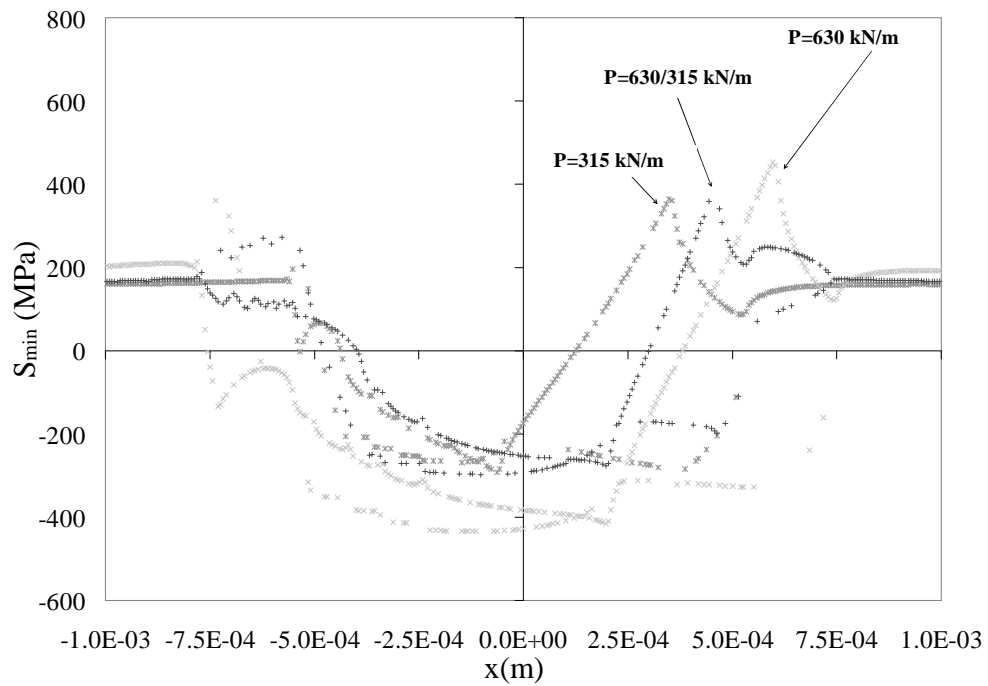
Figure 5.42. Comparison of MSSR Term, S$_{min}$, Along Contact Surface for Idealized Uni-Directional Shear Test

5.45

Figure 5.43. Comparison of MSSR Term, $|S_{max} - S_{min}|$, Along Contact Surface for Idealized Uni-Directional Shear Test.

Turning our attention to idealized test with bi-directional shear it can be seen in Figures 5.44 thru 5.52. , which start on the next page, that the terms of the MSSR parameter are nearly identical for the case of $P_{const}=350$ kN/m and the variable case with $\varphi_P= +90^o$. For the constant contact load of 700 kN/m and the variable case with $\varphi_P= -90^o$ the magnitude and location of the maximum value of the MSSR terms are very similar.

From the plots of MSSR term values along the surface of contact it can be seen that using the current formulations for the MSSR parameter the desired trend between fatigue life and experimentally observed loading condition cannot be achieved.
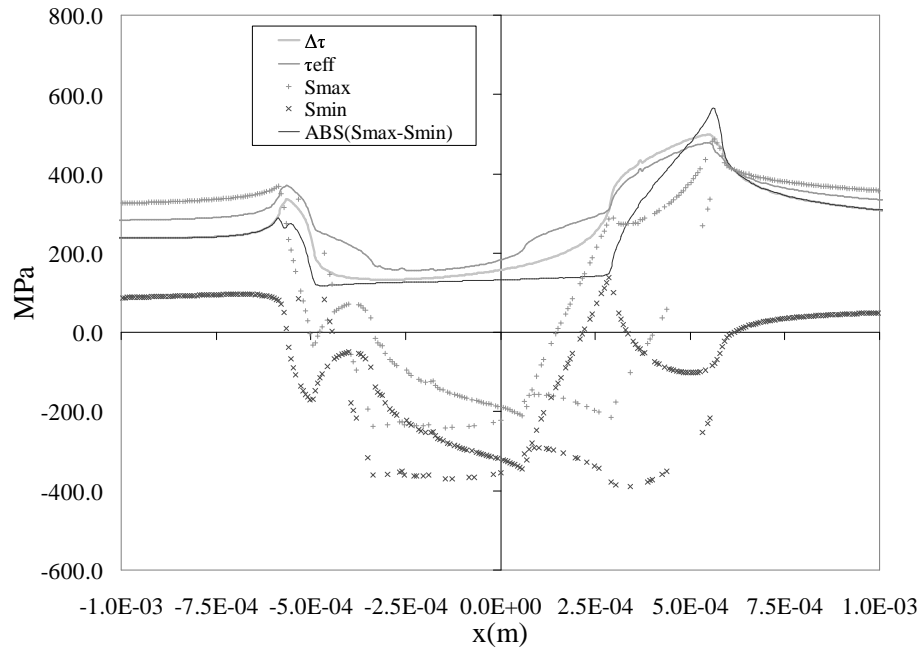
Figure 5.44. Comparison of MSSR Terms Along Contact Surface of Idealized Bi-Directional Shear Test, $P_{const} = 350$ kN/m

.
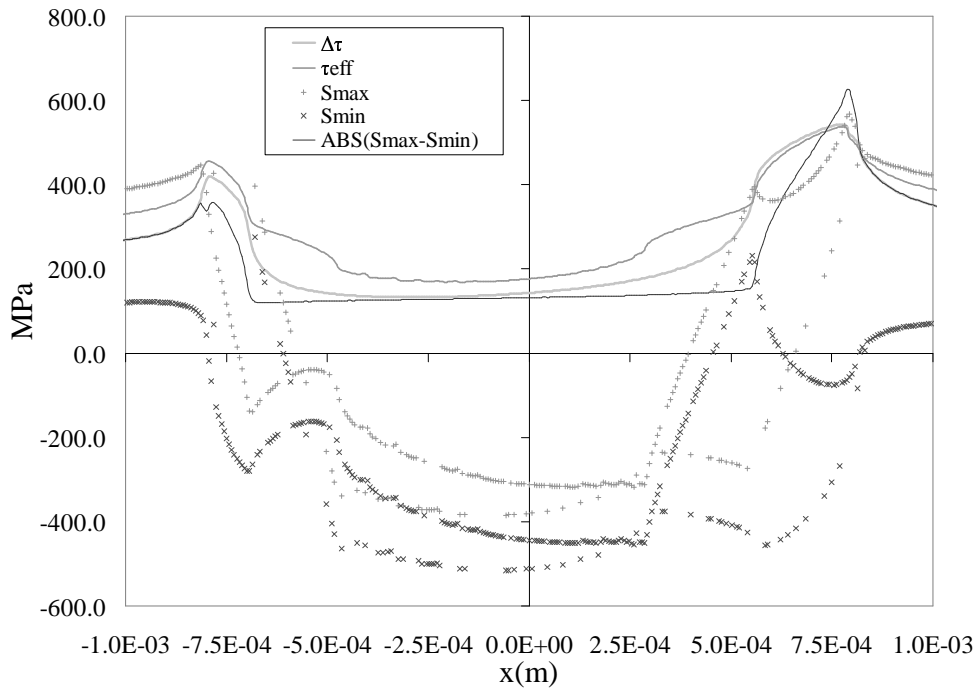
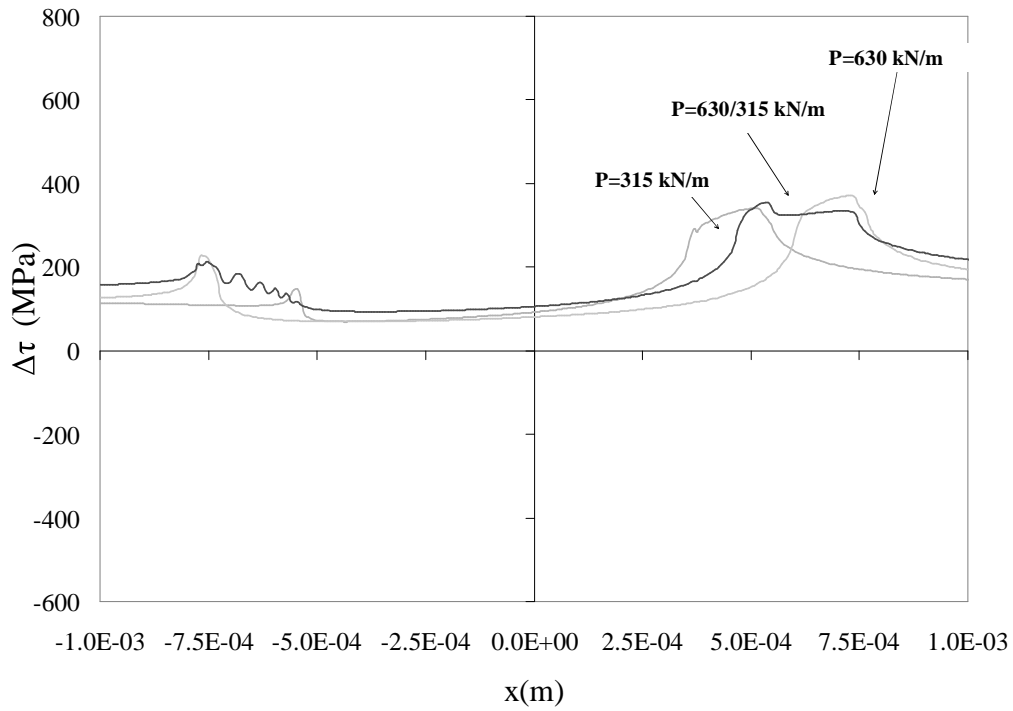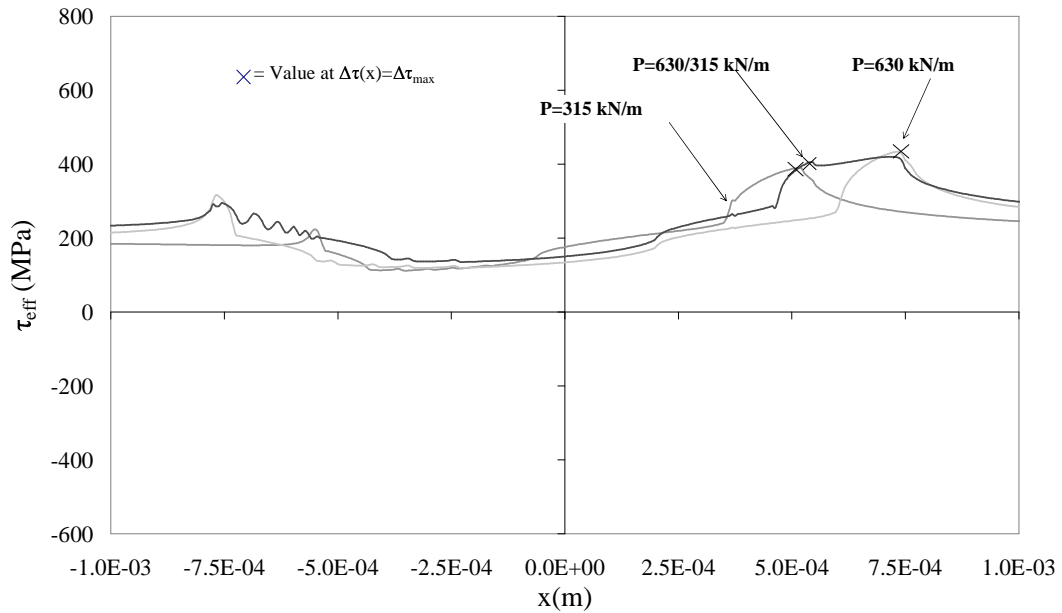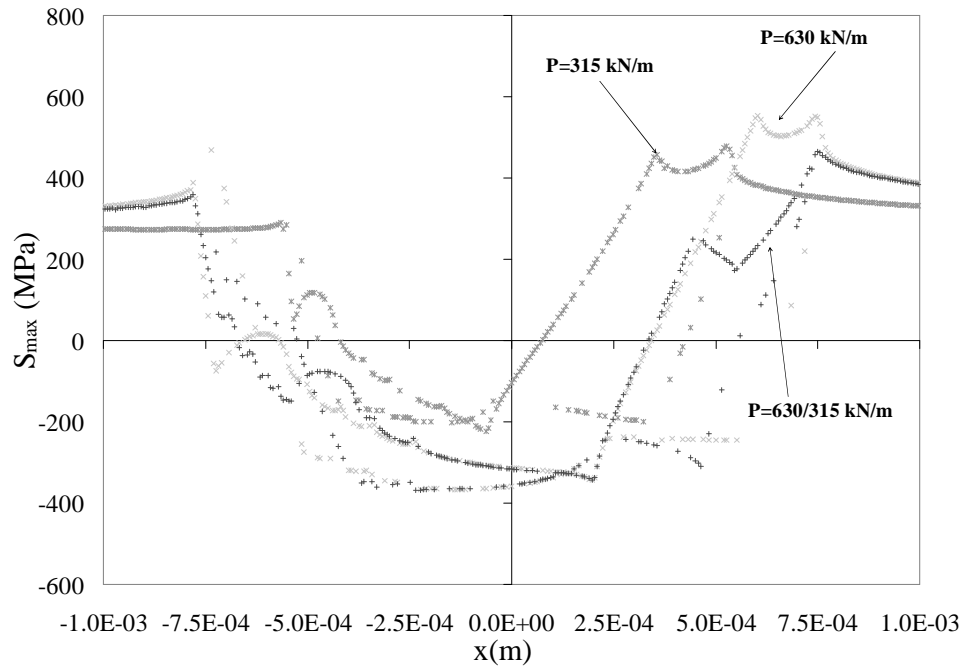Figure 5.45. Comparison of MSSR Terms Along Contact Surface of Idealized Bi-Directional Shear Test, $P_{const} = 700$ kN/m

5.47
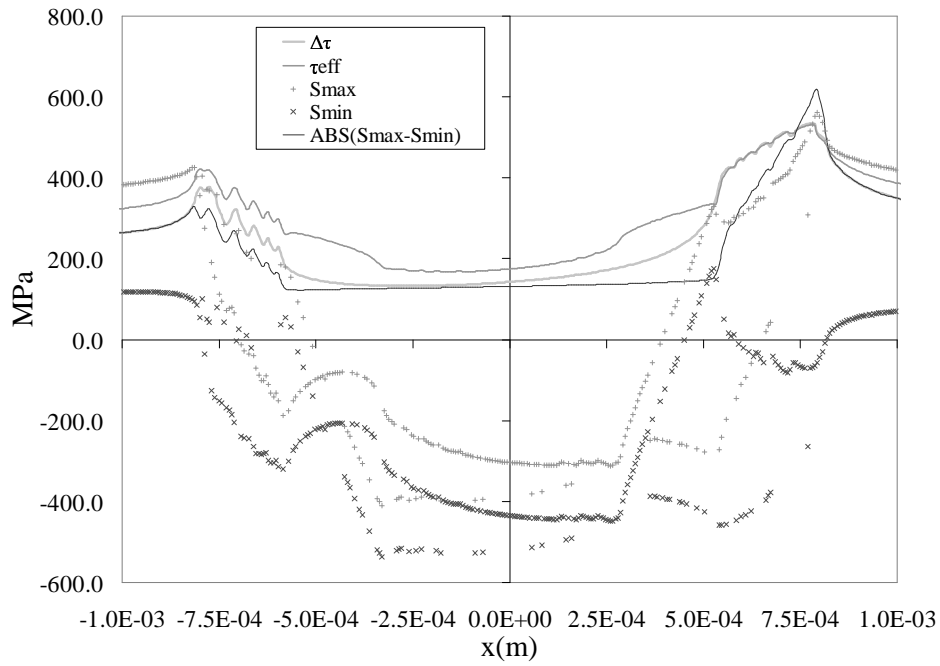
Figure 5.46. Comparison of MSSR Terms Along Contact Surface of Idealized Bi-Directional Shear Test; P_{max} = 700 kN/m, P_{min} = 350 kN/m with -90° phase
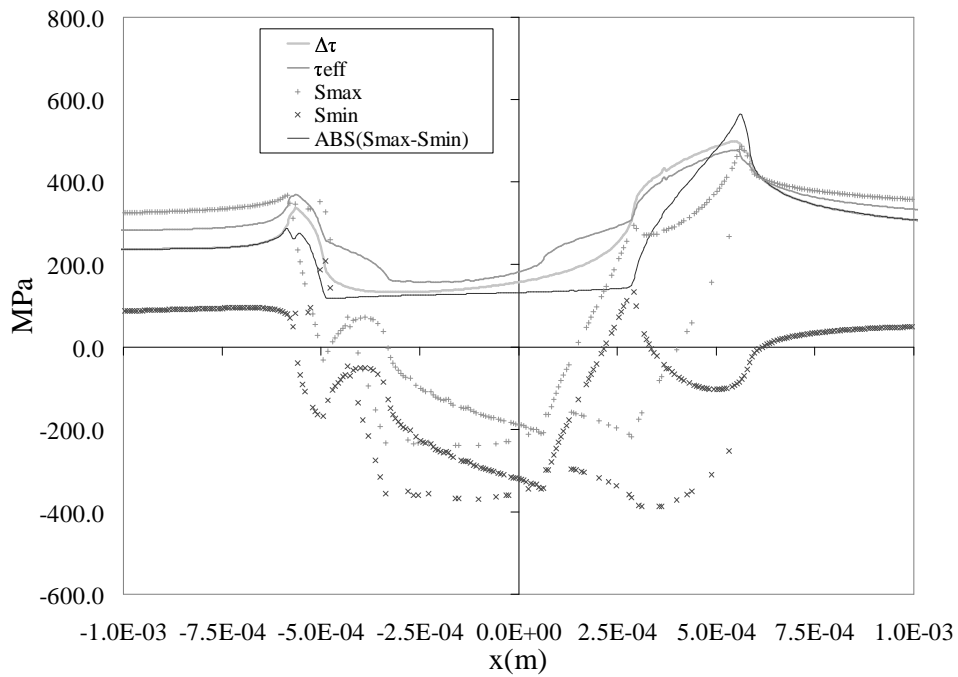
Figure 5.47. Comparison of MSSR Terms Along Contact Surface of Idealized Bi-Directional Shear Test; P_{max} = 700 kN/m, P_{min} = 350 kN/m with +90° phase

5.48
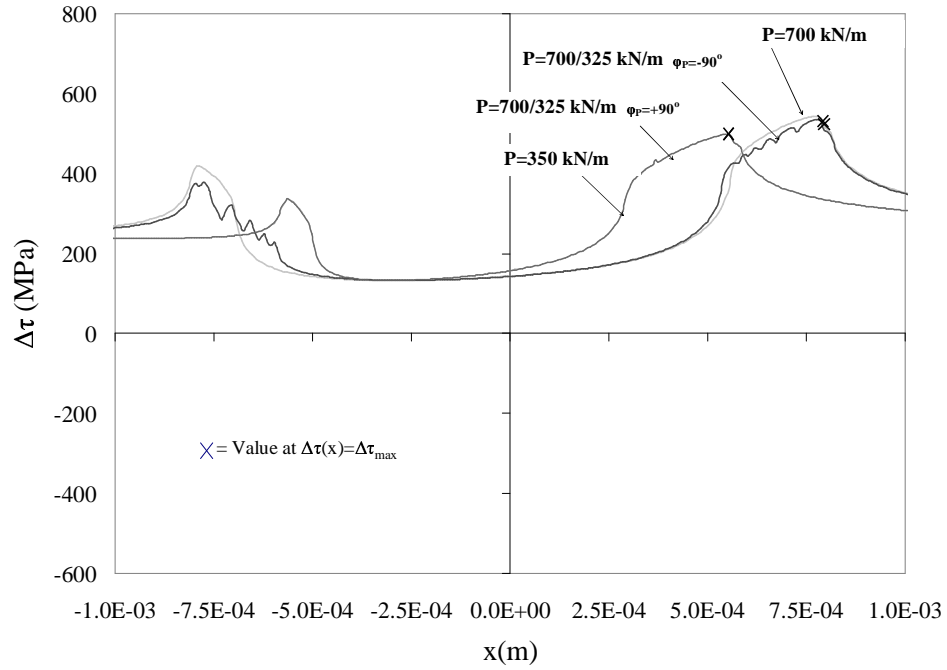
Figure 5.48. Comparison of MSSR Term, $\Delta\tau$, Along Contact Surface for Idealized Bi-Directional Shear Tests
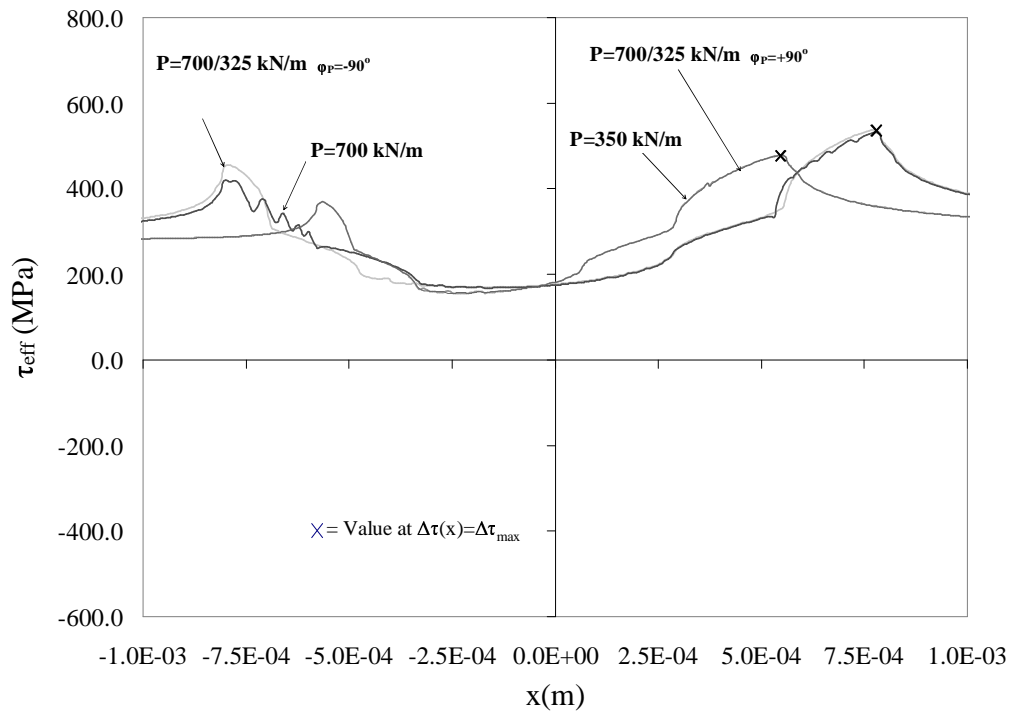
Figure 5.49. Comparison of MSSR Term, τeff, Along Contact Surface for Idealized Bi-Directional Shear Test.
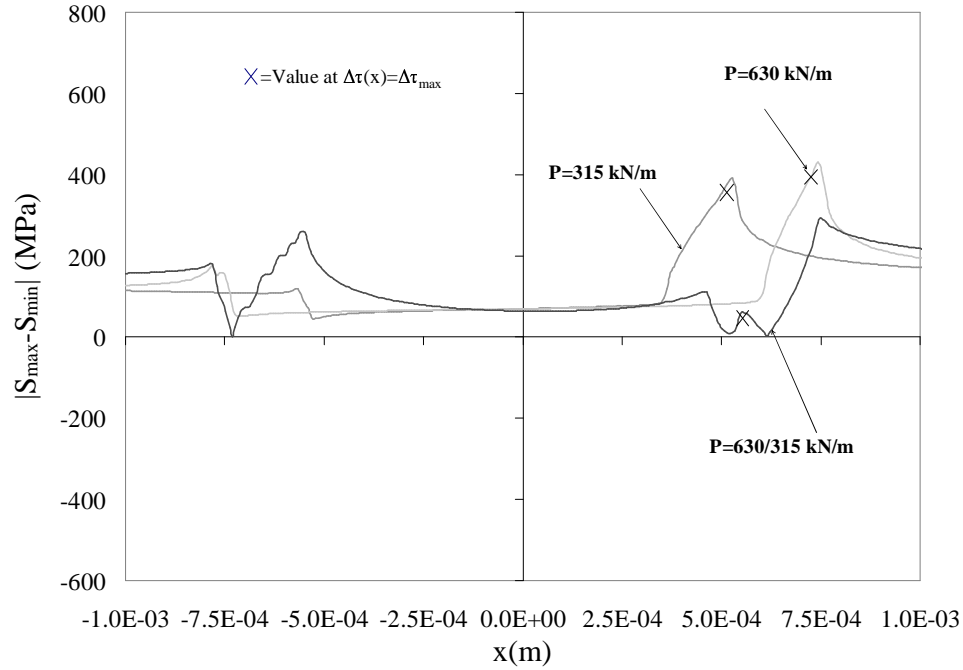
5.49
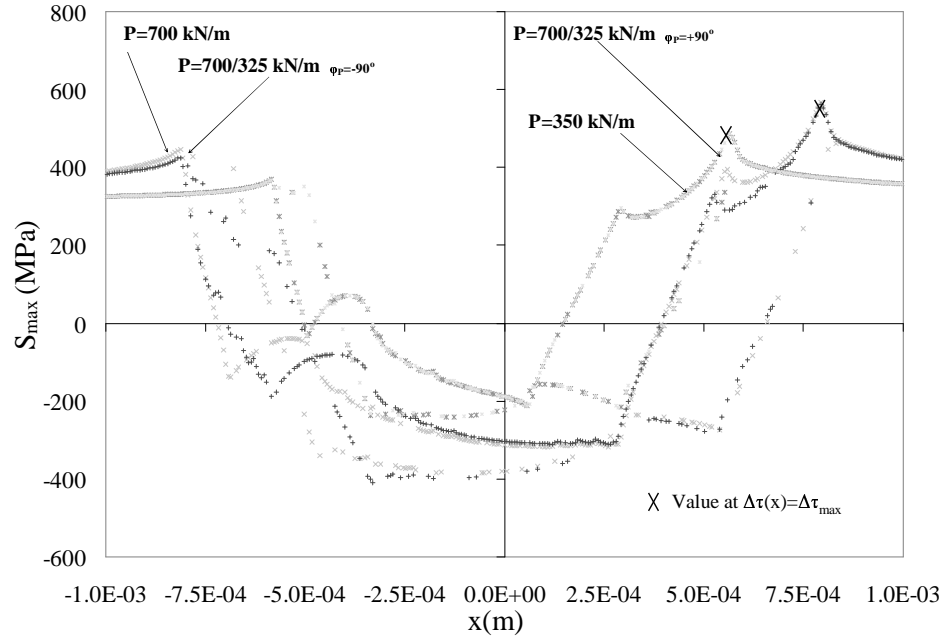
Figure 5.50. Comparison of MSSR Term, S_{max}, Along Contact Surface for Idealized Bi-Directional Shear Test.
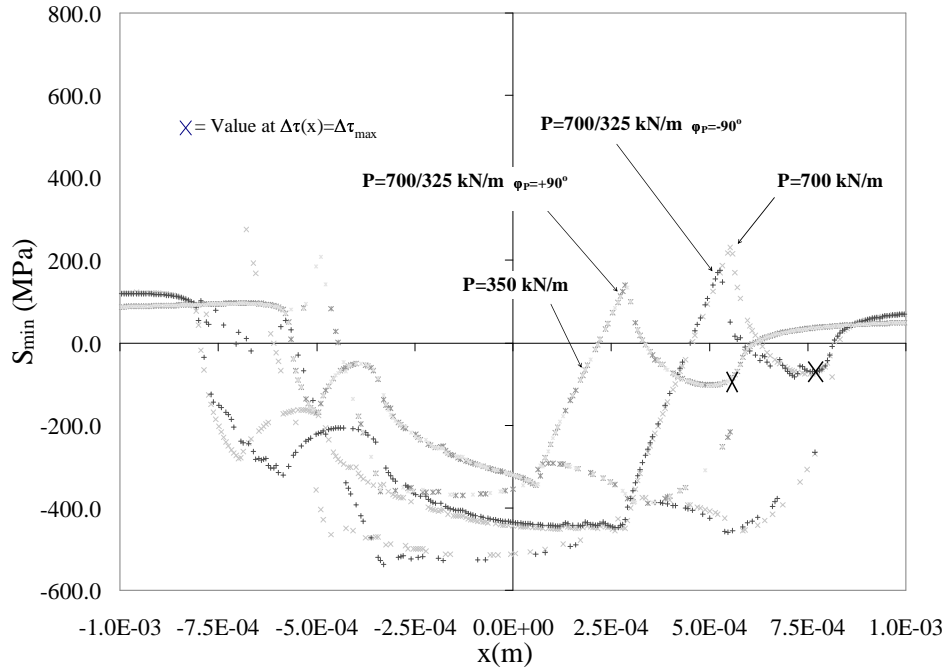
Figure 5.51. Comparison of MSSR Term, S_{min}, Along Contact Surface for Idealized Bi-Directional Shear Tests.
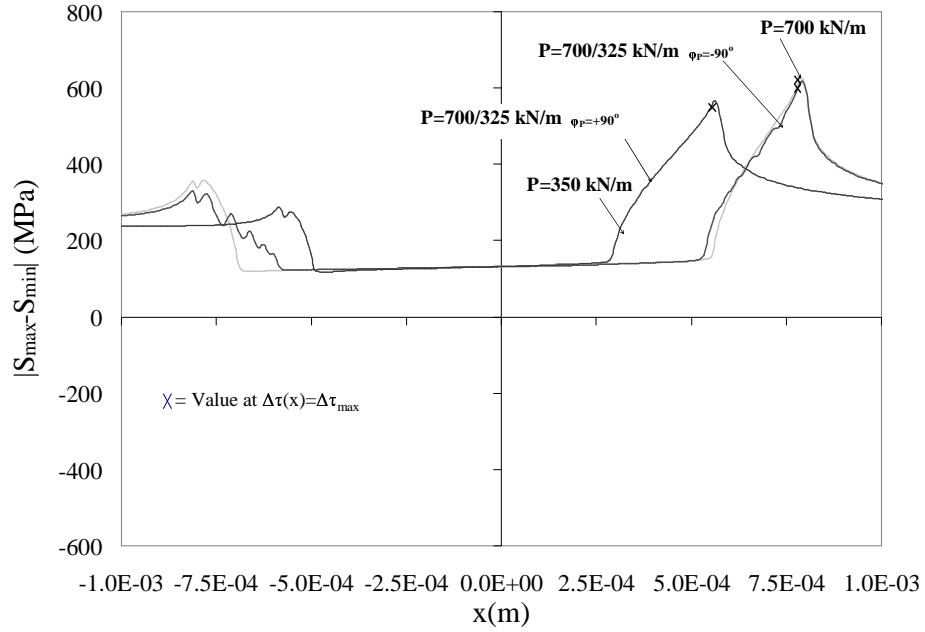
Figure 5.52. Comparison of MSSR Term, $|S_{max} - S_{min}|$, Along Contact Surface for Idealized Bi-Directional Shear Tests.

5.5. Proposed Modifications to MSSR Parameter

Namjoshi et al [29] were not able to conclude the exact role of normal stress on the critical plane from their study. Furthermore, the coefficients proposed by Namjoshi et al. were based on an empirical curve fit to experimental data for various pad geometries. Therefore, it is reasonable to modify the coefficients empirically to fit the experimental data from this study. In doing so it is desirable to maintain the relationship between fatigue life and the MSSR parameter for the data from Namjoshi et al.

In manipulating the coefficients of the MSSR parameter it is desired to select values which place the proper emphasis on the terms which compose the parameter i.e. τ_{eff} and σ_{max} or $|S_{max}-S_{min}|$ depending on the formulation used.

5.51

From the analysis of the MSSR terms for various loading conditions of the numerical experiments as discussed previously it was observed that at the location of $\Delta\tau_{max}$ all values of the MSSR terms for the variable contact load case were less than those of the constant contact load cases with τ_{eff} being near the value of τ_{eff} for the higher constant contact load. Also, S_{max}, was less than those values for the higher constant contact load and S_{min} and $|S_{max}-S_{min}|$ were less than the same terms for both constant contact load cases with uni-directional shear. Therefore, based on these observations, a new value for the coefficients, A and C, and exponents, B and D, of the MSSR parameter are proposed. In order to reverse the influence of the absolute difference in difference between S_{max} and S_{min} at the point where shear stress range is maximum the following coefficients and exponent values are proposed: A=.25 B=.75 C=25 and D=-1. Values of the MSSR determined using these coefficients are listed in Table 5.5. Figure 5.53 shows the MSSR parameter determined for test of this study as well as for the 2 inch radius pad case from Lykins using the newly proposed coefficients versus fatigue life. The curve fit used by Namjoshi et al is also included on Figure 5.53 for comparison. The MSSR formulation using $|S_{max}-S_{min}|$ as shown in Figure 5.53 shows a better relationship between MSSR values and fatigue life thus far.
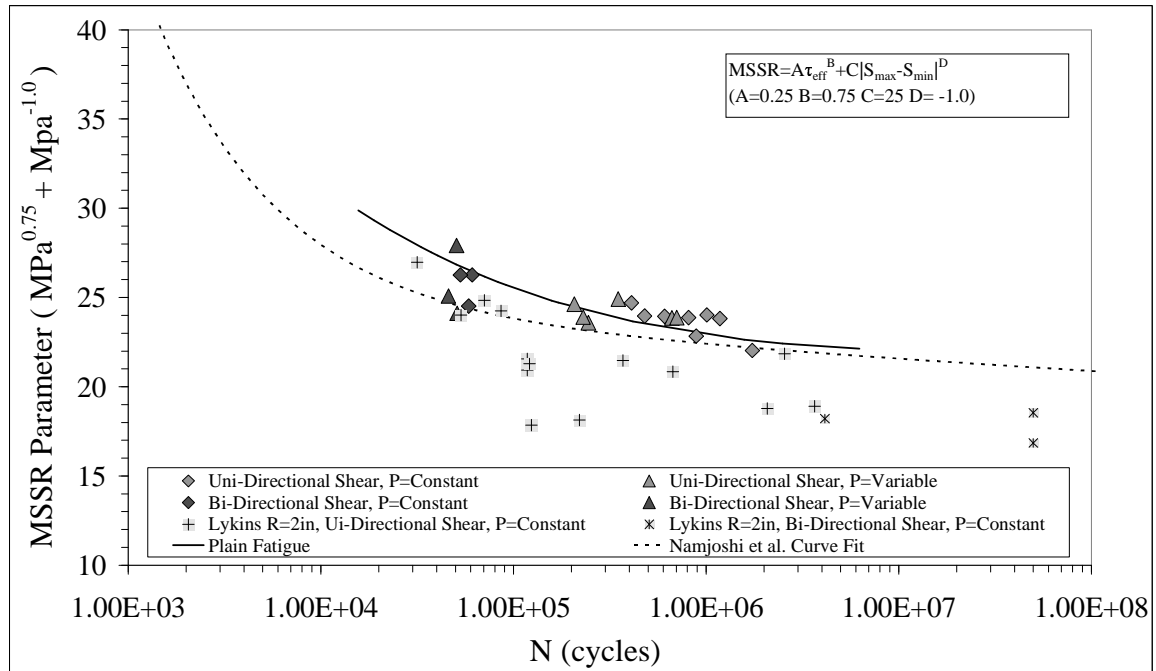
5.52

Figure 5.53. MSSR Parameter Value Relationship to Fatigue Life for Experimental Test Data from this Study and 2" Radius Pad from Lykins [19]

Table 5.5. Summary of Modified Shear Stress Range Predictive Parameter Values for Experimental Tests

Test #	P_{max} (kN/m)	P_{min} (kN/m)	P_{φ} (deg)	$MSSR_1$	$MSSR_2$	$MSSR_3$	N (cycles)
P=Constant: Uni-Directional Shear							
1	315	-	-	31.04	24.69	22.1	1.74E+06
2	350	-	-	32.03	25.43	22.9	8.89E+05
3	525	-	-	28.21	26.16	23.9	1.18E+06
4	525	-	-	33.16	26.29	24.0	6.10E+05
5	630	-	-	33.20	26.15	24.1	1.01E+06
6	630	-	-	33.13	26.08	24.0	4.80E+05
7	630	-	-	33.05	26.03	23.9	8.12E+05
8	700	-	-	34.07	26.56	24.8	4.10E+05

Test #	P_{max} (kN/m)	P_{min} (kN/m)	P_{φ} (deg)	$MSSR_1$	$MSSR_2$	$MSSR_3$	N (cycles)
P=Variable; Uni-Directional Shear							
9	630	315	0	32.90	26.39	23.9	6.64E+05
10	630	315	0	28.33	26.41	23.9	7.05E+05
11	700	350	0	26.69	27.24	24.4	2.45E+05
12	700	350	0	27.13	28.15	25.2	2.30E+05
13	700	525	0	30.69	21.53	25.7	3.50E+05
14	700	525	0	33.98	26.71	25.7	2.07E+05

Test #	P_{max} (kN/m)	P_{min} (kN/m)	P_{φ} (deg)	$MSSR_1$	$MSSR_2$	$MSSR_3$	N (cycles)
P=Constant; Bi-Directional Shear							
15	350	-	-	31.50	27.62	24.6	5.86E+04
16	525	-	-	33.27	29.08	26.3	6.10E+04
17	700	-	-	33.28	29.06	26.3	5.30E+04

Test #	P_{max} (kN/m)	P_{min} (kN/m)	P_{φ} (deg)	$MSSR_1$	$MSSR_2$	$MSSR_3$	N (cycles)
P=Variable; Bi-Directional Shear							
18	700	350	90	29.90	28.81	25.8	6.90E+04
19	700	350	90	32.61	29.02	26	4.95E+04
20	700	350	90	29.85	28.85	25.6	5.07E+04
21	700	350	-90	34.46	30.66	28	4.60E+04
22	700	350	90	31.96	28.16	25.1	5.10E+04
23	700	525	90	30.74	31.57	24.2	5.10E+04

$_1$ $MSSR = A(\tau_{eff})B + C\sigma_{max}^{D}$ A=0.75 B=0.5 C=0.75 D=0.5

$_2$ $MSSR = A(\tau eff)B + C(|\sigma_{max}-\sigma_{min}|)^{D}$ A=0.75 B=0.5 C=0.75 D=0.5

$_3$ $MSSR = A(\tau eff)B + C(|\sigma_{max}-\sigma_{min}|)^{D}$ A=0.25 B=0.75 C=25 D=-1.0

Table 5.6. Summary of Modified Shear Stress Range Fatigue Parameter Determined From FEA Stress Output and Namjoshi Parameter Program for Idealized Loads

P=Constant: Uni-Directional Shear											
Case #	P_φ deg	$\Delta\tau$max MPa	τ_{eff} MPa	θ deg	Smax MPa	Smin MPa	x/a		$MSSR_1$	$MSSR_2$	$MSSR_3$
1	-	341	389	-54	253	-112.59	-0.92		26.7	29.1	22.0
2	-	371	434	36	535	129.26	-0.93		33.0	30.1	23.8

P=Variable; Uni-Directional Shear											
Case #	P_φ deg	$\Delta\tau$max MPa	τ_{eff} MPa	θ deg	Smax MPa	Smin MPa	x/a$_{max}$	x/a$_{min}$	$MSSR_1$	$MSSR_2$	$MSSR_3$
3	0	355	403	26	192	207.29	-0.68	-0.96	25.4	18.0	24.1

P=Constant; Bi-Directional Shear											
Case #	P_φ deg	$\Delta\tau$max MPa	τ_{eff} MPa	θ deg	Smax MPa	Smin MPa	x/a		$MSSR_1$	$MSSR_2$	$MSSR_3$
4	-	499	478	-51	312	-229.18	-0.93		29.6	33.8	25.6
5	-	543	537	38	524	-70.89	-0.94		34.5	35.7	27.9

P=Variable; Bi-Directional Shear											
Case #	P_φ deg	$\Delta\tau$max MPa	τ_{eff} MPa	θ deg	Smax MPa	Smin MPa	x/a$_{max}$	x/a$_{min}$	$MSSR_1$	$MSSR_2$	$MSSR_3$
6	-90	535	532	40	532	-67.39	-0.94	-1.34	34.6	35.7	27.7
7	+90	499	478	40	447	-93.64	-0.66	-0.93	32.2	33.8	25.6

[1] $MSSR=A(\tau_{eff})^B+C\sigma_{max}{}^D$ A=0.75 B=0.5 C=0.75 D=0.5

[2] $MSSR=A(\tau eff)^B+C(|\sigma_{max}-\sigma_{min}|)^D$ A=0.75 B=0.5 C=0.75 D=0.5

[3] $MSSR=A(\tau eff)^B+C(|\sigma_{max}-\sigma_{min}|)^D$ A=0.25 B=0.75 C=25 D=-1.0

X. Summary, Conclusions, and Recommendations

6.1. Summary

Experiments were performed using a test setup modified to allow direct measurement of shear on both sides of a fretting fatigue specimen. Analytical and numerical techniques were employed to simulate the experimental test as well to perform a systematic study in which only contact load was varied. Furthermore, using results from numerical analysis the MSSR predictive fatigue parameter was evaluated based on crack location, crack orientation and fatigue life prediction of experimental tests. Experimental, analytical and numerical results were presented and discussed in light of previous works. New findings on the relationship between variable contact load and fatigue life were presented.

6.2. Conclusions

A distinction was made in this study between test with non-reversing i.e. uni-directional shear and those with fully reversing i.e. bi-directional shear, shear loads. The following conclusions are drawn for each

6.2.1. Uni-Directional Shear Test

1. Fatigue life was shown to be less for tests with uni-directional shear and a variable contact load in phase with applied axial stress than for tests with equal higher and lower constant contact loads at the same axial and shear stress levels.

2.   Differences in fatigue life for various contact loading conditions were greater for uni-directional shear test with lower axial stresses and contact loads.

3.   Contact width for test with a variable contact load was between that of constant contact load test of the same higher and lower constant contact loads.

4.   Stick zone size of test with variable contact load was determined from FEA and it was found to be between that of test with the same higher and lower constant contact loads

6.   The primary slip zone size range of test with variable contact loads was numerically determined to be greater than for test with the same higher and lower constant contact loads.

6.2.2. Bi-Directional Shear Test

1.   Fatigue life was less for bi-directional shear test with variable contact load than for constant contact loads with the same higher and lower contact loads for both phase angles tested i.e. -90° and $+90^o$ phase angles

2.   Decreases in fatigue life for variable contact load test were less distinguishable at higher contact loads

3.   Contact width was less for variable contact loads than higher constant contact loads.

4.   Relative Slip Range was numerically determined to be the same between test with -90° phase and a contact load test with the same higher contact

load as well as between test with $+90^o$ phase and constant contact load test with the same lower contact load.

6.2.3. Modified Shear Stress Range Fatigue Parameter

1.   MSSR predictive parameter was able to predict crack location and crack orientation, which agreed with experimental observations

2.   Two different formulation of the MSSR parameter failed to predict fatigue life for variable contact load test.

3.   New values for the coefficients and exponents of the MSSR parameter are proposed which provide a reasonable prediction of fatigue life for test with a variable contact load as well as test with constant contact loads

6.2.4. Global Application of Finding

It has been shown for the axial load and contact loads and variable contact load waveforms and relative phases that a variable contact load has a negative effect on the fretting fatigue life of Ti-6Al-4V. The exact cause of the decrease in fretting fatigue life under certain variable contact loads has not yet been established. However, using the trends observed in this study design engineers can take steps to avoid fretting fatigue induced failures.

6.3. Recommendations for Future Work

This study was one of the first studies on the effects of variable contact load on the fretting fatigue behavior in titanium alloy. Therefore, there are numerous possibilities for future work in this area. Nonetheless, results from this study point to specific areas which may help further understanding of the factors which influence fretting fatigue in general and in variable contact loading conditions specifically.

Certain factors were observed to be related to lower fatigue lives for variable contact load conditions based on the results of this study. In particular, relative slip range or amplitude and the relationship between contact width and contact load show a strong relation with a variable contact load. Much work has been done to establish relations between the variables involved in fretting fatigue i.e. slip range, contact load and contact width, however, most researchers utilize experiments where the contact load is static. Therefore analysis of these relationships under dynamic loading conditions may reveal factors behind the trends observed in this study. Including a method of measuring slip experimentally would greatly aid the study of the relationship between the variables. Numerical models offer the easiest means for such analysis. Through FEA analysis using idealized load conditions a study of the variables involved in variable contact loading i.e. contact load phase, frequency, and magnitude, future experimental studies could be designed based on observation from a numerical analysis.

For this study coefficient of friction was assumed to be constant during loading. The variation of friction force during variable contact loading could be examined to confirm of refute this assumption. A study of the cyclic variation of friction and other variables influencing fretting fatigue under a variable normal load could reveal insight into the points of maximum stresses along the contact surface for various loading conditions which may not be intuitively obvious.

This study only examined one type of waveform for unidirectional shear test and one waveform with different phases for bi-directional shear test. Numerical studies of various contact load waveforms and magnitudes could reveal frequency, phase and

6.4

magnitude threshold values above or below which contact load does not greatly decreases fatigue life.

        Much work could still be done using the data and samples from this study. A closer examination of the scar pattern using SEM or another tool to examine details of the damage and scar pattern along the contact region could reveal if the actual stick and slip zone follow a pattern as determined via FEA. Crack location and orientation was only determined for one test of this study. Crack orientation and location could be determined for other test of this study and continue to verify or disprove the ability of the MSSR parameter to predict crack orientation and location. Also, crack depth should be determined. Also, the effect of variable contact load on surface treatments i.e. shot peening or lubrication could be studied to see such conditions reduce the effects of a variable contact loading.

Appendix A: Experimental Test Development

The purpose of this Appendix is to provide a more detailed description of the development of the new variable contact load fretting fatigue test setup used in this study. This appendix will first discuss the test setup developed under contact by UDRI. Then improvements made to the new test setup during the course of this study will be discussed.

A.1. Test Setup Developed by University of Dayton Research Institute (UDRI)

This section will focus on the major finding of the test development study performed under contact by University of Dayton Research Institute and the transition from development of the new fretting fatigue test method to the work performed by this author.

As stated in Chapter 3, the basis for the test setup used in this study was developed under contract by UDRI [15] during an investigation into the feasibility of using a multi-axis test stand at the Air Force's Turbine Engine Fatigue Testing Facility. It was demonstrated in the work performed by UDRI that it was possible to apply a cyclically varying contact load to a fatigue specimen in a fretting configuration using a multi-axis test stand, servo-hydraulic actuators, and incorporating software to control the actuators. It was found that shear load could be measured using a set of calibrated flexure springs. However, there were several issues with the test setup as used in the study.

First, work by UDRI was only able to accurately conduct uni-directional shear load fretting fatigue test, or test in which the direction of the reacted shear load does not

A.1

change. This was due to hysteresis in the test configuration used in the study. The setup used in the work performed by UDRI contained hysteresis in the support bushings used to hold the flexure springs in place. This hysteresis reduced the effective stiffness of the flexure springs and prevented the flexure spring assembly from restricting the movement of the pads. This prevented an adequate reacted tangential shear load from developing in both directions. Yet, the configuration used in the study by UDRI did allow sufficient reacted shear loads if the direction of the shear load shear did not change. This was because hysteresis in the flexure spring assembly could be eliminated if the flexure was loaded in one direction. Hysteresis was eliminated in the work by UDRI by preloading the flexure springs with a small force in the same direction as the applied axial load prior to applying a contact load. This removed any freedom of movement or "play" from the flexure spring assembly and any further attempt to move the contact pads held by the flexure spring assembly resulted in a reacted shear load being developed on the fatigue specimen. Therefore, when the contact load was applied and the axial load increased, a shear load was produced immediately rather than after the flexure spring assembly had moved through the region of movement containing hysteresis. These tests were referred to as "uni-polar" in the report by UDRI [34] and are referred to as "uni-directional" shear test in this study. Experimental data collected during the study by UDRI [34] had a uniform contact zone and nearly equal shear on either sides of the specimen during a test. Therefore, they were useful in the study of the effect of variable contact load on fretting fatigue and are included in this study.

While the study performed under contract by UDRI investigated variable contact loading it was not possible to conduct fretting fatigue test with shear in both directions or

bi-directional shear loads. The next section will describe modifications to the test setup

used in the study by UDRI and made during the course of this study to allow fretting

fatigue test with bi-directional shear.

A.2. **Modifications Made to Test Setup for this Study**

Fretting fatigue tests typically involves loading conditions in which the direction

of the shear load changes direction between each cycle of applied axial load. Therefore,

it was desired to further develop this new variable contact load test so that results could

be better compared with those of pervious studies. However, the test stetup in the study

by UDRI did not allow for fretting fatigue test to be conducted with bi-directional shear

for two reasons. First, excessive hysteresis in the test setup used during the study by

URDI prevented the stiffness required for shear loads to be developed in both directions.

As mentioned earlier in order to develop a shearing load on the fatigue specimen

sufficient resistance had to be provided by the flexure spring assembly to hold the contact

pads in place. However, with the tolerances used in the setup by UDRI sufficient

resistance was not obtainable in both directions due to hysteresis being present in the

setup. Furthermore, in the setup used by UDRI only one load cell was placed in line with

the axial load train. With this setup there was no way to determine how much force was

being lost due to hysteresis nor could the effect of hysteresis on the accuracy of the shear

load measured by the flexure springs be quantified. Therefore, two major modifications

were made. First, it was found that a tight tolerance between the tappet shaft and the

support bushing which held the shaft largely affected the amount of hysteresis in the

experimental setup. Therefore, new oversized tappets were made and new bushings were

honed to match the new tappets. This provided the flexure spring assembly with a higher

overall stiffness relative to the old setup and the stiffness needed to develop a sufficient

reacted load for shear in both directions. Second, an additional load cell was placed in

the axial load train so that axial load could be measured and monitored at both ends of the

fatigue specimen. Using two axial load cells provided a means of ensuring the measured tangential load, Q, was accurate and the effects of hysteresis in the test stand fixturing was minimal.

A.3. Future Experimental Setup Modification Suggestions

In studying the effects of contact load it is desirable to keep all other variables i.e. bulk stress and shear stresses, the same between with related contact load magnitudes. An attempt was made to keep the bulk stress ratio, the shear stress ratio, and the span of both the bulk stress and shear stress the same between related test i.e. the constant contact cases, which corresponded to the maximum and minimum contract, loads for a variable loading condition. Actual loads did not always equal the loads desired for several reasons. First, this was a new experimental test configuration. Much time and effort was spent understanding the intricacies, quarks, and nuances of the test setup. Second, the stiffness of the two flexure spring assemblies was not identical. The stiffness of the flexure spring assemblies was found to be dependent on the clearance between the tappet shaft and support bushing as well as the reminder of the flexure spring assembly. Obtaining identical stiffness for each flexure spring assembly would require the addition of a method for adjusting the stiffness of the flexure spring in small incremental amounts. Therefore, it was very difficult to develop equal shear on each side of the specimen. Thirdly, in trying to achieve similar shear magnitudes, ratios, and spans and magnitude of the axial load was sometimes adjusted slightly to aid in achieving the desired shear.

Appendix B: Specimen Photos

This Appendix contains photos of the scar patter for all experimental tests.

B.1. Uni-Directional Shear Test Specimen Scar Photos

Figure B.1. Specimen #1 with P_{const}= 315 kN/m and Uni-Directional Shear
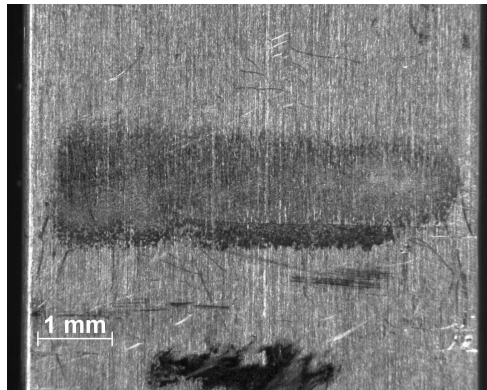

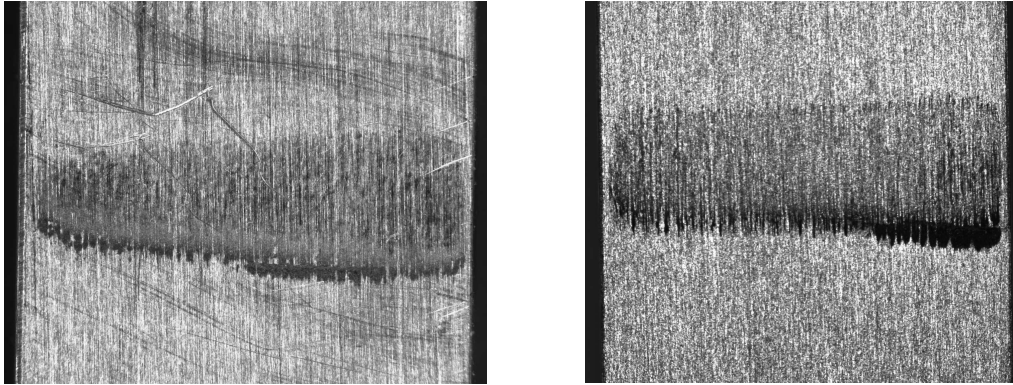Figure B.2. Specimen #2 with P_{const}= 350 kN/m and Uni-Directional Shear

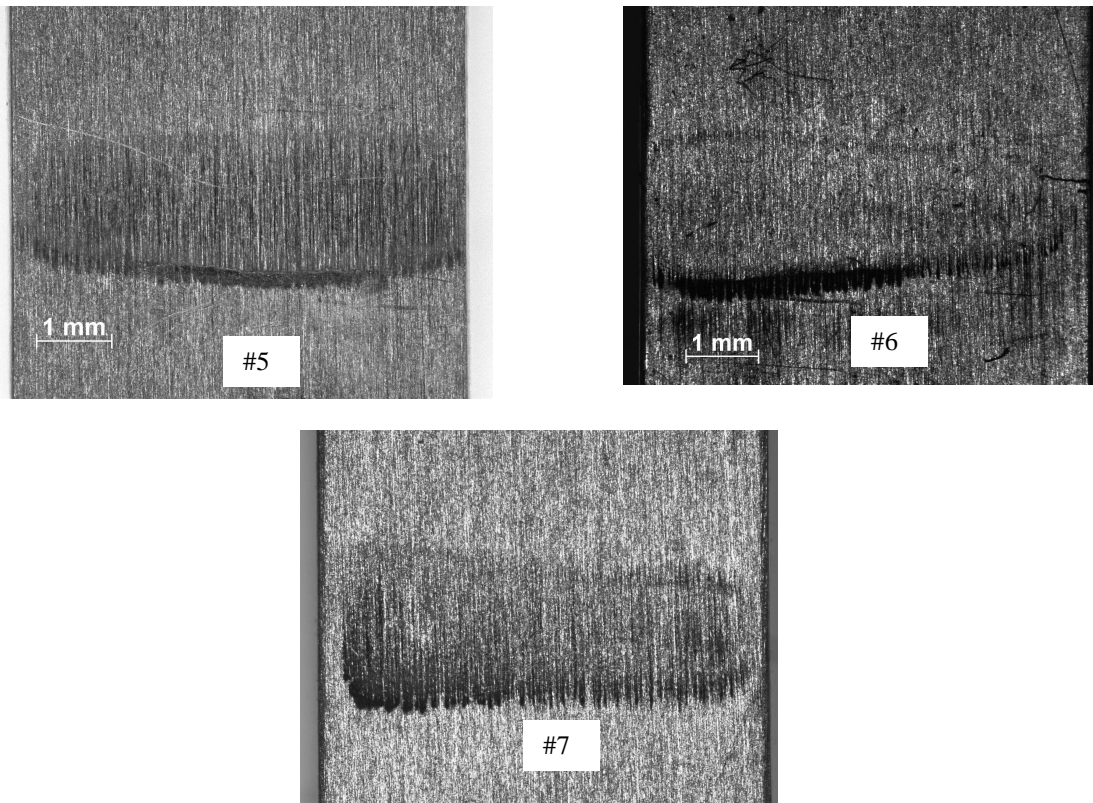Figure B.3. Specimens #3 (Left) and #4 (Right) with P_{const}= 525 kN/m and Uni-Directional Shear

Figure B.4. Specimens #5, #6 and #7 with P_{const}= 630 kN/m and Uni-Directional Shear
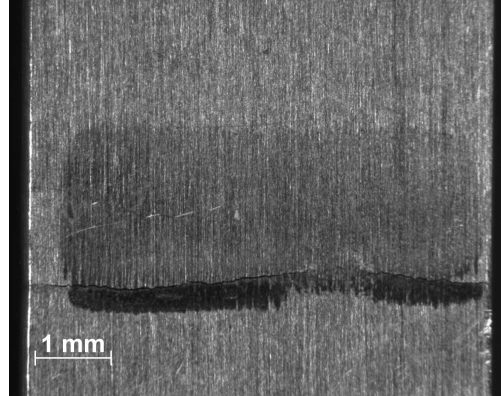
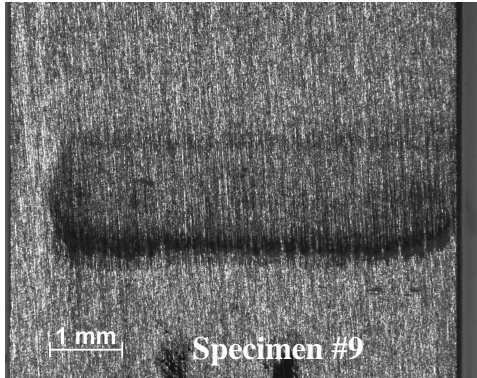Figure B.5. Specimen #8 with Variable Contact Load P_{max}= 630 to P_{min}= 315 kN/m and Uni-Directional Shear
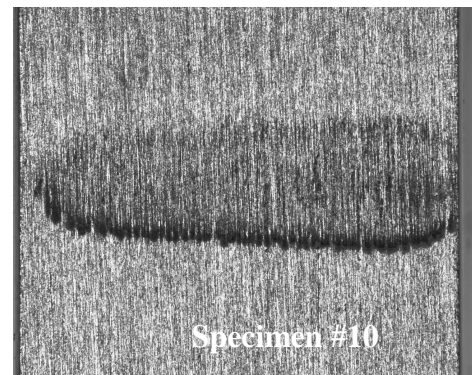
Figure B.6. Specimen #9 and #10 with Variable Contact Load P_{max}= 630 to P_{min}= 315 kN/m and Uni-Directional Shear
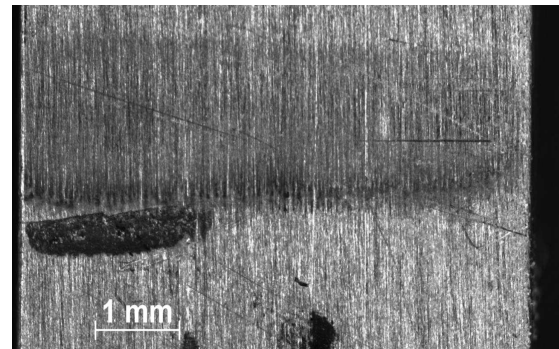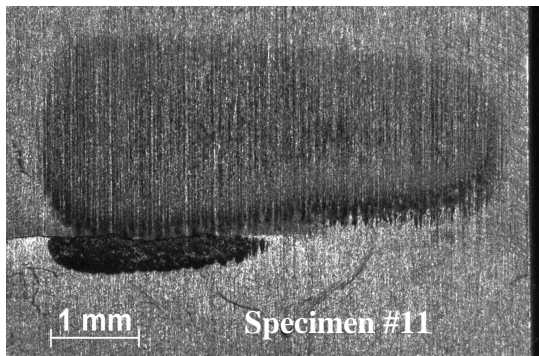

Figure B.7. Specimen #11 and #12 with Variable Contact Load P_{max}= 700 to P_{min}= 350 kN/m and Uni-Directional Shear
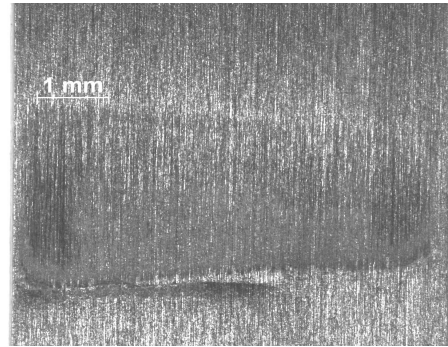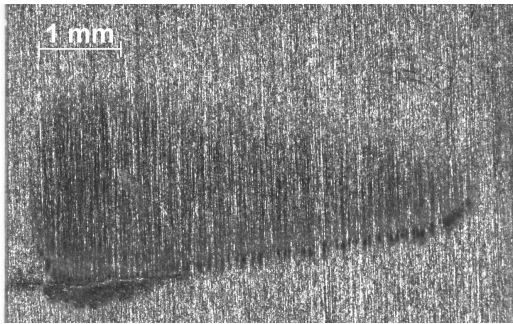
Figure B.8. Specimen #13 and #14 with Variable Contact Load P$_{max}$= 700 to P$_{min}$= 525 kN/m and Uni-Directional Shear
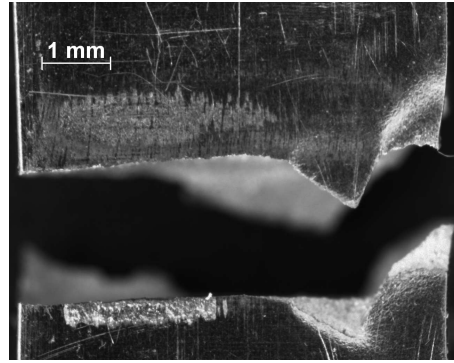
Figure B.9. Specimen #15; Constant Contact Load P_{const}= 350 kN/m, Bi-Directional Shear

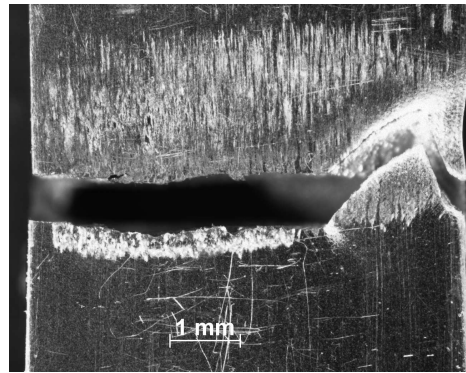Figure B.10. Specimen #16; Constant Contact Load P_{const}= 525 kN/m, Bi-Directional Shear

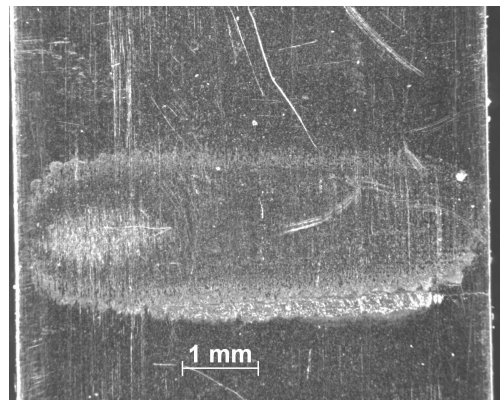

Figure B.11. Specimen #17; Constant Contact Load P_{const}= 700 kN/m, Bi-Directional Shear
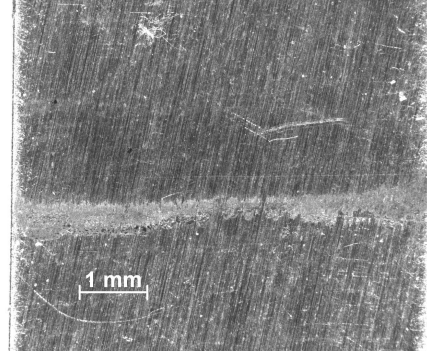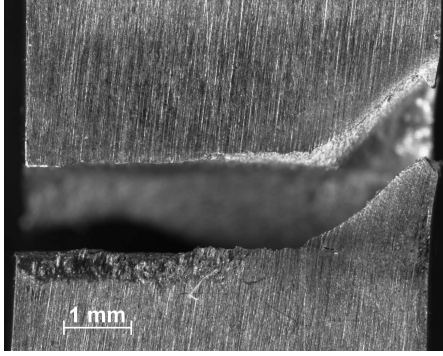
Figure B.12. Specimens #18 and 19; Variable Contact Load P_{max} = 700 kN/m P_{min}= 350 kN/m, Bi-Directional Shear +90° Phase

Figure B.13. Specimen #20 and #22; Variable Contact Load P_{max} = 700 kN/m P_{min}= 350 kN/m, Bi-Directional Shear +90° Phase
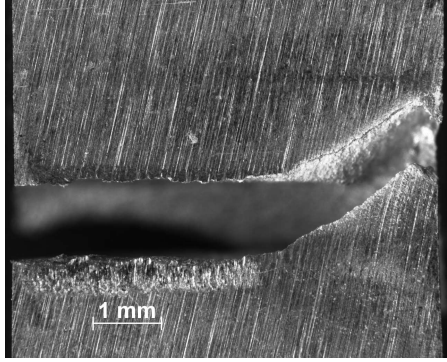
Figure B.14. Specimen #21; Variable Contact Load $P_{max} = 700$ kN/m $P_{min} = 350$ kN/m, Bi-Directional Shear -90° Phase

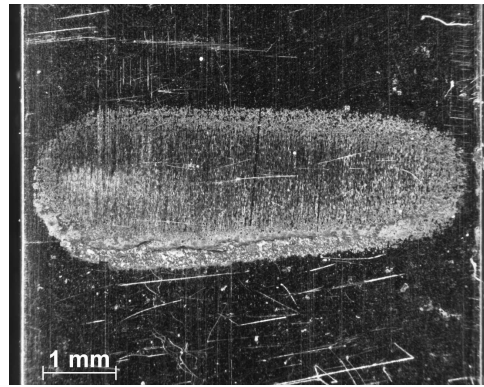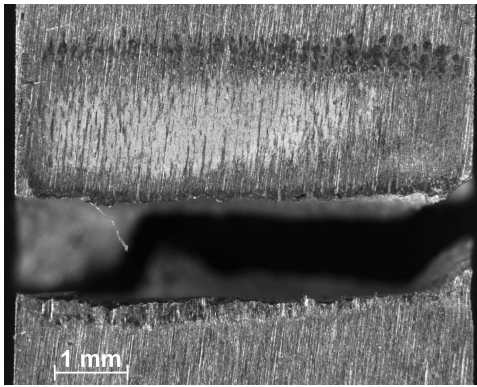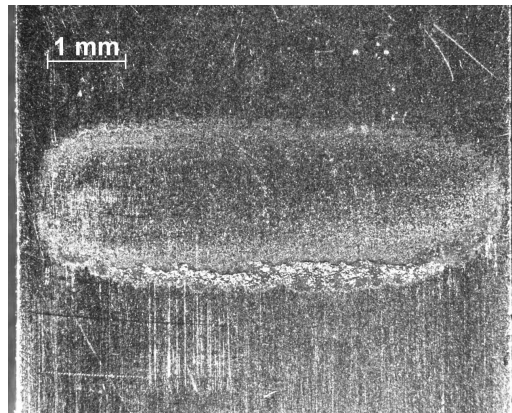
Figure B.15. Specimen #23; Variable Contact Load $P_{max} = 700$ kN/m $P_{min} = 525$ kN/m, Bi-Directional Shear +90° Phase

Appendix C: Finite Element Analysis Results for Experimental Loads

This Appendix contains finite element analysis results for experimental test not included in the main body of the report.

C.1. Uni-Directional Shear Tests

Figure C.1. , C.2, and C.3 with corresponding contact loads of P_{const}=315 kN/m, P_{const} = 630 kN/m and P_{max}=630 to P_{min}=315 kN/m are representative of the stresses along the surface for a uni-directional shear tests. Figures C.5 thru C.9 show comparisons of S_{11}, S_{22} and S_{12} along the contact surface for uni-directional shear tests #1, 5 and 9.
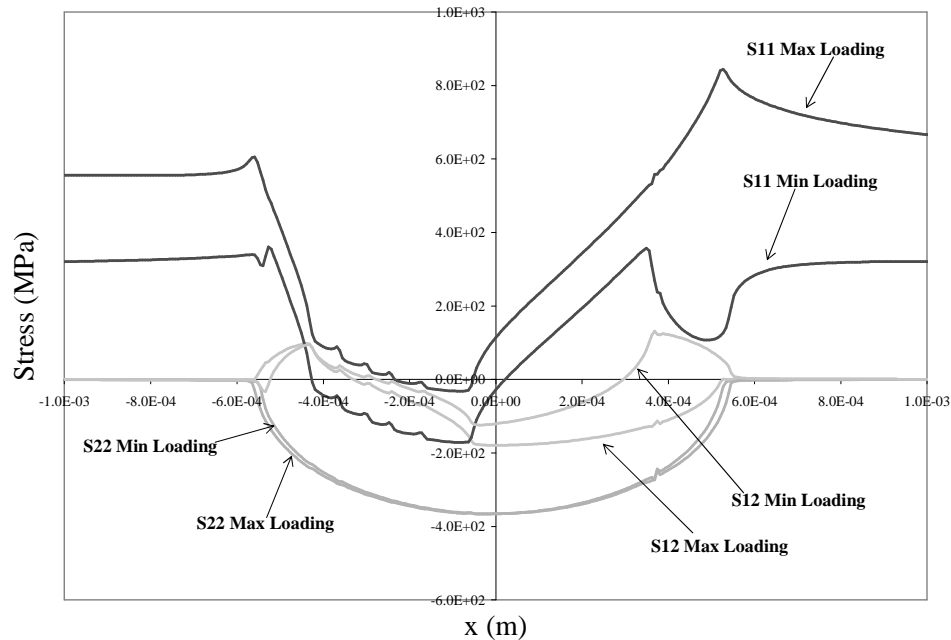
Figure C.1. Comparison of Stresses Along Surface of Contact for Maximum and Minimum Applied Loading Conditions for Uni-directional Shear Test with Constant Contact Load (Test #1: P_{const}=315 kN/m)
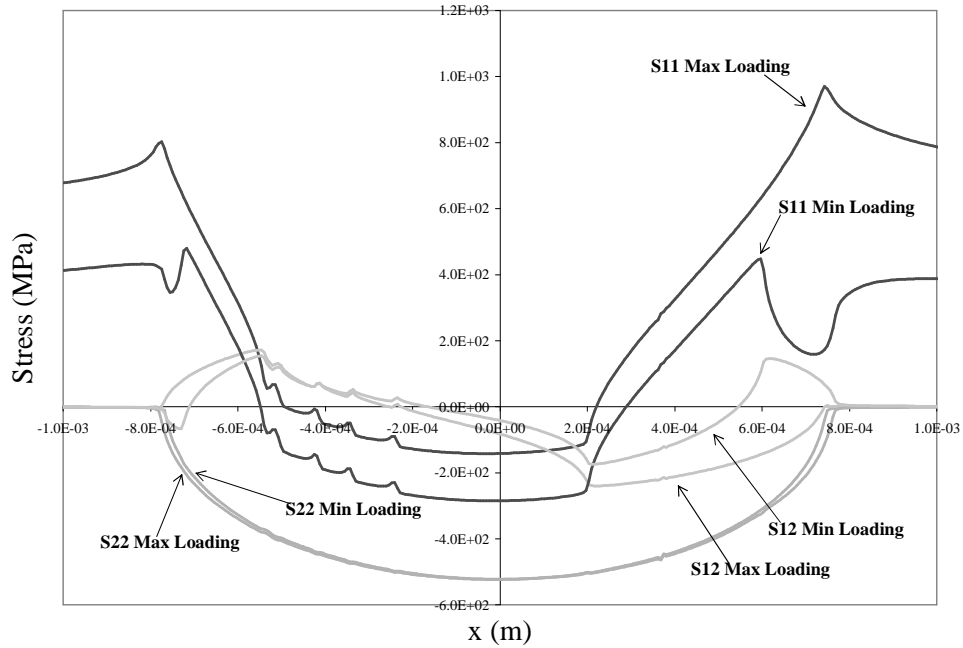
Figure C.2. Comparison of Stresses Along Surface of Contact for Maximum and Minimum Applied Loading Conditions for Uni-directional Shear Test with Constant Contact Load (Test #5: P_{const}=630 kN/m))
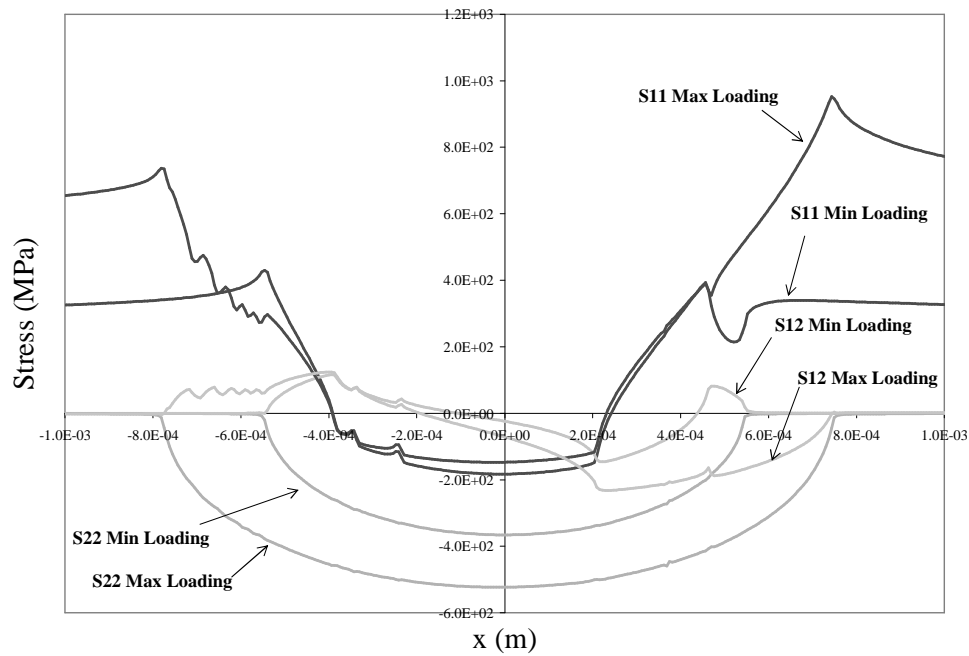
Figure C.3. Comparison of Stresses Along Surface of Contact for Maximum and Minimum Applied Loading Conditions for Uni-directional Shear Test with Constant Contact Load (Test #9: P_{max} = 630, P_{min} = 315 kN/m)

C.2

Figure C.5. Comparison of S_{11} Along Surface of Contact for Maximum Applied Loading Condition for Uni-directional Shear Tests for Tests 1,5 and 9

Figure C.4. S_{11} Along Surface of Contact for Minimum Applied Loading Condition for Uni-directional Shear Tests for Tests 1,5, and 9

C.3

Figure C.6. S_{12} Along Contact Surface for Maximum Applied Loading Condition for Uni-directional Shear Tests for Tests 1,5, and 9

Figure C.7. S_{12} Along Surface of Contact for Minimum Applied Loading Condition for Uni-directional Shear Tests for Tests 1,5, and 9

C.4
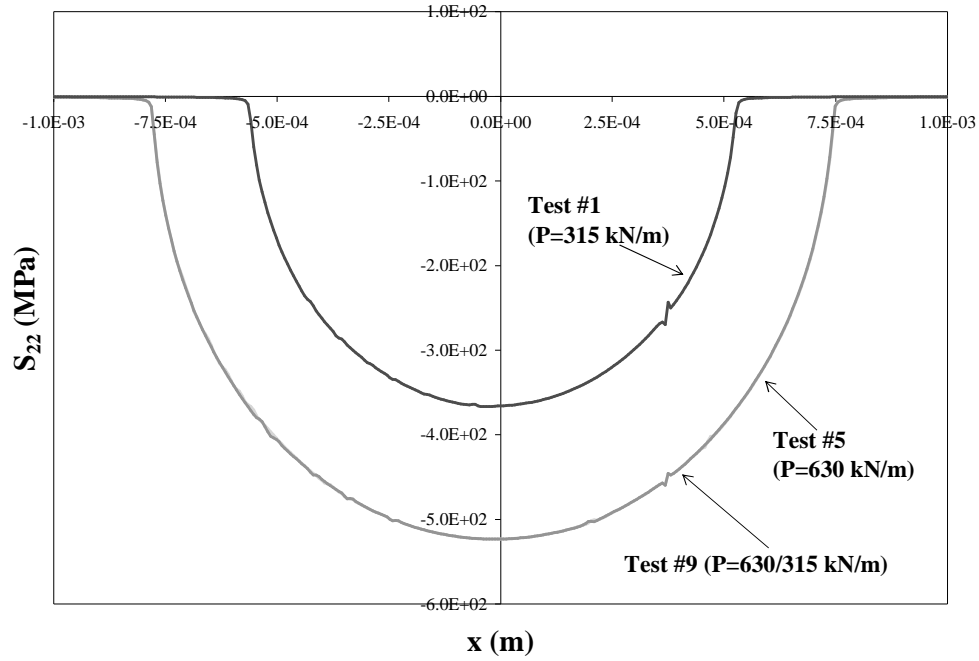
Figure C.8. S_{22} Along Surface of Contact for Maximum Applied Loading Condition for Uni-directional Shear Tests for Tests 1,5, and 9
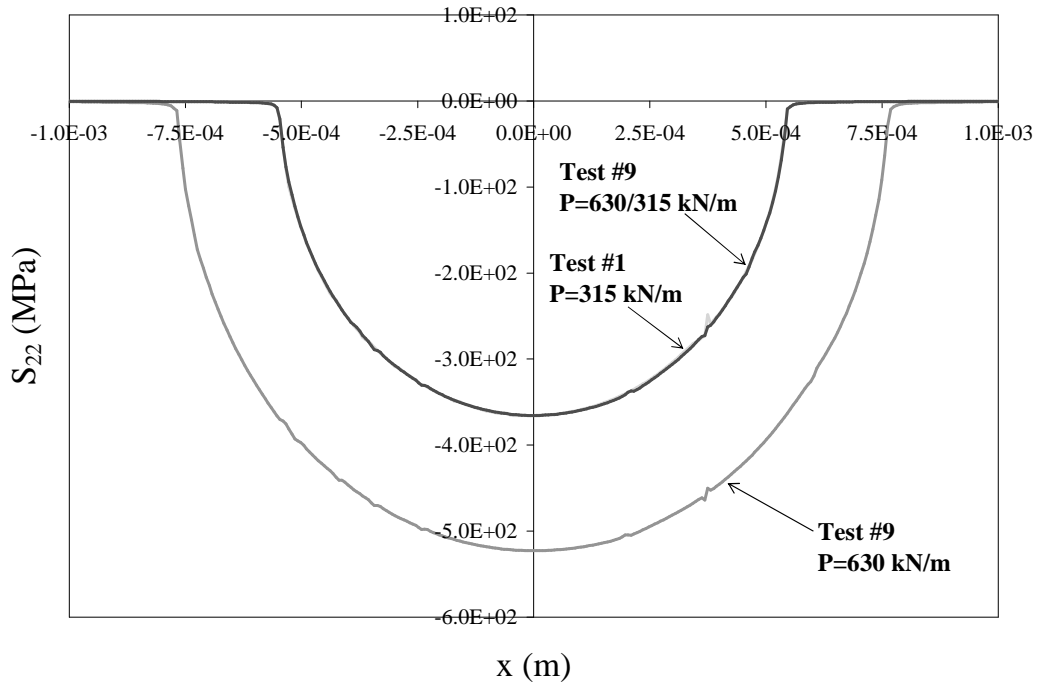
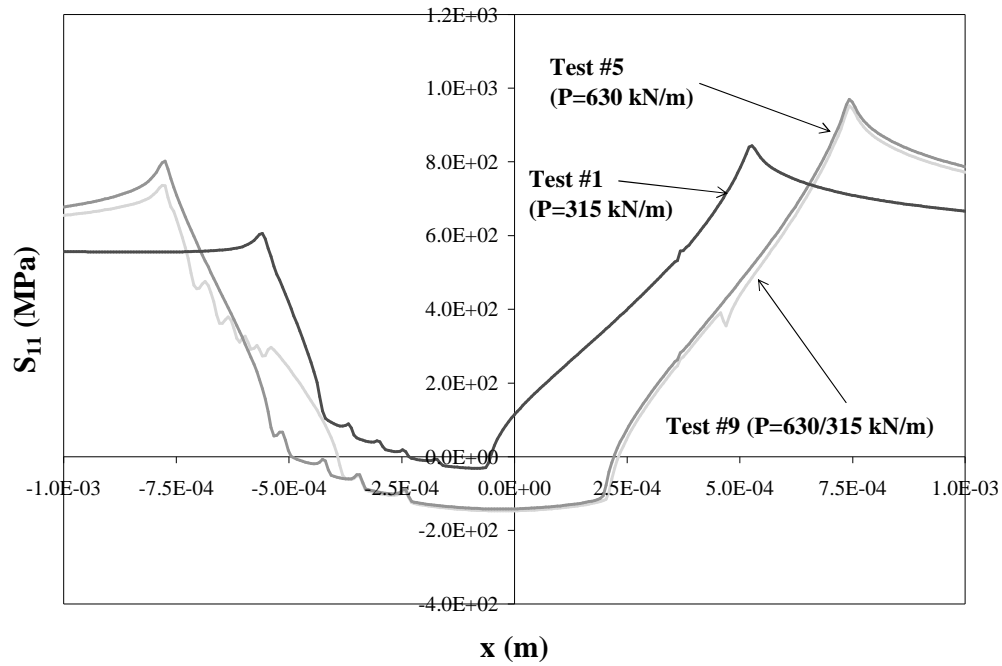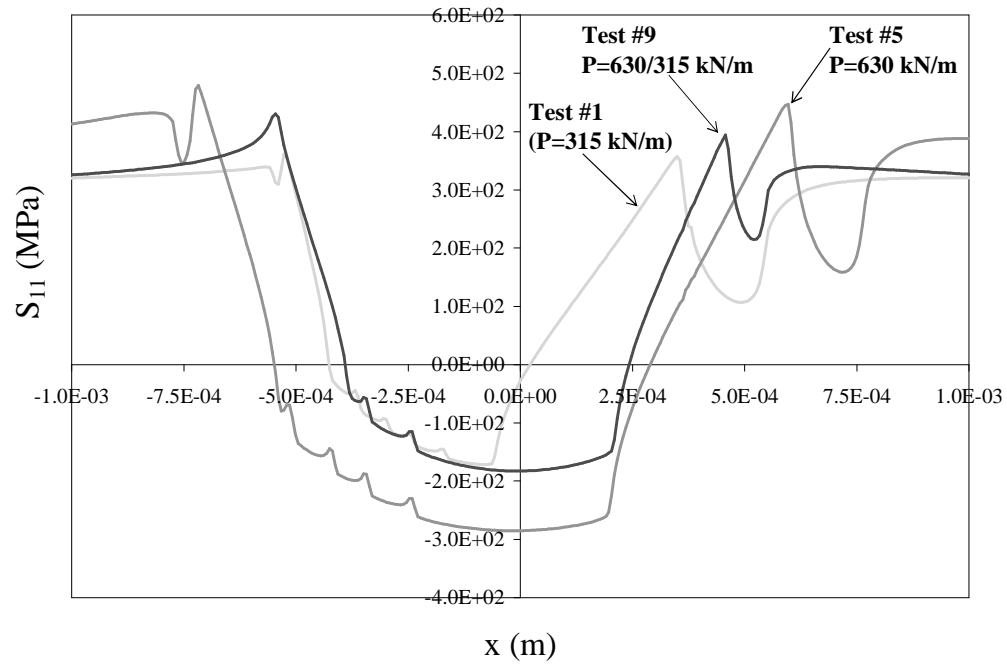Figure C.9. S_{22} Along Surface of Contact for Minimum Applied Loading Condition for Uni-directional Shear Tests for Tests 1,5, and 9
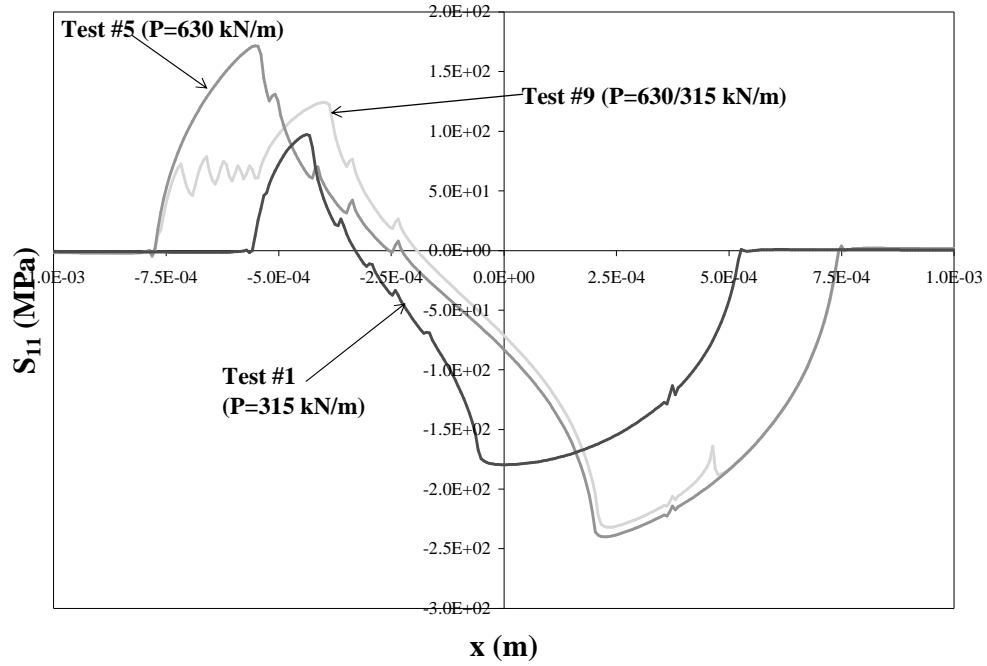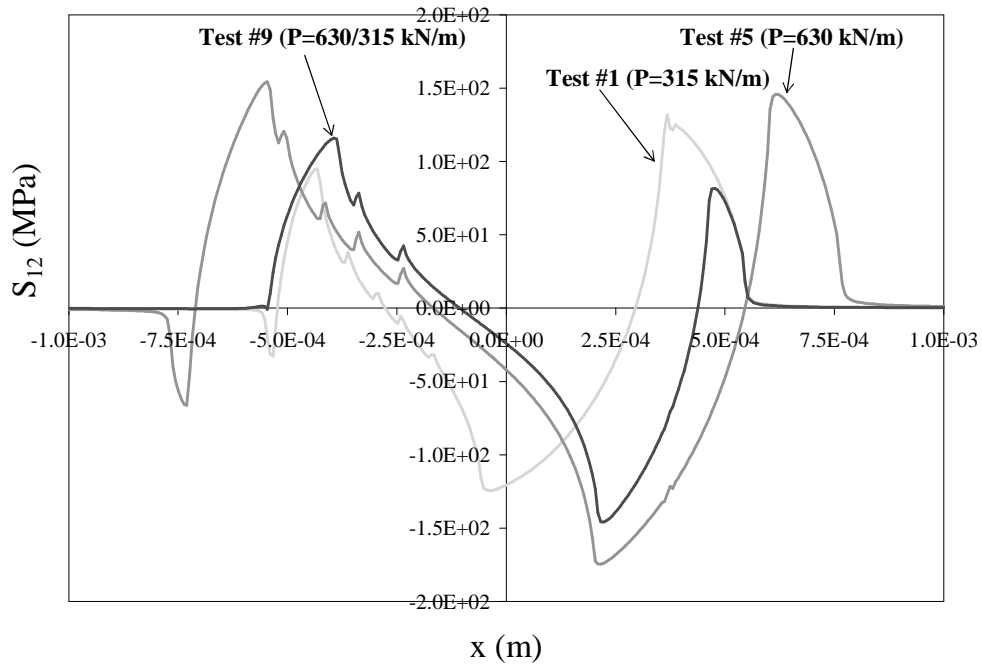
C.5

Appendix D: Additional Thoughts by Author

The purpose of this appendix is to convey some ideas developed by the author during the course. They are included here to serve starting point and points for consideration for future researchers in this area.

D.1. Local Mechanistic Parameters

As seen in equations 17 thru 21 the relationship between contact width and bulk axial stress is not defined. However, it has been shown by Iyer [16] and Magaziner [23], that the location of peak Herztian pressure shifts when an axial load is applied. Furthermore, Iyer established a relationship between contact width, peak contact pressure and bulk axial stress and states that "only peak contact pressure and local, maximum bulk stress range are found to be independent variables for determining fretting fatigue life [16]." He goes on to relate contact semi-width to peak contact pressure and states that slip-amplitude has "little or no direct effect on fretting fatigue life". In Iyer's study contact load was constant, therefore, Iyer concluded, "peak contact pressure and contact semi-width change only slightly during fretting fatigue and can be regarded as 'static' parameters. [16]." On the other hand, this study has shown that as expected peak contact pressure is not static when a variable contact load is applied. Therefore, the relationships between the local mechanistic parameters as stated by Iyer cannot be directly applied to this study.

Iyer also states that contact semi-width is a function of the contact pressure and does not itself have any effect on fretting fatigue life [16]." However, from this study it is unclear what the relationship is between semi-contact width, peak pressure, and fatigue

life since contact width was less for test with a variable contact load although the maximum and minimum peak pressures were the same as for constant contact loads with equivalent higher and lower constant contact loads.

Furthermore, Iyer [16] also states that slip-amplitude has "little or no direct effect on fretting fatigue life". However, it has been shown that slip amplitude is greater for uni-directional shear test with a variable contact. Therefore, it is unclear if slip amplitude for test with a variable contact load and uni-directional shear is dependent on peak contact pressure and not a major factor in effecting fatigue life as Iyer states or if slip amplitude resulting from a variable contact load is a major contributing factor to a decrease in fatigue life.

Iyer and Mall [15] found that the total width of the contact zone, primary and secondary slip as well as stick zone, is primarily a function of the contact load, however, the widths of the stick and slip zoned depended on the axial stress ratio, R. Furthermore they found a close correlation between the width of the measured contact zone as well as the primary slip zone from experimental test and computed values. From experimental test of this study it has been observed that the contact width falls between that of contact load test with equivalent higher and lower contact loads. Therefore, this may highlight the findings of other researchers [27] that at higher axial load the influence of the axial load is much greater than that of the contact load resulting in a less dramatic decrease in fatigue life.

In their study Iyer and Mall state "the width of the stick and slip regions and the location of the boundary between them may be expected to be a function of the applied axial stress ration, R [15]. This may explain the reason why the width of the stick and slip

regions were similar between variable and constant contact loads with bi-directional shear which were at higher axial stress ratios than uni-directional shear tests. Furthermore, they state that a reduction in life with increasing contact pressure may be attributed to the increased uniaxial stress concentration factor at the edge of contact [15]." This however, does not explain the decrease in life for a variable amplitude load, which has a uniaxial stress concentration factor at the edge below that of a constant contact load of the same higher contact load.

D.2. **Bulk Axial Stress Amplitude**

As seen from the plots of the FEA results for stresses, S_{11}, S_{22} and S_{12} along the surface of contact surface as discussed in Chapter 5 it was seen that test with a variable contact load had a maximum values less than that for higher constant contact load at the instance of maximum load application. However, at the point of minimum load application the maximum value of stresses along the surface was between those for test with higher and lower constant contact loads. Therefore, the range of maximum stress on the contact surface is greater for variable contact loads than for constant contact load test. Iyer and Mall [17] concluded from their study that the decrease in fretting fatigue life with increasing contact pressure can be related to the increase in the local stress range amplification alone, without any regard to interfacial shear stress or slip amplitude. The exact relationship between bulk stress amplitude on the contact surface and fatigue life should be investigated further.

From the results of this study peak contact pressure appears to influence fretting fatigue life for a variable contact load as well. However, the extent which the local maximum bulk stress and peak contact pressure influence fatigue life relative to one

another is unclear from the results of this study. Further work should be conducted to establish the relationship between bulk axial stress, contact width, and slip amplitude when contact load i.e. peak contact pressure, is variable.

Bibliography

1.   Adibnazari, S. and Hoepnner, D. W., "Characteristics of the fretting fatigue damage threshold," *Wear*, Vol. 159, 43-46, 1992.

2.   Anton, D. L., Lutian, M. J., Favrow, L. H., Logan, D., and Annigeri, B., "The effect of contact stress and slip distance on fretting damage in Ti-6Al-4V/17-4PH contact," *Fretting Fatigue: Current Technology and Practices*, *ASTM STP 1367*, D.W. Hoeppner, V. Chandrasekaran, and C.B. Elliots, Eds., American Society for Testing and Materials, West Conshohocken PA, 2000.

3.   Cattaneo, C., *Sul Contatto di due Corpi Elastici: Distrobuzion Locale Degli Sforzi Reconditi dell Academia Naziionale de Lincei*, Vol 27, 342-348, 1938.

4.   Chan, K., Lee, Y., FORTRAN program developed at South West Research Institute. Personal Communication of Lykins, 1998.

5   Dowling, Norman E., *Mechanical Behavior of Materials: Engineering Methods for Deformation, Fracture, and Fatigue*. Englewood Cliffs N.J., Prentice Hall, pp 400, 1993.

6.   Fellows, L., Nowell, D., Hills, D., "Contact Stress in a Moderately Thin Strip with Particular Reference to Fretting Experiments," *Wear*, Vol. 185, 235-238, 1995.

7.   Fernando, U. S., Brown, M. W., Miller, K. J., Cook, R., and Rayaprolu, D., "Fretting Fatigue Behavior of BS L65 4 percent Copper Aluminum Alloy under Variable Normal Load." *Fretting Fatigue*, R.B. Waterhouse and T.C. Lindley Eds. European Structural Integrity, Mechanical Engineering Publications Limited, London, 1994.

8   Findley, W. N., "Fatigue of metals under combinations of stresses," *Trans. ASME*, Vol 79, 1337-1348, 1957.

9.   Goss, G.L. and Hoeppner, D.W., "Normal load effects in fretting fatigue of titanium and aluminum alloys," *Wear*, Vol. 27, 153-159, 1974.

10.   Harris, W.J., "The Influence of Fretting Fatigue," *AGARD Advisory Group for Aerospace Research and Development*, Advisory Report 8, 1967.

11   Hibbeler, R. C., *Mechanics of Materials*. Upper Saddle River N.J., Prentice Hall, pp 452-454, 1997.

12. Hibbit, Karlsson and Sorensen, Inc. *ABAQUS Standard User's Manual Vol. II*, 2002

13 Hills, D., Nowell, D., Sackelfield, A., "Surface Fatigue Considerations in Fretting Interface Dynamic," *Proceedings of the 14th Leeds-Lyon Symposium on Tribiology*, D. Dawson, C.M. Taylor, M. Godet, D. Berthe Eds. Elsevier, Amsterdam, 1988.

14. Hutson, A., Nicholas, T., and Goodman, R., "Fretting fatigue of Ti-6Al-4V under flat-on-flat contact," *International Journal of Fatigue*, Vol. 21, 663-670, 1999.

15. Iyer, K. and Mall, S., "Effects of cyclic frequency and contact pressure on fretting fatigue under two-level block loading," *Fatigue and Fracture of Engineering Materials and Structures*, Vol. 23, No. 4, 335-346, April 2000.

16. Iyer, K., "Peak contact pressure, cyclic stress amplitudes, contact semi-width and slip amplitude: relative effects on fretting fatigue life," *International Journal of Fatigue*, Vol. 23, No. 3, 193-206, March 2001.

17. Iyer K, and Mall, S., "Analyses of contact pressure and stress amplitude effects on fretting fatigue life," *Transactions of the ASME Journal of Engineering Materials and Technology*, Vol. 123, No. 1, 85-93, 2001.

18. Lindley, T., Nix, K., "The Role of Fretting in the Initiation and Early Growth of Fatigue Cracks in Turbo Generator Material," *Multiaxial Fatigue*, ASTM, 340-360, 1985.

19. Lykins, C., *An Investigation of Fretting Fatigue Crack Initiation Behavior of the Titanium Alloy Ti-6Al-4V*. PhD dissertation, University of Dayton, December 1999.

20. Lykins, C., Mall, S., and Jain, V., "An evaluation of parameters for predating fretting fatigue crack initiation," *International Journal of Fatigue*, Vol. 22, No 8. 703-716, Sept 2000.

21. Lykins, C., Mall, S., and Jain, V., "A shear stress-based parameter for fretting fatigue crack initiation," *Fatigue Fracture Engineering Material Structure*, 2000, Vol. 24, No 7. 461-473, July 2001.

22. Lykins, C., Mall, S., and Jain, V., "Combined experimental-numerical investigation of fretting fatigue crack initiation," *International Journal of Fatigue*, Vol. 23, No. 9, 703-711, Sept. 2001.

23. Magaziner, Russell, S., *Examination of Contact Width on Fretting Fatigue.* MS Thesis, AFIT/GAE/ENY/02-08. School of Aeronautics and Astronautics, Air Force Institute of Technology (AU), Wright-Patterson AFB, OH, March 2002 (AD-A401279)

24. Mindlin, R., "Compliance of Elastic Bodies in Contact," *Journal of Applied Mechanics*, Vol. 16, 259-268, 1949.

25   Morel, F., "A critical plane approach for life predictions of high cycle fatigue under multiaxial variable amplitude loading," *International Journal of Fatigue*, Vol. 22, 101-119, 2000.

26. Nakazawa, Kozo, Maruyama, and others, Effect of contact pressure on fretting fatigue of austenitic stainless steel," *Tribology International*, Vol. 32,79-85, 2003.

27. Nakazawa, K., Sumita, M., and Maruyama, N., "Effects of contact pressure on fretting fatigue of high strength steel and titanium alloy," *Standardization of Fretting Fatigue Test Methods, ASTM STP 1159*, M. Attia and R.B. Waterhouse, Eds., American Society for Testing and Materials Philadelphia PA 1992.

28. Namjoshi, S., *Parameters Program.* Fortran Program

29. Namjoshi S., Mall S., Jain V., and Jin, O., "Fretting Fatigue Crack Initiation Mechanism in Ti-6Al-4V," *Fatigue and Fracture of Engineering Material and Structures*, Vol. 25, No. 10, 955-964, Oct 2002.

30. Nishioka, K., and Hirakawa, K., "Fundamental Investigation into Fretting Fatigue, Part 2," *Bulletin of JSME*, Vol. 12, No. 50, 180-187, 1969.

31. Nishioka, K., and Hirakawa, K., Fundamental Investigation into Fretting Fatigue, Part 3," *Bulletin of JSME*, Vol. 12, No. 50, 397-407, 1969.

32 . Nix, K., Lindley, T., "The Application of Fracture Mechanics to Fretting Fatigue," *Fatigue and Fracture of Engineering Materials and Structure*, Vol. 8, No. 2, 143-160, 1985.

33. Nowell D., Hills, D. A., *Mechanics of fretting fatigue*. The Netherlands: Kluwer Academic Publishers, 1994.

34. Propulsions Directorate, Air Force Research Libratory, Air Force Material Command. Contract F33615-96-C-264 with University of Dayton Research Institute. Wright-Patterson Air Force Base, OH. December 2002.

35.   Ruiz, C., Bodington, P., and Chen, K., "An Investigation of Fatigue and Fretting in a Dovetail Joint," *Experimental Mechanics*, Vol. 24, No. 3, 208-217, 1984.

36.   Socie, D., "Multiaxial Fatigue Damage Models," *Journal of Engineering Materials and Technology*, Vol. 109, 293-298, Oct 1987.

37.   Szolwinski, M., and Farris, T., "Mechanics of Fretting Fatigue Crack Formation," *Wear*, Vol. 198, No. 1-2, 93-107, Oct. 1996.

38.   Walker, K., "The Effects of Stress Relaxation During Crack Propagation and Fatigue for 2024-T3 and 7075-T6 Aluminum," Presented to Subcommittee E-9V Winter Meeting, Feb 1969.

39   Walker, K. "Effects of Environment and Complex Load History on Fatigue Life," *American Society for Testing and Materials*, West Conshohocken, PA., STP 462, 1-14, 1970.

40.   Wallace, J. M., and Neu, R. W., "Fretting fatigue crack nucleation in Ti-6Al-4V," *Fatigue and Fracture of Engineering Material and Structures*," 26, No. 03, 199-214, March 2003.

Vita

       Lieutenant Andrew J. Jutte was born in Dayton, OH and grew up in Englewood, OH until college. He graduated from Northmont High School, Clayton, OH in June 1996. In May 2003 he graduated from the University of Dayton with a Bachelor of Science in Mechanical Engineering with a concentration in Aerospace. He was commissioned upon graduation in May 2000. In July 2000 he was assigned to F-15 System Program Office, Warner Robins Air Logistics Center, Robins AFB, GA as a Developmental Engineer. In August 2002 he was reassigned to AFIT as a graduate student to pursue a Masters of Science in Aeronautical Engineering. Upon graduation, Lt Jutte will be assigned to the Propulsions Directorate of the Air Force Research Lab, WPAFB, OH to work as a research engineer.

REPORT DOCUMENTATION PAGE

Form Approved
OMB No. 074-0188

The public reporting burden for this collection of information is estimated to average 1 hour per response, including the time for reviewing instructions, searching existing data sources, gathering and maintaining the data needed, and completing and reviewing the collection of information. Send comments regarding this burden estimate or any other aspect of the collection of information, including suggestions for reducing this burden to Department of Defense, Washington Headquarters Services, Directorate for Information Operations and Reports (0704-0188), 1215 Jefferson Davis Highway, Suite 1204, Arlington, VA 22202-4302. Respondents should be aware that notwithstanding any other provision of law, no person shall be subject to an penalty for failing to comply with a collection of information if it does not display a currently valid OMB control number.
PLEASE DO NOT RETURN YOUR FORM TO THE ABOVE ADDRESS.

1. REPORT DATE *(DD-MM-YYYY)* 23 Mar 04	2. REPORT TYPE **Master's Thesis**	3. DATES COVERED *(From – To)* Aug 2002 – Mar 2004

4. TITLE AND SUBTITLE	5a. CONTRACT NUMBER
EFFECT OF A VARIABLE NORMAL LOAD ON FRETTING FATIGUE BEHAVIOR OF Ti-6Al-4V	5b. GRANT NUMBER
	5c. PROGRAM ELEMENT NUMBER

6. AUTHOR(S)	5d. PROJECT NUMBER
Jutte, Andrew, J., 1LT, USAF	5e. TASK NUMBER
	5f. WORK UNIT NUMBER

7. PERFORMING ORGANIZATION NAMES(S) AND ADDRESS(S) Air Force Institute of Technology Graduate School of Engineering and Management (AFIT/EN) 2950 Hobson Way WPAFB OH 45433-7765	8. PERFORMING ORGANIZATION REPORT NUMBER AFIT/GAE/ENY/04-M09

9. SPONSORING/MONITORING AGENCY NAME(S) AND ADDRESS(ES) AFRL/PRTC Attn: Dr. Charles Cross 1950 5th Street, Bldg 18 WPAFB OH 45433-7765 DSN: 986-5530	10. SPONSOR/MONITOR'S ACRONYM(S)
	11. SPONSOR/MONITOR'S REPORT NUMBER(S)

12. DISTRIBUTION/AVAILABILITY STATEMENT
    APPROVED FOR PUBLIC RELEASE; DISTRIBUTION UNLIMITED.

13. SUPPLEMENTARY NOTES

14. ABSTRACT

Effects of a variable contact load on the high cycle fretting fatigue behavior of Ti-6AL-4V were investigated. Experimental tests were performed using a new test setup capable of applying a contact load varying in amplitude, frequency, and phase and independently measuring shear forces on opposite sides of a specimen. Finite element analysis (FEA) of experimental and idealized loading conditions was performed and local mechanistic parameters and the Modified Shear Stress Range (MSSR) fatigue parameter were determined. Correlations between contact width, slip amplitude, fatigue life and a variable contact load were established with variable contact loading shown to have a damaging effect. Predicted values of crack location and orientation using the MSSR parameter were verified experimentally. The MSSR parameter unsuccessfully predicted fatigue life for variable contact loads. A new formulation of the MSSR parameter is proposed.

15. SUBJECT TERMS
    Fretting Fatigue, Variable Normal Load,

16. SECURITY CLASSIFICATION OF:			17. LIMITATION OF ABSTRACT	18. NUMBER OF PAGES	19a. NAME OF RESPONSIBLE PERSON Prof. Dr. Shankar Mall, AFIT (ENY)
REPORT U	ABSTRACT U	c. THIS PAGE U	UU	174	19b. TELEPHONE NUMBER *(Include area code)* (937) 255-3636, ext 4587; e-mail: Shankar.Mall@afit.edu

Standard Form 298 (Rev: 8-98)
Prescribed by ANSI Std. Z39-18